PREPARATION AND CHARACTERIZATION OF ULTRA THIN FILMS CONTAINING SILVER-COPPER NANOALLOYS USING LAYER-BY-LAYER DEPOSITON TECHNIQUE FOR ANTIBACTERIAL APPLICATIONS

A THESIS

SUBMITTED TO THE DEPARTMENT OF CHEMISTRY AND

THE GRADUATE SCHOOL OF ENGINEERING AND SCIENCE

OF BILKENT UNIVERSITY

IN PARTIAL FULFILLMENT OF THE REQUIREMENTS

FOR DEGREE OF

MASTER OF SCIENCE

By

MERVE TANER CAMCI

JUNE 2012

I certify that I have read this thesis and that in my opinion it is fully adequate, in scope and in quality, as a thesis for the degree of Master of Science

……..

Prof. Dr. Şefik Süzer (Principal Advisor)

I certify that I have read this thesis and that in my opinion it is fully adequate, in scope and in quality, as a thesis for the degree of Master of Science

……..

Prof. Dr. Ömer Dağ

I certify that I have read this thesis and that in my opinion it is fully adequate, in scope and in quality, as a thesis for the degree of Master of Science

……..

Assoc. Prof. Dr. DönüşTuncel

I certify that I have read this thesis and that in my opinion it is fully adequate, in scope and in quality, as a thesis for the degree of Master of Science

……..

Assoc. Prof. Dr. Işık Yuluğ

I certify that I have read this thesis and that in my opinion it is fully adequate, in scope and in quality, as a thesis for the degree of Master of Science

……..

Assist. Prof. Dr. Gülay Ertaş

Approved for the Graduate School of Engineering and Science:

……..

Prof. Dr. Levent Onural

Director of Graduate School of Engineering

ABSTRACT

PREPARATION AND CHARACTERIZATION OF ULTRA THIN FILMS CONTAINING SILVER-COPPER NANOALLOYS USING LAYER-BY-LAYER DEPOSITON TECHNIQUE FOR ANTIBACTERIAL APPLICATIONS

Merve TANER CAMCI

M.S. in Chemistry

Advisor: Prof. Dr. Şefik SÜZER

June, 2012

The main objective of this master thesis is to explore the preparation, characterization and antibacterial applications of Layer-by-Layer (LbL) assembled ultra thin films containing AgCu nanoalloys. Within this purpose, first part of the research mainly focused on the preparation of Ag nanoparticles and AgCu nanoalloys in order to prevent the oxidation of copper to copper oxide and the formation of polyelectrolyte-AgCu nanoalloy films by Layer-by-Layer assembly. Accordingly, Ag nanoparticles and AgCu nanoalloys were synthesized by the chemical reduction of silver and copper salts in aqueous solution with the help of strong reducing agents sodium borohydride or hydrazine hydrate in the presence of complexing agent and stabilizer, then ultra thin polyelectrolyte layers containing pre-prepared AgCu nanoalloys were constructed by Layer-by-Layer deposition technique in different combinations. Also the stability of these nano sized binary alloys in solution phase were

prolonged in the presence of third metal zinc as a sacrificial anode. In the second part of the study, characterization of LbL assembled ultra thin polyelectrolyte and metal nanoparticle thin films using Optical (UV-visible) and X-ray Photoelectron Spectroscopy (XPS) was studied. In order to get further information on the optical response of single and bimetallic nanoparticles, Ag nanoparticle and AgCu nanoalloy incorporated ultra thin polyelectrolyte films were investigated by optical spectroscopy. In addition the LbL films were analyzed by Static XPS to extract atomic level chemical information due to elemental and chemical state analysis. In order to get further understanding at the molecular level, samples were analyzed under external bias application by Dynamic XPS and it was shown that Ag and Cu respond in the same way to applying external electrical stimuli when both are in the same environment as a result of alloy formation, as reflected by the same shifts in Ag3d and Cu2p binding energy positions. Lastly, in the third part of the study detailed antibacterial analysis of synthesized monometallic and multimetallic nanoparticle solutions and the organized ultra thin polyelectrolyte layers containing Ag and AgCu nanoclusters against *Escherichia coli* strain was performed. These approaches enabled us to show the better antibacterial behavior of AgCu nanoalloys as a result of successful synthesis of AgCu nanoalloy without any copper oxide formation as the end product.

Keywords: Ultra-Thin Film Coatings, Layer-by-Layer Deposition, Ag Nanoparticles, AgCu Metal Nanoalloys, Antibacterial Applications, XPS

ÖZET

ANTİBAKTERİYEL UYGULAMALAR İÇİN GÜMÜŞ-BAKIR NANOALAŞIMLAR İÇEREN VE KATMAN-KATMAN-KAPLAMA YÖNTEMİ İLE HAZIRLANAN ULTRA İNCE FİLMLERİN HAZIRLANMASI VE KARAKTERİZASYONU

Merve TANER CAMCI

Kimya Yüksek Lisans Tezi

Danışman: Prof. Dr. Şefik SÜZER

Haziran, 2012

Bu yüksek lisans tezinin ana amacı, AgCu nanoalaşımlar içeren ve katman-katman-kaplama (KKK) tekniği ile oluşturulmuş ultra ince filmlerin hazırlanması, karakterizasyonu ve antibakteriyel uygulamalarını incelemektir. Bu kapsamda araştırmanın ilk bölümü esas olarak Ag nanoparçacık ve bakır oksit içermeyen AgCu nanoalaşım sentezi, depolama süresince bakır oksit oluşumunun engellenmesi ve Katman-Katman Kaplama yöntemi ile polielektrolit filmlerin hazırlanması üzerine yoğunlaşmaktadır. Bu noktadan hareketle, Ag nanoparçacıkları ve AgCu nanoalaşımlar kompleks yapıcı ajan varlığında, çok güçlü indirgeyici ajanlar olan sodyum borohidrür ve hidrazin hidrat yardımı ile gümüş ve bakır tuzlarının sulu çözeltilerinin indirgenmesi ile sentezlenmiştir. Ayrıca, bu nano boyuttaki ikili alaşımların çözelti fazında kararlığı, üçüncü bir metal olan çinkonun 'sacrificial anode' olarak mevcudiyetinde uzatılabilmiştir. Daha sonra da, önceden sentezlenen Ag ve AgCu nano-

parçacık/alaşım içeren ultra ince polielektrolit filmler Katman-Katman kaplama tekniği kullanılarak farklı kombinasyonlarda inşa edilmiştir. Çalışmanın ikinci kısmında katman-katman-kaplama tekniği kullanılarak hazırlanan ultra ince polielektrolit ve metal nanoparçacık içeren filmlerinin Optik (UV-visible) ve X-ray Fotoelektron Spektroskopi (XPS) teknikleri kullanılarak karakterizasyonu ele alınmıştır. Tek ve bimetalik nanoparçacıklar hakkında optik yanıt ve bilgi alabilmek için, Ag nanoparçacık ve AgCu nanoalaşım dahil edilmiş ultra ince polielektrolit filmleri de optik spektroskopi ile incelenmiştir. Bu noktadan sonra KKK filmleri, elemental ve kimyasal durum analizleri yapılarak atomik düzeyde bilgi elde etmek için 'Statik XPS' metodu ile incelenmiştir. Ayrıca, moleküler düzeyde daha fazla bilgi elde etmek amacıyla numuneler 'Dinamik XPS' yöntemi ile dışarıdan uygulanan elektriksel gerilim altında incelenmiştir. Gümüş ve bakırın nanoalaşım oluşturmasının sonucu olarak aynı yapısal çevrede bulunması halinde dışarıdan gelen elektriksel uyarana aynı şekilde tepki verdiği Ag3d ve Cu2p tepeciklerinin bağlanma enerjilerindeki kaymalarla kanıtlanmıştır. Son olarak, çalışmanın üçüncü bölümde sentezlenen mono-metalik ve multi-metalik nanoparçaçık çözeltilerinin ve Ag ya da AgCu nanopartiküller içeren organize ultra ince polielektrolit katmanlarının, *Escherichia coli* bakterisi oluşumuna karşı detaylı antibakteriyel özellikleri analiz edilmiştir. Bu yaklaşımlar AgCu nanoalaşımların çok daha iyi antibakteriyel özellik gösterdiğini ve bakır oksit içermeyen başarılı bir sentez yolunun antibakteriyel özellik üzerindeki etkisini açıkça ortaya koymaktadır.

Anahtar Kelimeler: Katman-Katman Kaplama, Ultra-İnce Filmler, Ag Nano-Parçacık, AgCu Metal Nano-Alaşımları, Anti-Bakteriyel Uygulamaları, XPS

ACKNOWLEDGEMENTS

Before starting a new academic education and at the end of comprehensively scientific survey throughout last three years as impressive introduction to my academic carrier, I have always been proud of the privilege of work with my supervisor Prof. Dr. Şefik Süzer who taught me "how to swim in the sea". I have my deepest gratitude and respect to him because of his great interaction, guidance and counseling in every stage of my life and scientific study.

I would also like to show my appreciation with my sincere gratefulness to Assist. Prof. Dr. Gülay Ertaş, who supported me during each step of my life for the last six years. I express my thanks to Assoc. Prof. Işık Yuluğ from Molecular Biology and Genetics Department for her cooperation in this research study. I also thank to our past lab group members Hikmet Sezen, EdaYılmaz, Dr. Ivalina Abramova and Chemistry Department members Emine Yigit and Ethem Anber. I never forget my dear friends Müge Artar, Vusala İbrahimova, Gözde Barım, Özlem Ünal and Şeyma Ekiz and express my special thanks to Nilüfer Sayar for her contribution, friendship and support for this scientific study for three years.

I would like to express my thankfulness to my respectable doctor Assoc. Prof. Dr. Selahattin Özmen, who has provided me the medical treatment and enabled me to continue my life and reach these days, and also I thank his team in Gazi University, Faculty of Medicine profoundly.

My inclusive education and scientific research survey in Bilkent University has been most pleasant period of my life with my special family: a father whom I am always proud to be a daughter of him, a mother who devotes her life like an angel with her endless dearness, a sister who always shares each moment of her life and peerless friendship with me and a very special husband who makes every single day of my life special for me with his fabulous love and support.

And I dedicate this thesis to my unborn daughter *Masal Mercan*…

TABLE OF CONTENTS

LIST OF FIGURES

LIST OF TABLES

LIST OF ABBREVATIONS

CFA: Colony Forming Abilities

CFU: Colony Forming Units

DC: Direct Current

DF: Dilution Factor

E.coli: Escherichia coli

LbL: Layer - by -Layer

LB: Langmuir – Blodgett

LB: Luria Broth

MBC: Minimum Bactericidal Concentration

MIC: Minimum Inhibitory Concentration

NAs: Nanoalloys

NPs: Nanoparticles

PAH: Poly (allyamine hydrochloride)

PE: Polyelectrolyte

PEI: Poly (ethyleneimine)

PSS: Poly (sodium 4- styrene- sulfonate)

SAM: Self Assembled Monolayer

SQW: Square wave

OD: Optical Density

UNC: Uncountable

UV- vis: Ultraviolet- Visible

WCA: Water Contact Angle Measurements

XPS: X-ray Photoelectron Spectroscopy

1. INTRODUCTION

1.1. METAL NANOPARTICLES

Metal nanoparticles have been heavily investigated because of their particle characteristics, size dependent properties, easy syntheses and chemical modifications. The metallic nanoparticles are also challenging for functionalization and surface modification. The increased surface-to-volume ratio imparts high reactivity to nano-sized clusters than their bulk counterparts. Accordingly smaller, smart and more efficient materials can be built up as nano-sized particles which behave different than their bulk and atomic forms. On account of the attractive and easily tunable properties of nanoparticles of the metals exhibiting increased photochemical activity, chemical and biological features because of their high surface to volume ratio, nanoparticles have been used in wide range of nano scale applications such as electronics, biology, catalysis, optics and chemical sensing.

1.1.1. Synthesis of Metal Nanoparticles

1.1.1.1. Monometallic Nanoparticles

Nanoparticles of metals can be synthesized from noble and transition metal precursors or even in the form of oxides of transition metals referring to smart materials in the 1nm – 100nm size range. In addition, bimetallic or multi-metallic nanoparticles being composed of combination of two or more metal atoms, have distinct and enhanced properties from their monometallic counterparts.

Preparation of metallic nano-clusters is executed by using a variety of methods such as galvanic exchange reactions, wet-chemical synthesis via assorted reducing agents, electrochemical, photo-reductive, microwave enhanced or biological techniques.[1-9] Rather

than the sophisticated physical synthesis routes, metal nanoparticle synthesis can be regularly carried out via using solution chemistry. The nano-sized particles possess few meter square interface as in form of colloidal solutions, thus facilitate the surface modification in solution in terms of ease in controlling reaction parameters such as temperature, concentration, pH, reducing agent or solvent without the need of expensive or complex equipment. [4, 10-12]

Monometallic nanostructures such as silver-only or copper-only nanoparticles can be synthesized by chemical reduction of silver and copper ions, which are produced by dissolving the salts of silver and copper in aqueous media, with the help of a reducing agent according to various wet-chemical reduction procedures. Reduction takes place with the formation of metal in zero-oxidation state on account of electron uptake of metal ions, then as a next step these reduced-metal atoms migrate and form nanoparticles.

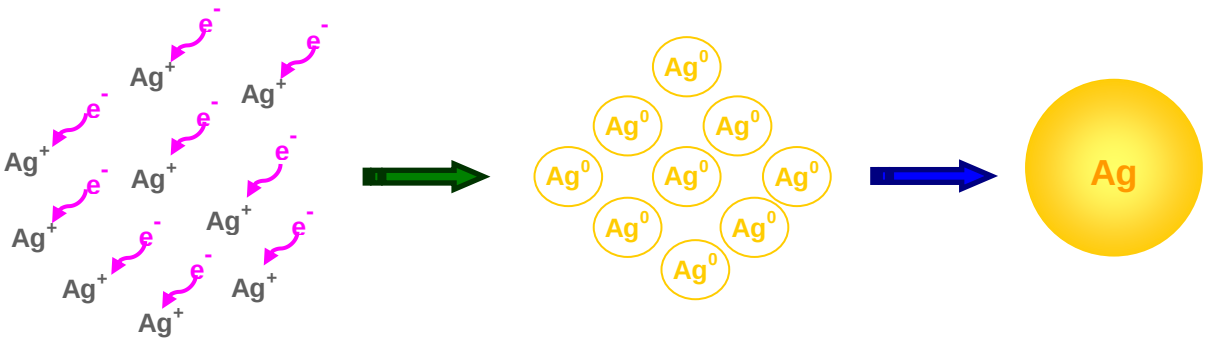

Figure 1. Illustration of silver-only nanoparticles formation after reduction of silver ions (Ag^{+}) to silver atoms (Ag^{0}).

Because of the increased surface-to-volume ratio of the nano-sized materials, their high surface energy and reactivity impose limitations in their shell-life and use in different applications. Naked-nanoparticles are not stable in the absence of any protecting agents. For example naked nano-sized straightforwardly move towards each other causing aggregation and increase in particle size uncontrollably or react with other species in their medium yielding cumulative species with entirely different chemical and physical properties. Therefore, different kinds of stabilizer and / or surfactants are used to prevent particle aggregation, control over particle-size, impart stability to nanoparticles. In the presence of stabilizer and / or surfactants there exists a repulsive force between the capped nanoparticles preventing their attractive migration to each other. Henglein et al. demonstrated the capping of silver nanoparticles by citrate in terms of being an efficient protecting surfactant, furnishing long-term stability to the capped-nanoparticles. Furthermore the size and the structure of silver nanoparticles were controlled in the presence of citrate as capping agent via changing the concentration of this surfactant allowing the diameter dispersion.[13] In order to impart further stability to the highly reactive nanoparticles and prevent nano-sized metal clusters at different oxidation states rather than zero, assortment of techniques are used in association with different kinds of surfactants by virtue of the steric effects, and by keeping nucleation sites of stabilizers and nanoparticles with the help of electrostatic interactions as far as possible, [13-15] chemical and biological protecting agents under different reaction conditions. [11, 16-20]

Highly dispersed metal nanoparticles of uniform size, shape and purity can easily be synthesized in solution by reduction of metal ions that have higher standard reduction potentials whereas species having relatively low reduction potential have a tendency toward contamination with reactive species in the medium, forming non-zero oxidation states. Varghese et al. represented the advance stabilization of Ag nanoparticles using chemisorption

of very strong protecting agent which is an amino acid containing sulphhydryl group (-SH) [19] and found their stabilization with high affinity of metal atoms toward sulfur- containing reagents. [18, 21]

In the presence of suitable complexing, reducing and protecting agents Ag and Au nanoparticles are stable under ambient conditions against oxidation. However for the synthesis of copper nanoparticles, the main handling problem is their high air sensivity, low stability and reactivity of the copper nanoparticles that cause the formation of copper oxide in the end product due its lower standard reduction potential (+0.34V) as compared to Ag (+0.80V) and Au (+1.50V). In the presence of appropriate reducing agents, reduction of Ag or Au is more favorable than Cu as a result of difference between their reduction potentials.

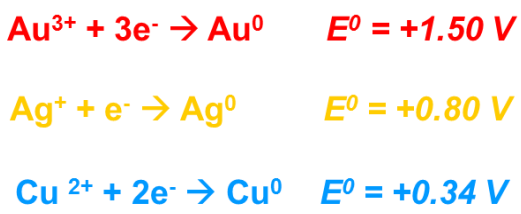

Figure 2. Representation of reduction potentials of gold (Au^{3+}), silver (Ag^{+}) and copper (Cu^{2+}) ions.

Especially for the wet-chemical synthesis under ambient conditions oxidation of copper nanoparticles is nearly inevitable without presence of extremely strong reducing and protecting agents because of the highly reactive oxygen species in air or solution. To suppress the oxidation problem of copper, purging of the reaction media with inert gases, use of non-aqueous media or inert atmosphere, use of very strong reducing and, complexing agents, surfactants, stabilizers are used against copper oxide formation during preparation and/or storage periods.

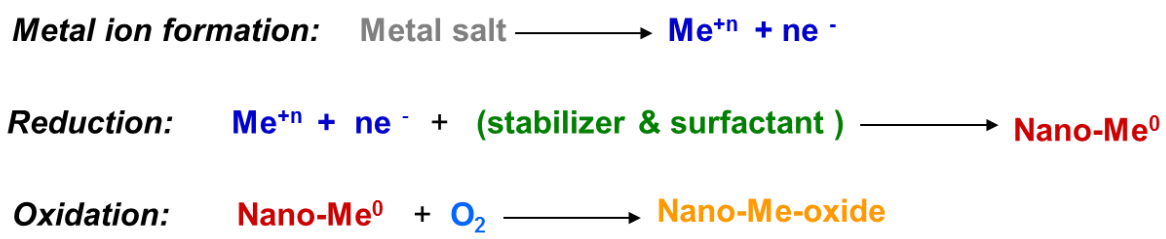

Figure 3. Representation of metal nanoparticle formation by reduction of metal ions and oxide contamination of synthesized nanoparticles.

1.1.1.2. Bimetallic and Multimetallic Nanoparticles

Synthesis of the monometallic nano-sized clusters using different preparation routes have been heavily investigated for many years, whereas metal nanoalloy syntheses have not been so widespread due to handling problems and difficulties in preparation. Bimetallic or multi-metallic nanoclusters can be synthesized by the co-reduction of two or more kinds of metal ions forming nanoalloys sharing the same crystal structure. However, reductive deposition of one kind of metal ion over another reduced metal nucleus results in forming core-shell nanoparticles. [3]

In favor of incorporating two different metals to form nanoalloys, suitable reducing agent which has the capability to reduce both types of the metal ions is used for the reduction of both metal ions to zero valent metals at the same time. Furthermore, as an alternative way to the monometallic counter parts of nano-sized structures, surfactants are utilized in bimetallic nanoclusters synthesis not only for stabilization of nanoclusters but also to bring the reduction potentials of two different metals closer in the direction of co-reduction of these metal ions together. [42]

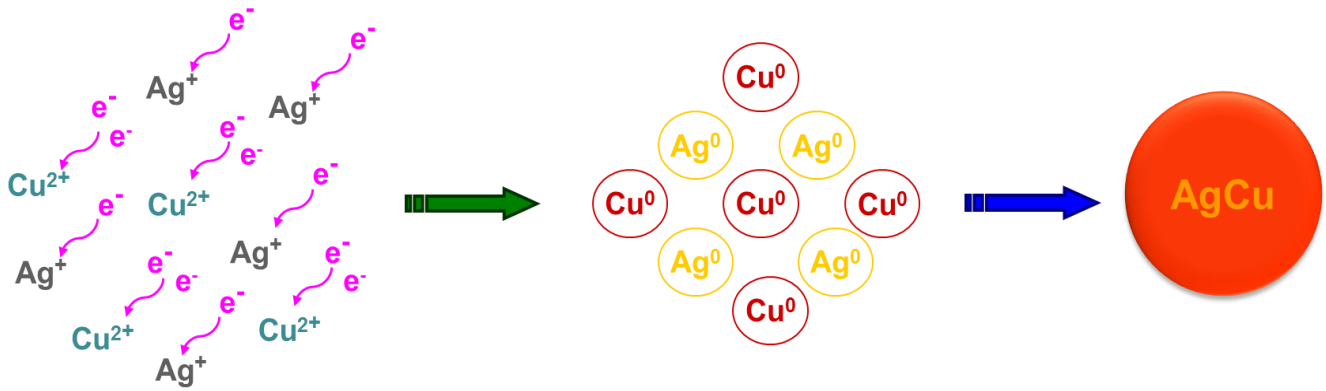

Figure 4. Illustration of silver-copper nanoalloys formation after co-reduction of silver and copper ions (Ag^{+} and Cu^{2+})to silver and copper atoms (Ag^{0} and Cu^{0}).

Also, after the synthesis of monometallic or multimetallic nano-sized clusters with high dispersity and stability, these nanoclusters can be further functionalized by surfactants or capping agents in order to use in various applications. For instance, negatively capped Ag nanoparticles, which are produced by carboxylic group surrounding around zero-valent silver nano-sized metals, can be used to construct ultra thin multilayers as a result of electrostatic attachment of negatively charged nanoparticles in between the positively charged polyelectrolyte layers effectively.

1.1.2. Antibacterial Applications of Metal Nanoparticles

For many years metals such as zinc, gold, silver and copper containing materials have been used for antibacterial applications. While the exact mechanism responsible for antibacterial action is still unknown, these antibacterial metals have the ability to penetrate into bacteria causing cell death or else interact with microbial cell membranes and active proteins as a result of high affinity of transition metals toward sulphur and phosphorus containing proteins that cause enzyme denaturation and deactivation their bacterial activity as a result of interaction between metal and bacteria.[17, 19, 22-29] These antibacterial species show strong and fatal toxic action against prokaryotes including all kinds of bacteria and microorganisms whereas much less toxicity can be omitted for eukaryotes including all other organisms. Thus, as compared to heavy metal ions, nano-sized metal particles show lower toxicity toward humans with remarkably higher antibacterial impact.

Antibacterial activity of these species robustly related with their size and decreases with increasing size, so nano-size metal particles exhibit higher antibacterial activity over their larger colloidal, ionic and bulk counterparts. High surface-to-volume ratio and small size of nanoparticles impart an advantage of close interaction with cell membranes or active sites of the bacteria cells causing deactivation of microbial action. Hence this nanometer-size advantage allows the penetration of nanoparticles through the cell membrane causing cell death. Bacteria cell membranes consist of many sulphur containing proteins, so these sulphur containing parts are privileged sites for transition metal nanoparticles to interact causing disruption of bacterial activity. The infiltrated metal nanoparticles lean towards the interior proteins containing sulphur or phosphorus such as DNA and react with these proteins causing cell death.

Aggregation of nanoparticles is also a crucial problem for antibacterial applications because when the nano-sized particles aggregate they deteriorate their antibacterial properties as a result of increasing size and alteration of chemical and physical properties. Immobilization of antibacterial metal nanoparticles on different kinds of host materials increase the effectiveness of antibacterial application in terms of longer release time and prevented particle aggregation via attachment on supported materials so imparting higher durability.

Subsequently, with recent technological developments and emerging demand for health promoting products, metal particles in nanometer size are suitable candidates for innovative biotechnological applications in industry and hospitals in terms of the desired antimicrobial modification of surfaces and materials to prevent bacterial activity of microorganisms. Advances in coating technology and ability to design intelligent nano-sized materials elicit innovation of antibacterial coatings for broad variety of applications such as in biomedical devices, packaging, textile and cosmetic industries.

Ruparelia and his co-workers [28] studied on bacteria growth profiles in the presence of 3 nm silver and 10 nm copper nanoparticles against various strains of *Staphylococcus aureus, Escherichia coli* and *Bacillus subtilis* bacteria and they showed the superior antibacterial characteristics of silver nanoparticles over oxide-contaminated copper nanoparticles against E. *coli* and S. *aureus* where copper nanoparticles are more effective against B. *subtilis*. In addition, they stated that the combination of Ag and Cu nanoparticles, as physical mixtures, give rise to more effective antibacterial effect against mixed bacteria populations as in real life systems.

Sambhy et al.[23] presented their work on antibacterial composites consisting of embedded AgBr nanoparticles in poly (4-vinyl-N-hexylpyridinium bromide) as cationic polymer matrix and the surfaces coated with these AgBr/polymer nano-composites forming

biofilms on glass microscope slides show antibacterial characteristics toward both Gram negative and Gram positive bacteria. Likewise, they demonstrated the tunable antibacterial properties of the AgBr/polymer nano-composite coating via changing the size of embedded AgBr nanoparticles impart higher antibacterial activity of 10 nm AgBr nanoparticles as compared to 71 nm AgBr nanoparticles to the higher surface-to-volume ratio of smaller nanoparticles.

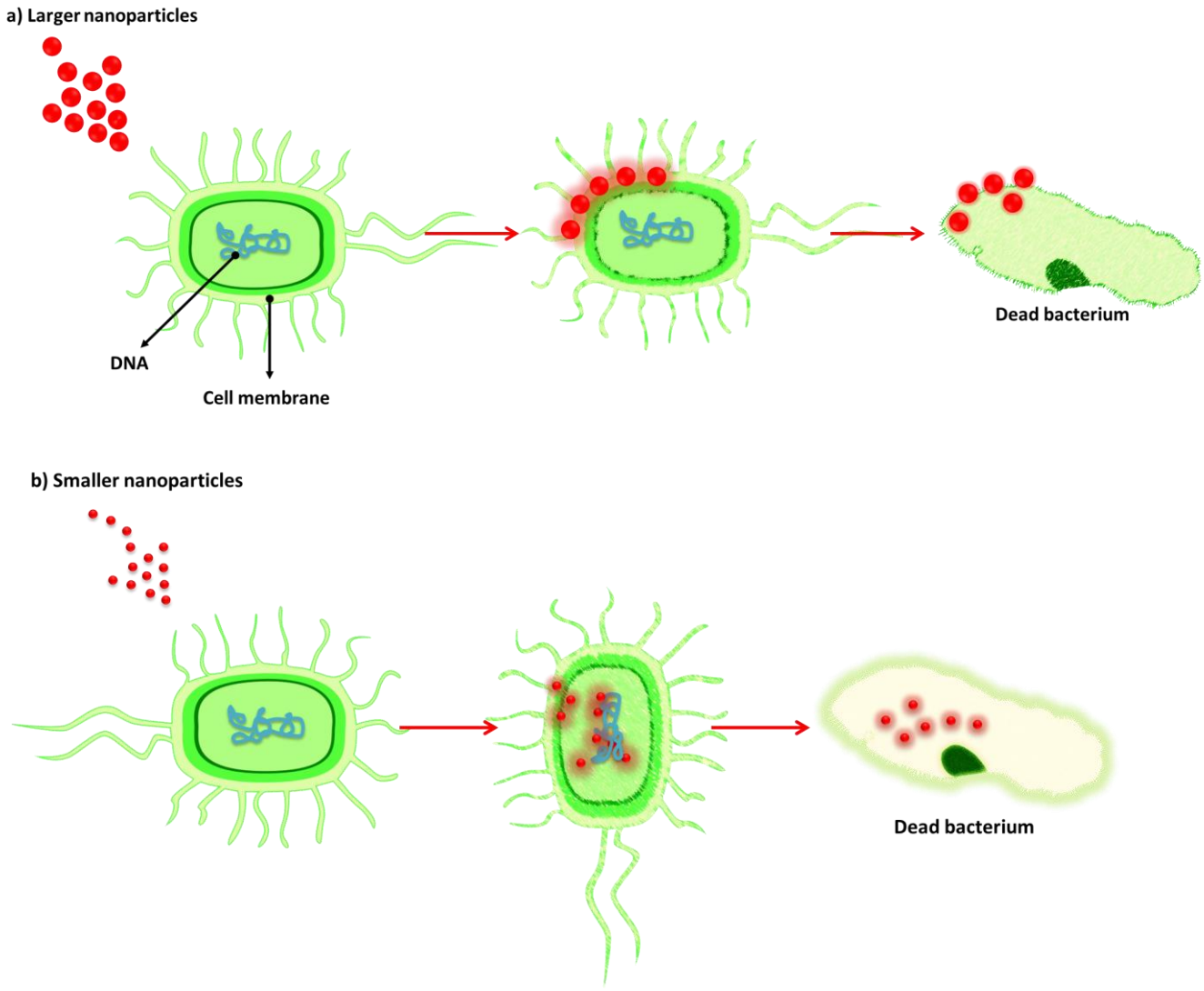

Figure 5. Illustration of antibacterial action of **(a)** larger **(b)** smaller nanoparticles.

1.1.2. LAYER-BY-LAYER ASSEMBLED ULTRA THIN FILMS

Layer-by-Layer assembled PEs multilayer incorporated with antibacterial nanoparticles are ideal materials for studying chemical and physical properties of desired surfaces and interface between these smart surfaces and bacteria cells. LbL deposition technique for this purpose is preferred over other deposition techniques because; it combines inorganic nanoparticles with organic polyelectrolyte layers using `very small amount of materials` and constructs surfaces without any chemical modification of coated polyelectrolytes, metal-nanoclusters or substrate as well as inducing stability during antibacterial applications.

LbL is also applicable to various kinds of materials and can be used to coat the common substrates like glass, with high efficiency. Besides the control of ultra thin layers in nanometer scale is easy because of the tunable parameters such as pH of the medium, temperature, supporting PEs' concentration present during the adsorption process. Ability to control the chemical and physical properties of layer components allows the design of ultra thin films as surface properties of the multilayers can be controlled and modified. In addition, this highly efficient and cheap technique can be carried out at room temperature without requiring vacuum equipment or any kind of special instrumentation for chemical and biological applications.

1.2.1. Layer-By-Layer Assembly

In 1960s, with the help of Langmuir- Blodget (LB) technique[30], which uses the principle of monolayer formation on water-air interface firstly and transfer of the monolayers onto a solid support, Kuhn and co-workers showed that functional units can be formed exhibiting different properties for individual layers in nanoscale.[31] In 1966 a new method was

developed in order to provide alternative technique to limitations of LB technique and Iler had proposed a method that constructs multilayers by using inorganic colloids.[30] Afterward this application was used as basis of multilayer formation process, and in 1990s Decher proposed a method for fabrication of multi composite films depending on electrostatic attraction between oppositely charged polyelectrolyte species. This method is now called the Layer-by-Layer (LbL) assembly that opens a new route potentially leading other new developments.

For the biological and material applications, thin solid films consisting up many different polyelectrolyte layers using the LbL deposition technique provides advanced coatings and smart surfaces with the creation of functional and controllable properties using polyelectrolytes for modification of surfaces. This LbL process assembles the organic polymers with the inorganic nanoparticles combining the unique responses of macro molecules and micro molecules. Also LbL technique imparts unique properties to nano-materials in opposition to the expensive instrumentation, long fabrication period for film preparation, instability of prepared films resulting from weak interactions under ambient conditions and limited number of substrates in LB technique and Self Assembled Multilayers (SAMs).[32] Owing to the fact that, particles are most useful in the form of thin films LbL technique allows the formation of tunable and homogenous films that contain metal nanoparticles rather than the mechanical mixing of nanoparticles and building blocks which may result non-homogenous thin films and unsuccessful coverage of materials with unusual properties of geometry.[33]

1.2.2. Building Blocks of Layer-by-Layer Assembly

The building blocks of the LbL technique are polyelectrolytes (PEs), and it was developed for polyelectrolyte-polyelectrolyte systems because oppositely charged polyelectrolytes have also the complexation ability in multilayer structures.[30] Polyelectrolytes

have been used in analytical and colloidal chemistry which are defined as macromolecular species dissociating into charged polymeric molecules in solution. The multilayers constructed from PEs show indistinguishable properties than each other in terms of multilayer structures due to their high penetration ability in molecular level. [34]

LbL deposition technique is used for consecutive adsorption of oppositely charged polyelectrolytes for constructing multilayer structures and the type of polyelectrolyte which is used for deposition process to form the first layer is an important factor on the stability of the ultra thin multilayer, because the attaching of the whole film to the different substrates is highly dependent of the first layer. When the adsorption of first layer on the substrate is completed, surface charge is inverted by the adsorption of oppositely charged second layer using enough concentration of opposite charges. With the purpose of stabilization of each PE layer, washing process is used after adsorption of monolayer to remove either unreacted or weakly bonded PEs.

In LbL process generally poly (allylaminehydrochloride) (PAH), poly(diallyldimethylammoniumchloride) (PDDA), polyethyleneimine (PEI) are used as the positively charged polyelectrolytes and poly (acrylic acid) (PAA), poly (styrene sulfonate) (PSS), poly (vinyl sulfate) are used as the negatively charged polyelectrolytes, where all polyelectrolytes are broadly available and have enough density of positive or negative charges on their polymer chains for the preparation of multilayers easier.[30-32, 35-37]

Manipulation for improvement of LbL ultra thin layers is related not only with the choice of oppositely charged polymer partner but also parameters such as ionic strength to control the availability and density of ionic charges on polymer chains. In an ionizing solvent, successful deposition of these PEs requires maintenance of electro-neutrality for the neutralization of charge on repeating units of PEs with the help of smaller counter ions which are oppositely charged since macromolecular species such as PEs likely to be in their most

expanded form with higher availability of charges on polymer sides, due to intermolecular repulsions of each charged monomeric unit when ionic strength of solution.[34, 38, 39] Therefore the charges on the monomeric units of PEs are balanced either by oppositely charged PEs or counter ions.

Using LbL approach, to reach the desired multilayer combination after the deposition of charged polyelectrolyte layer, oppositely charged polyelectrolyte layer is deposited. This sequential cyclic process is continued until the desired multilayer configuration is achieved and single monomeric layers can also be easily obtained by adsorption of the positively charged polycation or negatively charged polyanion on charged substrate directly.

LbL deposition technique is available not only for PEs but also any type of common type of charged species. In order to incorporate three dimensional inorganic metallic nanoclusters with various functionalities in the ultra thin PE layers, after the deposition of the charged polyelectrolyte layers, the charged metallic nanoclusters are deposited imparting a net negative charge to the nanoclusters requires oppositely charged polyelectrolyte partner for LbL assembly constructing nano scale functional ultra thin films consisting of organic and inorganic layers.[40-44] Also by the use of colloidal nanoclusters three dimensional construction of these ultra thin films basically uses the irreversible strong electrostatic forces between charged PE layers and the required – oppositely charged nanoclusters partners as driving force for stable film assembly but also multiple intermolecular interactions such as hydrogen bonding [37, 41, 45], hydrophobic interaction [46] and charge transfer [47] cooperatively contributes to the formation so as the stability of the films.

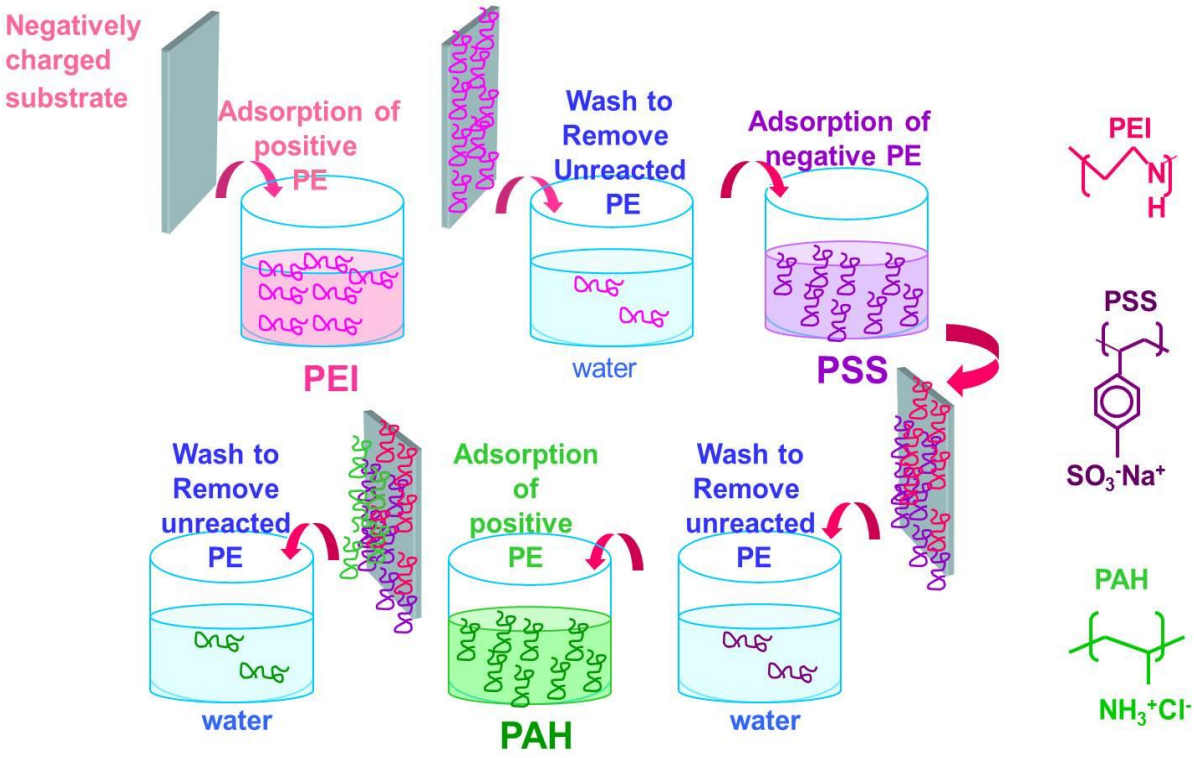

Figure 6. Schematic representation of polyelectrolyte adsorption on negatively charged substrate showing molecular structures for commonly used polyelectrolytes: Polyethyleneimine (PEI), Poly(styrene sulfonate) (PSS) and Poly(allylaminehydrochloride) (PAH).

The thickness of polymer layer is related to both the amount of polyelectrolyte and the nature of polyelectrolyte and the films can be constructed by LbL deposition at the molecular level. Also, the nanoscale control over thickness of adsorbed thin layers related to the dipping time of the substrate in PEs' aqueous solution on account of improvement in the amount of adsorbed charged polyelectrolyte chains.[48] As very important parameter for nano scale precision thickness of single bilayer consisting of one positively charged and one negatively charged layer is in the range of 1nm- 5nm allowing the nanometer scale control for thickness of these layers.[32, 49]

1.2.3. Design of Antibacterial Ultra Thin Polyelectrolyte Layers Using Layer-by-Layer Assembly

Surface modification has been advocated for better controlling of the interactions between bacteria and substrate inducing biochemical death of bacteria in consequence of interaction with antibacterial functional groups [50-52] and propagation of antibacterial compounds over time from material surface to bacteria with respect to releasing ability of antibacterial agents from polymer multilayers.[17, 32, 53-55]

Both Gram negative bacteria, having single peptidoglycan layer between lipopolysaccharide rich layers, and Gram positive bacteria, having multilayered peptidoglycan cell at outermost layer, are susceptible for the antibacterial activity control of nanoparticle loaded multilayer thin films.[54, 55] Additionally, ultra thin antibacterial layers can be studied in terms of their effectiveness by different kinds of methods as well as counting the number of bacteria after a certain incubation time, antibacterial drop test, determination of colony forming units, following the optical density at 600nm referring to the bacteria number in aqueous medium after definite incubation time or disk-diffusion (Kirby- Bauer) test.[26, 28, 54-59]

Polyelectrolyte multilayers provide numerous opportunities to design intelligent surfaces with nanostructures to explore antibacterial characteristics combined with chemical properties for biotechnological applications. Incorporation of antimicrobial metal nanoparticles with charged PEs via immobilization on to the various types of materials for antibacterial applications in this intelligent ultra thin surface construction is effectively used for antibacterial purposes.[26, 42, 55, 60-62] With the use nanoparticles with charged polymers these ultra thin layers achieve high reactivity as a result of large interface area between nanoparticles and PEs. [17, 22] These immobilized antibacterial nanostructures reveal long term stability and are much more environment friendly. The surface density and arrangement of the resulting antibacterial PE thin layers are controlled by different number of antibacterial

reagent-PEs dipping cycles and time. As a function of nanoparticle containing thin layer thickness and nanoparticle density, the effectiveness of the layers can be controlled for antibacterial purposes.[55, 60, 63]

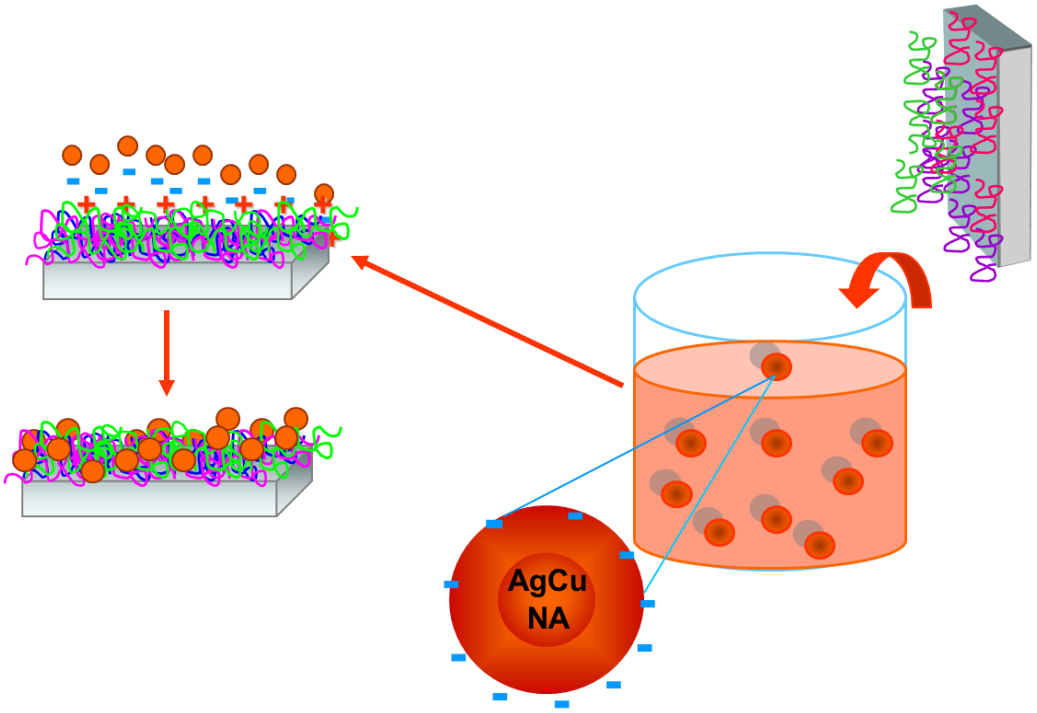

Figure 7. Schematic representation of metal-nanoalloy/polyelectrolyte ultra thin film construction with adsorption of negatively capped AgCu NAs on PEI/PSS/PAH polyelectrolyte layers via LbL assembly.

1.3. CHARACTERIZATION TECHNIQUES

1.3.1. UV-visible Spectroscopy

For the characterization of the nanoparticles NMR, IR, Raman, UV-Visible and X-ray Photoelectron Spectroscopy, AFM, SEM, TEM, and XRD diffraction are the commonly used techniques. Unfortunately, the most common techniques used by chemist like Infrared or Nuclear Magnetic Resonance cannot be used for the characterization of ultra thin layers containing metal nanoclusters because of their lack of sensivity.

UV-visible spectroscopy, that gives important informations for samples, is the most commonly used optical technique because it is easy in application and cheaper than other techniques. UV-visible spectroscopy records the absorption spectrum in ultraviolet and visible region in electromagnetic radiation containing electronic transition in molecular orbitals from ground state to excited state in terms of absorbed light at different wavelengths. This technique is also used for determination of different properties such as average particle size, shape, concentration and composition of metal nanoparticles.

In this work, UV-visible spectroscopy is used to characterize both the nanoparticles which are prepared by chemical reduction via solution chemistry, and the nanoalloys embedded into the ultra thin multi-layers which are prepared by LbL assembly.

1.3.1.1 Optical Response of Metal Nanoparticles

Metal nanoparticles exhibit strong plasmon resonance (SPR) extinction band in the visible spectrum as a consequence of interaction between conduction electrons of metal nanoparticles and incident electromagnetic radiations.[4] SPR band is the outcome of resonance frequency as a result of restoring force to compensate polarization that is generated by

electron motion in phase for the particles having much smaller size than wavelengths of incident light. [4]

Particles which have smaller diameter than 3 nm do not exhibit significant surface plasmon absorption covering visible region unless the particle size becomes higher than 5 nm surface plasmon bands broaden where the dimensions of the nanoparticles are comparable with the wavelength of interacting light.[4, 64] The metal particles of silver and gold show distinct and well-defined plasmon absorption in the visible region exhibiting drastic color effects due to the surface plasmon absorption in the metal nanoparticles, as a result of the collective oscillations of the free conduction electrons.[65] For the bimetallic nanoclusters, in case of nanoalloys where the particles of two metals distributed homogenously, position of surface plasmon band lies between two distinct absorption bands of single metal nanoparticles.[64, 66] Alternatively for the core-shell bimetallic nanoclusters, surface plasmon absorption is mainly determined by absorption of the metal at the shell as a result of alternating oscillation mode of surface conduction electrons.[67] In addition, since resonance wavelength depends on the orientation of the electrical fields and the oscillation modes of the shape of the nanoclusters, optical properties also change as shape of the nanoclusters change.[7]

Silver nanoparticle existence can easily be detected with their optical spectra with a characteristic peak around 390-400nm.[68] However, characterization of copper as nanoparticle or in nanoalloy cannot be directly observed with their UV-visible spectra, because the surface plasmon band for copper nanoparticles is not in the UV-visible region and the oxidative property of copper makes plasmon frequency determination in this region harder. In order to prove the existence of copper nanoparticles by UV-visible optical spectra, indirect characterization techniques are used such as controlling the decrease in the broad absorption band of the cupric ions in the solutions with the addition of reducing agent to the reaction media.[69, 70] What is more, absence of copper plasmon peak in UV-visible region depends on

the small cluster size with high dispersity of nanoparticles whereas the silver nanoparticle surface plasmon peak is much more intense as it can be detectable as compared to copper nanoparticle counterparts. [16, 71, 72]

For the optical characterization of co-reduced silver and copper nanoparticles from the metal salts of silver and copper in aqueous media, silver in silver-copper alloy nanoparticles can be detected by the broadening of the peak in absorption spectrum towards 410 nm-450 nm, which has a different position than the characteristic Ag nanoparticle peak, as a result of the Cu and Ag interaction and alloy formation. Thus the red shift in the Ag-Cu nanoalloy optical spectrum to the higher wavelengths and the broadening in the absorption spectrum is a proof of the existence of the silver and copper together in the nanoalloy.

1.3.1.2. Optical Response of LbL Films Containing Metal Nanoparticles

Layer-by-layer assembly allows the nano-scale organization of nanoparticles and the thickness via alternating adsorption of the optically active nanoclusters and polymeric electrolytes resulting ultra thin film formation.[33, 37] Tunable properties of metal nanoparticle-polyelectrolyte films at the molecular level give opportunity for tunable optical properties. Red-shift is expected in the absorption spectrum of these particles since introduction of the nanoclusters into an organic matrix with different dielectric constant affect the dipolar-dipolar interactions resulting surface plasmon resonance shifts to different position in their spectrum.[49, 67]

Nanoclusters are not only subjected to the dipolar interaction of the nanoclusters with their matrix and adjacent layer but also the interparticle distance between nanoclusters and embedding matrix have effect on the optical properties of ultra-thin polyelectrolyte layers.

In view of the fact that measured absorbance is directly related with the concentration of the nanoparticles absorbing species due to Beert-Lambert law, which defines absorption at specific wavelength (A) as multiplication of extinction coefficient (ε), path length (b) and the concentration of absorbing species (c), there exists a significant decrease at the intensity of absorbance in the optical spectrum of LbL deposited metal nanoclusters films and this can be clarified by the fact that LbL assembly uses very small amounts of materials to construct ultra thin films. Besides as the number of nanoclusters-polyelectrolyte layers increases, absorbance in the optical spectrum also increases with respect to the deposited bilayer on the substrate indicating the uniform assembly and distribution of the nanoclusters in each bilayer.[37]

1.3.2. X-ray Photoelectron Spectroscopy

X-ray Photoelectron Spectroscopy (XPS) which is used for surface analysis of materials is one of the most common techniques for characterization of nano-particles which are obtained by layer-by-layer deposition on polyelectrolyte multilayers. This non-destructive technique gives valuable quantitative and qualitative information about the surfaces with high precision and sensivity. As being a powerful technique for surface analysis, XPS has ability to give chemical information and high surface sensitivity for thin films, solids and nano clusters.[73, 74]

1.3.2.1. Basic Principles of XPS

XPS is based on the kinetic energy determination of emitted photoelectrons of the sample under radiation with highly energetic X-rays. X-rays of the photon source are directed to the analysis sample and photoelectrons are emitted from the sample. Generally conventional XPS instruments work with photon energies of 1486.6 eV for Al Kα and 1253.6 eV for Mg Kα. Electron analyzer collects the emitted photoelectrons and analyze their kinetic energies. Ultra high vacuum conditions are necessary to increase the probability of emitted photoelectron to reach the electron energy analyzer where only the escaped photoelectrons can arrive at the detector.[75] Binding energies of emitted photoelectrons are determined by the theory of conservation of energy [73-77] using following Einstein relation:

$$BE = h\nu - KE - \Phi$$

where BE is the binding energy of emitted photoelectrons, hν is the incident photon energy of X-rays, KE is the measured kinetic energy of the analyzed photoelectrons and Φ is the work function of spectrophotometer in terms of minimum energy required to eject one electron

from the Fermi level of the solid matrix to the vacuum level. Each spectrometer has its own characteristic work function and electronic behavior and this work function correction in binding energy eliminates the errors coming from spectrometer. After kinetic energy determination of the emitted photoelectrons by analyzer, spectrum of the photoelectron peaks in terms of their corresponding binding energies is obtained.

Ejection of electrons by X-rays during the measurements generates a positive charge on the surface of the sample as photoelectron flow toward electron analyzer. In case of conductive materials, generated positive charge is compensated by the electron flow from the ground, whereas non-conductive, poor conductive or not grounded materials cannot compensate this generated charge on the surface of the sample and cause shifts and drifts in the binding energy peak positions. Therefore, flood gun which supplies flow of low energy electrons to the sample surface is used to eliminate these generated positive charges and the unwanted shifts in the binding energies.

From the binding energies of the photoelectron peaks, XPS spectrum gives characteristic and element specific information about the sample. Binding energies are robustly specific to each atom and give distinctive information about corresponding atoms and elements except for hydrogen and helium. Chemically specific XPS not only allows the determination of type of atoms on the surface but also give information about chemical states and type of atomic orbitals where photoelectron is ejected such as s, p, d or f with respect to binding energies. In addition to qualitative analysis via XPS, quantitative analysis can be performed by calculating relative atomic ratios of the surface with the help of intensity of peaks and the monitored area of corresponding photoelectron peaks in the XPS spectrum.[78, 79] This property enables the determination of the stoichiometry between elements of the sample.

The chemical and physical information of the sample can be collected from about few outermost atomic layers of the sample's surface by XPS. X-rays have the ability to penetrate micron-depth through the sample but information can only be collected from 10-20 nm probe length. Emitted photoelectrons cannot travel micron-depth distances through the sample without any loss in their kinetic energy; accordingly due to the energy loss as a result of inelastic collisions between emitted photoelectron and other atoms in traveled-solid ejected photoelectron can only result from the outermost 10-20nm depth. This short probe length is material specific and is determined by the inelastic mean-free path (λ), which is defined as the distance traveled by ejected photoelectron without loosing its energy when intensity reduced to value 1/e factor of the its initial intensity, also enables the high surface sensitive investigations for nano-sized structures and thin films.[74, 76]

1.3.2.2. Static and Dynamic XPS Measurements

Flow of X-rays generated photoelectrons from sample to the vacuum generates a current during XPS measurements. This current for conductive and grounded samples, is the result of the withdrawn electrons from the ground. Also, in the presence of extra electrons from flood gun current is altered. XPS studies which are performed with a grounded sample system under no additional or external electron sources to control surface charging other than the flood gun are called "Static XPS Measurements". In another application, the degree and the sign of the surface charging is controlled by an external bias applied to the sample, the charging of the sample during photoemission process is controlled, which is an essential tool to obtain additional information about the sample. The XPS studies regarding charging as a tool under use of a time varying external bias are called as "Dynamic XPS Measurements".[80-85] Figure 8 depicts the schematic representation of the Static and Dynamic XPS measurements.

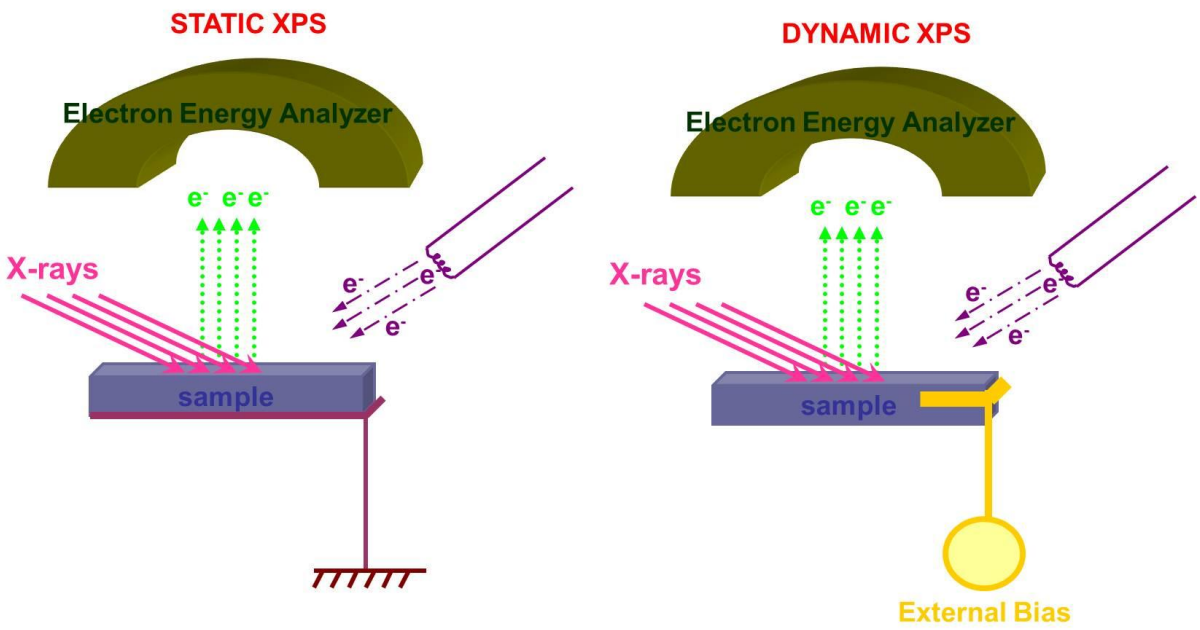

Figure 8. Schematic representation of XPS measurements using Static XPS and Dynamic XPS techniques.

Applying external DC voltage stress to the sample is one of the ways to use surface charging as a tool at various voltages. For conductive materials positions of the photoelectron peaks are displaced by application of either positive or negative external bias potential as much as the bias applied in a linear fashion. For non-conductive or poorly-conductive materials this behavior is non-linear. For example, if +10V is applied to the conductive sample, photoelectron peaks will shift towards higher binding energy positions by exactly 10 eV. On the other hand, application of same +10V to non-conductive material results shifts in binding energies smaller than 10 eV because of the created positive potential on the non-conductive material surface. If -10V is applied to the conductive material, negative surface charge accumulates on the surface of sample so electrons are repelled from the surface and the peak positions shift toward lower binding energies. Again for the case of non-conductive materials the overall shift as a result of negative voltage application is smaller than 10 eV

because of a shift toward higher binding energies due to positive charge accumulation on the surface.

In order to extract additional information, application of external square wave (SQW) pulses to the sample under analysis is an alternative way to utilize surface charging as a tool. SQW pulses can be described as alternating potentials at a given frequency and potential, so application of SQW pulses enables the use of response time via alternating potentials with different time intervals. Amplitude of the pulses is generally +10V / -10V while the frequency of pulses ranges in 10^{5} to 10^{-3} Hz for the sample under investigation. Application of positive and negative voltages leads the splitting of the binding energy peak into two peaks at a given frequency toward higher and lower binding energies respectively. Similar to the DC voltage stress results, if the sample is non-charging exactly 20 eV difference is observed between two splitted peaks' binding energies but with the increasing charging phenomena the binding energy difference decreases. As well as external DC voltage application facilitates the extracting information on extent of surface charging, SQW pulse application allows getting additional information about the degree of the response of sample to the potential changes in the applied frequency range, giving enough time for the sample to build up surface charging. In short either external DC stress or SQW pulse application are new tool to control surface charging and extract additional information from charging of the samples, DC stress furnishes information on resistance of the sample whereas SQW pulse furnishes information on both resistance and capacitance.

1.3.2.3. Application of XPS to Metal Nanoparticle Incorporated Ultra Thin Polyelectrolyte Multilayers

XPS that give valuable information in elemental identification, composition and chemical state depending on the characteristic binding energies is an essential tool for the investigation of metal nanoparticles and metal nanoparticle embedded ultra thin polyelectrolyte multilayers. For metal nanoparticles, besides the elemental analysis successful synthesis of the nano-structures is followed by the specific binding energies of the elements in their zero-oxidation state. Additionally, the successful nanoalloy synthesis can be analyzed by XPS without the need for electron microscopy. If the reduced nano-sized metal particles of different metals are in the same chemical structure forming nanoalloys, the binding energy shifts in the XPS spectra of different regions such as Ag3d and Cu2p for AgCu nanoalloys under external DC bias or SQW pulses are expected to be equivalent as a result of the response coming from the same domains where non-equivalent binding energy shifts are expected for the non-uniform or core-shell structured nano-sized particles.

Also the reduction level to determine the ratio of reduced / non-reduced species can be followed by the characteristic binding energies of the elements at different oxidation states and peak shape analysis in their XPS spectra.[86-88] Especially, in the case of copper nanoparticles shake up satellites and the peak-shape analysis in the spectrum of Cu2p region, precisely determine the oxidation state of copper whether at zero-one or two and the formation of different kinds of copper-oxide species such as CuO or Cu_2O.[89, 90]

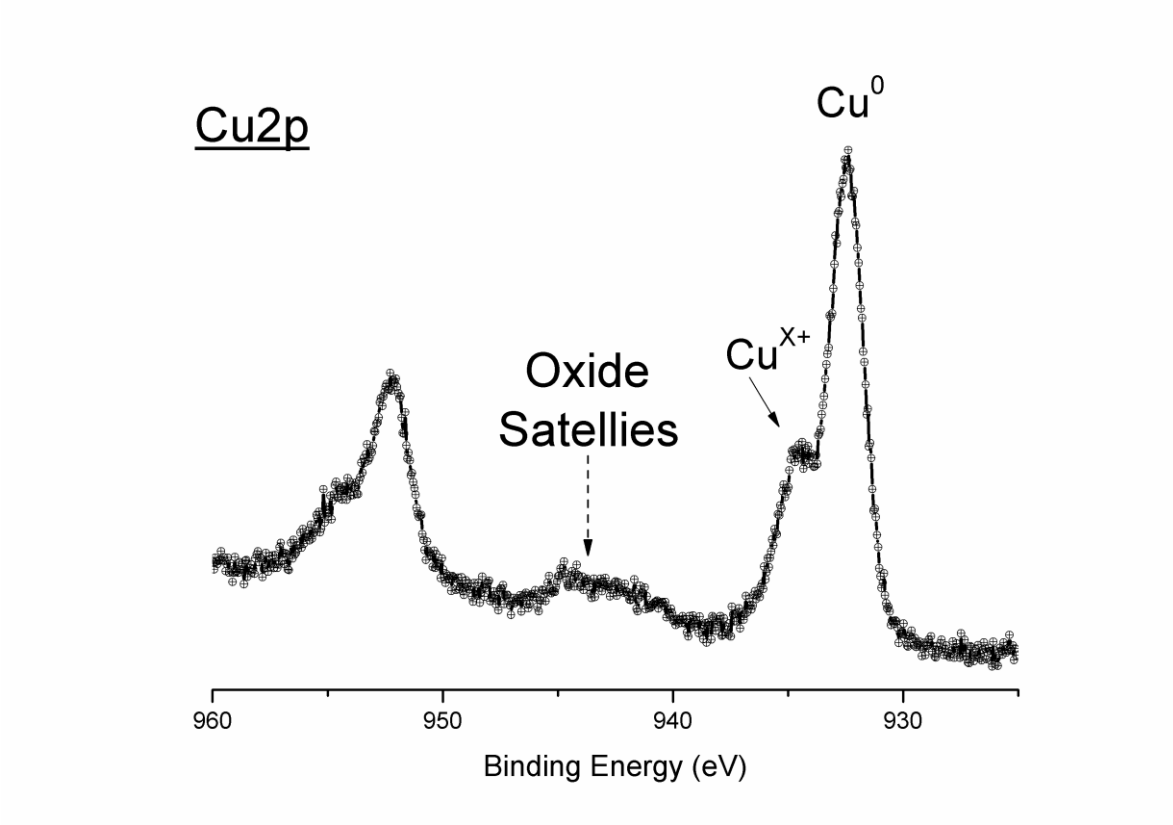

Figure 9. Cu2p region of XPS spectrum showing zero-valent Cu ^{0}, Cu $^{x+}$ peaks and copper-oxide satellites.

Construction of ultra thin multilayers containing metal nanoparticles can be monitored directly by XPS. Since adsorption of each polyelectrolyte layers can be screened by the elemental analysis of XPS spectra of constructed films corresponding specific elements of the construction materials. Conger et al. represented their XPS analysis on polyelectrolyte multilayers on SiO_2 / Si substrate and proved the adsorption of positively charged polyelectrolyte PAH (Poly (ally amine hydrochloride)) with the presence of N1s peak and the adsorption of negatively charged PSS (Poly (styrene sulfonate)) with the presence of S2p peak in XPS spectrum of layer-by-layer assembled bilayer system.[82] Furthermore, incorporation of the metal nanoparticles in ultra thin polyelectrolyte layers can be attested by the characteristic spin orbit splittings of metals such as Au4f or Ag3d corresponding to the presence of gold and silver nanoparticles on LbL multilayers respectively. The thickness of each adsorbed

polyelectrolyte layers can also be determined by using the proper relationships of the electron attenuation of XPS signals or analysis of collected spectra at grazing angles.[82, 91, 92]

More to the point of XPS studies on nanoparticles, Chen et al. presented the size-controlled synthesis of copper nanoparticles and comparison of Cu nanoparticles, Cu fibers and polycrystalline Cu in terms of size effect using core-level XPS spectra of Cu2p region.[93] Formation of nanoparticles is confirmed by XPS and by comparing binding energies in the core-level spectra of nanoparticles, fibers and polycrystalline they demonstrate the size effect with the light of information of that as the particle size reduces to nano scale, the core-level binding energy shifts to larger values as compared with that of bulk one.

Above and beyond of qualitative analysis, quantitative analysis can be performed by XPS investigations by means of combining monitored peak areas of corresponding XPS peaks with cross-sections of the interested orbitals and determined kinetic energies. In the light of recorded peak intensities so as the peak areas, stoichiometry between functional groups, surface atomic concentration of polyelectrolyte multilayers and the atomic ratios of elements or species are determined and constructed thin films can be developed for further applications.[79, 94-96]

1.4. AIM OF THE STUDY

This thesis focuses on three main objectives: (i) synthesis of silver nanoparticles and silver-copper nanoalloys, and preparation of ultra thin polyelectrolyte layers via incorporation of synthesized nanoclusters into the layer-by-layer assembled polyelectrolyte multilayers, (ii) characterization of metal nanoclusters and the metal nanoclusters/polyelectrolyte ultra thin films using different spectroscopic techniques, and (iii) antibacterial investigation of synthesized nanoclusters solutions and nanoclusters containing ultra thin polyelectrolyte multilayers.

In the first part of the study, preparation of ultra thin polyelectrolyte multilayers containing silver and silver-copper nanoclusters will be discussed. This part includes the wet-chemical synthesis of silver-only nanoparticles and silver-copper nanoalloys using different chemical procedures with different reagents for stable nanoclusters formation in details.

Second part focuses on primarily the characterization of synthesized nanoparticle and nanoalloys solution using UV-visible absorption spectroscopy and X-ray photoelectron spectroscopy and then the characterization of metal nanoclusters incorporated ultra thin polyelectrolyte layers by both optical and X-ray photoelectron spectroscopy. Also, investigation of response of ultra thin multilayers under external stimulus during XPS measurements will be discussed.

The last part of the study discusses the antibacterial properties of Ag-only and AgCu nanoalloys solutions following colony forming abilities and optical density changes against Gram negative bacteria *Escherichia coli.* Additionally, antibacterial effects of layer-by-layer assembled ultra thin films containing these metal nanoclusters will be discussed.

2. EXPERIMENTAL

2.1. MATERIALS

The water used in all experiments was prepared in a three-stage Millipore Milli-Q Synergy 185 purification system. Glasses that are used for LbL deposition were obtained from ISOLAB Microscope Slides. Sodium chloride (NaCl), sodium hydroxide (NaOH), zinc nitrate hexahydrate ($Zn(NO_3)_2.6H_2O$), hydrazine hydrate (HH) and formaldehyde (CH_2O) were purchased from Merck. Sodium borohydride was obtained from BDH chemicals and silver nitrate ($AgNO_3$) and L-cystein ($C_3H_7NO_2S$) were purchased from Fluka. Poly (allylaminehydrochloride) (PAH), polyethyleneimine (PEI), poly (styrene sulfonate) (PSS), polyvinylpyrrolidone (PVP), sodium citrate dihydrate ($C_6H_5O_7 \cdot 2H_2O \cdot 3Na$) and copper (II) acetate monohydrate ($C_4H_6CuO_4.H_2O$) were purchased from Sigma-Aldrich.

2.2. INSTRUMENTATIONS

For contact angle measurements Tantec Contact Angle Meter was used. Double Beam Thermo Scientific Evolution 160 UV-visible Spectrophotometer was used for the optical characterization of nanoparticles, nanoalloys and LbL films. Measurements were obtained acquiring absorbance spectrum of nanoparticles, nanoalloys and LbL films between 300 nm and 700 nm with scanning rate 100 nm/min. The optical measurements were performed against reference samples: deionized water which was the solvent for all synthesis processes of solutions' characterization and identical clean glass substate except NPs and NAs for LbL samples. For the purpose of spectrum aquisiton, the sample cuvettes and glass microscope slides were directly placed in the path of light between light source and detector.

XPS measurements were performed by AlKα Thermo Scientific K-Alpha X-ray Photoelectron Spectrometer with monochromotized photon energy 1486.68eV. Samples were

analyzed under X-rays with 45° angle and analyzer with 90° with respect to the surface of sample plane. The sample holder can be connected to either ground or power supply. Static XPS was used when sample was connected to the ground while recording the spectra. Dynamic XPS measurements were performed under external bias through a power supply with DC bias or SQW pulses connected to isolated sample holder while monitoring the changes during charging process. DS340 Synthesized Function Generator obtained from Stanford Research Systems was used for DC bias and SQW pulses generation.

The sample holder that was used for the dynamic XPS measurement is modified for external bias applications. Samples were placed on a rotatable sample holder and for the bias connection gold foil, as a very good conductor, was assembled on the top of the samples. In order to get the bias connection, sample holder was turned in the anti-clockwise direction until a gold wire touched to isolated edge of the sample holder which was also connected to the function generator.

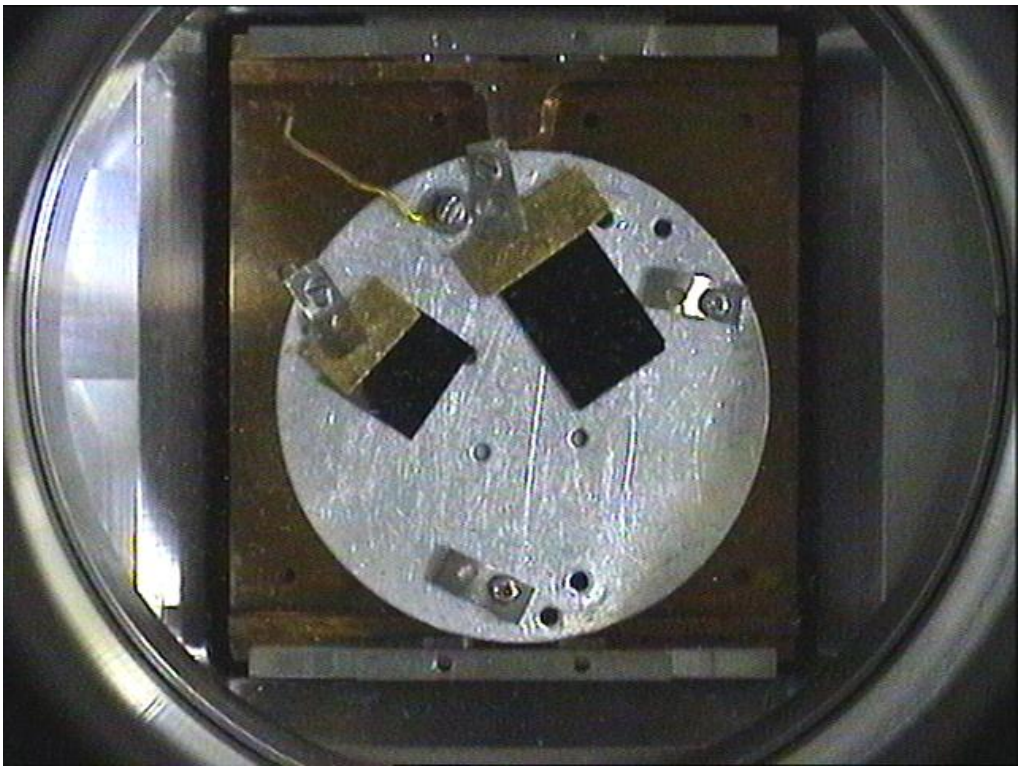

Figure 10. Representative image of rotatable sample holder used in Dynamic XPS measurements.

2.3. PROCEDURES

2.3.1. Synthesis of Ag Nanoparticles

98ml of 0.3 mM of sodium citrate dihydrate solution is cooled for 30 min and mixed with 1 ml of 1 mM of sodium borohydride solution. 1 ml of ice-cold 0.01 M $AgNO_3$ solution is drop wise and very slowly added to the reaction solution under vigorous stirring. Color change into bright yellow indicates the formation of nearly 10 nm Ag nanoparticles and the absorbance at 400 nm in UV-vis. Spectrum of the synthesized solution confirms successful Ag nanoparticle synthesis.

2.3.2. Synthesis of AgCu Nanoalloys

0.5 ml of each 0.01 M silver nitrate and 0.01 M copper acetate solutions are mixed and ultrasonicated for 2 min. 1ml mixture of Ag and Cu metal salt solutions are drop wise added to a mixture of 2 ml 0.01M cystein and 2 ml 0.01 M NaOH solution very slowly. After the formation of reaction mixture containing metal salts, this prepared solution is drop wise added to another solution mixture of 45ml of 1.1 mM solution of sodium citrate and 5ml of 0.4 mM solution of hydrazine hydrate. The reaction is allowed for 30 min under vigorous stirring as slow color change to dark wine-brown indicates the formation of AgCu nanoalloys in the solution. UV-vis optical spectrum gives broad peak between 420 nm and 450 nm.

2.3.3. Synthesis of AgCu-Zn Nanoalloys

0.5 ml of each 0.01 M silver nitrate, 0.01 M copper acetate and $4x10^{-4}$ M zinc nitrate solutions are mixed and ultrasonicated for 2 min. 1.5 ml of metal salt solution drop wise added to first reaction mixture of 2 ml 0.01M cystein and 2 ml 0.01 M NaOH solution and this solution drop wise added to second reaction mixture of 45ml of 1.1 mM solution of

sodium citrate and 5ml of 0.4 mM solution of hydrazine hydrate. After allowing reaction for 30min color change into dark wine-brown indicates the formation of AgCu-Zn ternary nanoalloys.

2.3.4. Preparation of Ultra Thin Polyelectrolyte Layers

To construct polyelectrolyte multilayers poly (allylamine hydrochloride) (PAH), polyethyleneimine (PEI) were used as positively charged polyelectrolytes and poly (styrene sulfonate) (PSS) was used as negatively charged polyelectrolyte. Glass microscope slides and silicon wafers were used as support materials for ultra thin construction. Negatively charged glass substrates were obtained by nearly 1 hour immersion in fresh piranha solution. In case of HF – cleaned Si (100) substrates, firstly silicon wafers were cleaned by 2 min immersion into HF solution to dispose native oxide layer onto substrates and other chemically bonded organic/inorganic contaminants and then thin oxide layer on Si (100) surface was grown by thermal treatment at 700°C for 3hours followed by dipping into the 0.1M NaOH solution.

The first layer of ultra thin films was constructed by dipping the negatively charged substrates into 1 g/l PEI solution, which renders preparation of multilayers easier as a result of high density of positive charges per unit length of the polyelectrolyte, for 40 min. Further adsorption procedure was performed from sequential dipping into 0.15 M NaCl solution with an amount of separate 1 g/l PSS and 1 g/l PAH solutions respectively. Each polyelectrolyte adsorption period has lasted 40min and followed by washing process. Desired number of multilayers can be obtained by sequential adsorption of PSS and PAH layers via dipping into polyelectrolyte solutions in an alternate fashion. Besides, different dipping periods (10 min – 40 min) and different polyelectrolyte concentrations (0.5 g/l – 2.0 g/l) were tried to obtain optimum dipping time and concentration. All films were dried under flow of nitrogen gas after adsorption processes were completed.

2.3.5. Preparation of Metal Nanoparticle Inserted Ultra Thin Polyelectrolyte Layers

Synthesis of Ag nanoparticles and AgCu nanoalloys yield negatively charged metal nano-particles/alloys as a result of citrate capping. Polyelectrolyte-metal films are prepared in the same way with polyelectrolyte multilayers. After the deposition of desired number of PEI-$(PSS\text{-}PAH)_x$ layers on negatively charged microscope slides or silicon substrates, adsorption was followed with dipping into pre-prepared nano-particle/alloy solutions. Also alternating deposition enables the adsorption of positively charge polyelectrolyte layer on top of the nano-particle/alloy layer; subsequently as many layers of nano-particle/alloys as needed can be constructed with the help of sequential adsorption of metal and polyelectrolyte layers.

2.3.6. Antibacterial Activity Tests

Antibacterial analysis of Ag nanoparticles and AgCu nanoalloys were performed against Gram-positive *Escherichia coli* DH5-alpha strain for different experiments. Luria-Bertani (LB) broth, which is a liquid media for propagation of *Escherichia coli* strains, was used for all of the experiments.

For different sets of experiments at the beginning of each set, E.*coli* colonies were grown in 10 ml liquid LB medium at 37°C with constant agitation at 225 rpm to minimize any possible settlement and aggregation during incubation. The change in optical density at 600 nm wavelength was determined by a Beckman DU 640 Spectrophotometer to follow the bacteria cell growth. All controllable parameters such as concentration, incubation time, incubation and application conditions, and bacteria suspensions were exactly the same for Ag-only NPs, AgCu NAs and their different concentrations.

2.3.6.1. Antibacterial Investigation of Ag Nanoparticles – AgCu Nanoalloys Inserted Agar Plates

E.coli DH5α strain has been grown to known optical densities of 0.05 OD, 0.1 OD and 0.2 OD in addition to control of optical density change at 600nm constant wavelength that the beginning of the experiment. Agar plates were prepared by using liquid LB Broth and Sterile Petri Dishes as materials. Sterile liquid agar was pour into each sterile plastic Petri dish and the lid of Petri dish was covered immediately. Agar medium became like stiff gelatin at room temperature in plates.

After the preparation of agar plates 100 µl *E.coli* DH5α of selected optical densities were cultured on LB agar plates supplemented with different concentrations (3 - 30 µg/ml) of synthesized silver-only nanoparticles and silver-copper nanoalloys. Control groups were prepared exactly in the same way described above except for addition of nanoparticles or nanoalloys. LB plates were incubated for 24 h at 37 °C. Agar plates were incubated upside down in order to prevent any condensation from dripping down onto agar surface containing bacteria and nanoparticles and nanoalloys. The growth of colonies was observed directly on plates and plates were straightforwardly comparable with each other in terms of visual colony formation.

2.3.6.2. Batch Growth Profiles of Ag Nanoparticles – AgCu Nanoalloys for Antibacterial Efficiency

The bacterial growth was followed in the liquid LB medium supplemented with *E.coli* cells having initial optical density of 0.05, 0.1, 0.2 OD_{600}. Dynamics of the bacterial growth was followed by the change in the optical density at constant wavelength 600 nm in order to acquire batch growth profiles of *E.coli* cells in the presence of nanoparticles or nanoalloys. 100 µl *E.coli* DH5α of selected optical densities was injected into liquid LB medium in the

presence of Ag NPs or AgCu NAs at different concentrations where LB medium was used as carrier to dilute nanoparticle and nanoalloy solutions to different concentrations. Negative controls were prepared without supplement of NPs or NAs but with same conditions of bacteria and LB medium.

Dynamics of bacterial growth was followed by the change in the optical density at constant wavelength 600 nm after certain incubation periods (1-24 hours) at 37 °C with constant agitation at 225 rpm. For each set of measurements clear sterile medium in spectrophotometer cuvette was used and intensity of the light that reaches to detector was taken as reference intensity to correct any light absorption caused by medium because we want to measure only the optical density caused by *E.coli* cells not medium as well as readjustment for reference sample was repeated for each of the OD measurements with sterile medium to prevent any drift. The batch growth profiles of *E.coli* DH5α in liquid LB broth were constructed by plotting determined optical density values with respect to incubation time for negative control, nanoparticles and nanoalloys.

2.3.6.3. Quantification of the Antimicrobial Properties of Ag Nanoparticles and AgCu Nanoalloys

Colony forming abilities of *E.coli* DH5α cells in the presence of nanoparticles and nanoalloys was determined by incubation of *E.coli* DH5α of 0.2 OD ($7x10^8$ CFU/ml) with different dilutions in the range of 10^0 - 10^7. 100 µl *E.coli* DH5α of each dilutions was spread on LB agar plates containing different concentrations of nanoparticles and nanoalloys with 10^1-10^5 dilutions from 30 µg/ml amount of Ag NPs and AgCu NAs solutions. The agar plates were incubated for 18 h at 37 °C, then the growth of colonies were observed and counted directly.

The minimum growth inhibitory concentration (MIC) which is the lowest concentration of antibacterial agent that inhibits the visible growth of bacteria used to quantify antimicrobial efficiency of nanoparticle and nanoalloy solutions. In this test, pure culture of *E.coli* DH5α was grown in LB broth and standardized to have optical density of 0.5 OD ($1.7x10^8$ CFU/ml). Ag NPs and AgCu NAs as antibacterial agents were diluted 2-128 times through sterile diluent, LB broth in our case. After dilution of antibacterial agents same volume of inoculums equal to the volume of NPs or NAs was added to the dilution test tube and same amount of bacteria were incubated overnight in serial dilutions of NPs and NAs, (from 30 µg/ml to 58 ng/ml) at 37 °C. Bacteria growth in all dilution test tubes were followed by optical density measurement and minimum concentration of nanoparticles and nanoalloys at which no bacterial growth was observed was selected to be the "MIC".

After MIC determination of Ag nanoparticles and AgCu nanoalloys minimum bactericidal concentration (MBC) was determined by spreading 100 µl aliquots from all dilution test tubes in which no visible bacteria growth was observable on sterile agar plates. The plates were incubated for overnight at 37°C and MBC values were selected as the lowest concentration of Ag NPs and AgCu NAs that kills >99.9% of the initial bacterial population where no visible growth of the bacteria was observed on the agar plates.

2.3.6.4. Investigation of Antibacterial Effects of Ag Nanoparticles and AgCu Nanoalloys Incorporated Ultra Thin Metal Polyelectrolyte Films

E.coli DH5α strain has been grown to known optical densities of 0.05 OD under the control of optical density change at 600nm constant wavelength at the beginning of the experiment. Agar plates were prepared by using liquid LB Broth and Sterile Petri Dishes as materials as described previously by pouring enough sterile liquid agar into each sterile plastic Petri dish and allowing agar medium to become like stiff gelatin at room temperature in plates.

Afterwards 2 cm x 2 cm LbL assembled PEI-PSS-PAH-AgCu NAs ultra thin films, which were prepared by dipping cycles of 40 min in 1g/l polyelectrolyte solutions and overnight dipping into NAs solution, were placed on the pre-prepared agar plates and 100 µl *E.coli* DH5α of optical density at 0.6 were inoculated on LbL films with 100 µl of liquid LB Broth to protect bacteria cells against desiccation and to elicit nutrients for bacterial growth. Growth of bacteria was monitored after incubation of plates for 24 h at 37 °C.

3. RESULTS AND DISCUSSION

3.1. PREPARATION OF Ag NANOPARTICLES

Silver nanoparticles were synthesized by the reduction of silver ions, which are produced via dissolving $AgNO_3$ salt in aqueous medium, with the help of strong reducing agent sodium borohydride under ambient conditions without any oxidation or precipitation problems. Color change into bright yellow indicates the formation of silver nanoparticles with size 10 nm. [97] Hence, successful synthesis of Ag NPs was detected by the change of color into bright yellow after reduction of the colorless silver ion solution.

Main handling problem in Ag NPs synthesis was the agglomeration of nanoparticles after reduction process. Particle aggregation was detected by color change from yellow to gray-green indicating the accumulation of nanoparticles. The side reaction between borohydride and water produce side products of borate anions and there borate anions provide important electrostatic barrier to aggregation.[98] As a convenient solution for particle aggregation, capping nanoparticles with negatively charged citrate imparts electrostatic protection against accumulation of nanoparticles then yields nanoparticles in smaller size.

3.2. PREPARATION OF AgCu NANOALLOYS

Although Ag nanoparticles do not have spontaneous oxidation problem under ambient conditions; during the preparation of AgCu nanoalloys in the presence of relatively weaker reducing agents spontaneous oxidation, reaction kinetics and stability were problematic. The synthesis had handling problems and the unstable behavior of AgCu NAs is governed by the instability of copper nano-sized particles in alloy as a result of rapid air oxidation of metallic copper to copper ions and copper oxide species. Hence, synthesis of copper nanoparticles or

copper containing nanoalloys has not been easy due to the low reduction potential of Cu^0/ Cu^{2+}.[11]

Substantially, unstable behavior of the copper nanoparticles in the presence of air was easily followed by the color change of the solution into bright yellow indicating copper being oxidized from zero to the +2 oxidation state.[99] Different synthesis routes were performed to obtain AgCu NAs without any copper oxide contamination in terms of controlling stability of copper nanoparticles through changing reaction medium and using different reducing, protecting and complexing agents.

3.2.1. Complexing Agent Effect on AgCu Nanoalloy Synthesis

The large difference in the standard reduction potentials between Ag°/ $Ag^+$and Cu°/ Cu^{2+}, makes preparation of AgCu nanoalloys from simple ionic solutions of their salts very difficult. Because complexing agents have the ability to bring reduction potentials of two species closer to each other, [42] so as to bring the Ag and Cu reduction potentials closer suitable complexing agent sodium citrate was added to the reaction solutions during synthesis of nanoalloys.

This anionic type complexing agent also enables electrostatic protection against particle agglomeration[17, 22] via repulsive forces between negatively charged surfactant groups around AgCu NAs (Figure 11). Additionally, surrounding of particles with negatively charged citrate ions allows the synthesis of AgCu NAs with smaller diameter size and high dispersity due to excessive stabilization ability of the anions by the attractive forces between charged groups. The successful synthesis of AgCu NAs was directly followed by the wine-brown color of the solution and in the absence of complexing agent color of nanoalloy solution immediately turned into light yellow as a result of oxide contamination of copper nanoparticles.

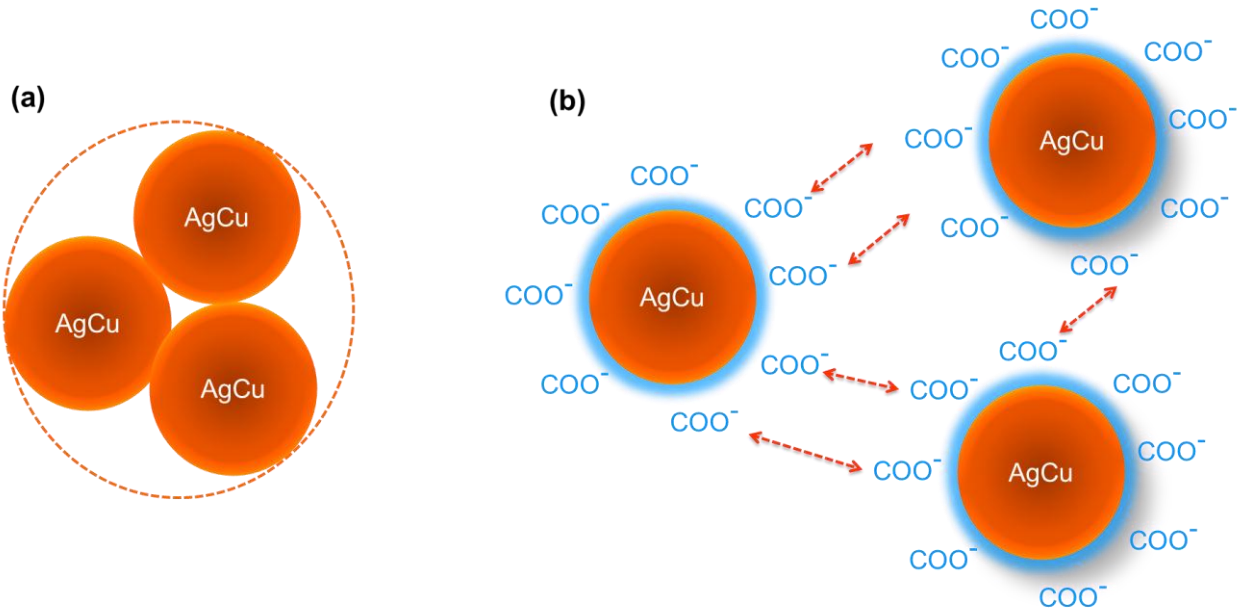

Figure 11. Schematic representation of **(a)** AgCu NAs particle agglomeration in absence of complexing agents **(b)** Electrostatic protection of AgCu NAs via citrate ions against agglomeration with the help of attractive forces between negatively charged COO^- groups.

In the presence of the complexing agent, not only the synthesis of AgCu NAs was succeed without any copper oxide formation at the end product, but also the deposition of the Ag-Cu nanoalloy on the polyelectrolyte layers was effectively carried out by surface modification of nanoalloys by capping them using negatively charged citrate anions, which increased the interaction between positively charged polyelectrolyte layer and the negatively charged nanoalloys, to affect the stability of the ultra thin layers. Likewise, the sequential attachment of nanoalloys on polyelectrolyte layers and adsorption of the next layer on nanoalloys was performed by electrostatic attraction between oppositely charged nanoparticles and polyelectrolyte layers.

3.2.2. Reducing Agent Effect on AgCu Nanoalloy Synthesis

Weaker reducing agents fail in reduction process of metal salts because of their poor electron donating ability in aqueous media where the strength of reducing agent is associated with their electron donating ability thus ease of losing electron .[4, 100] Relatively very weak reducing agent formaldehyde was firstly tried in attempt to observe the reduction ability for copper in AgCu NAs but reduction of copper and silver salts had not been succeed for several hours where reaction was allowed to continue overnight under stirring in the presence of formaldehyde and regrettably just after the injection of the copper salt solution to the reaction mixture color of the reaction solution turned into light yellow due to oxidation of copper because of weakness of reducing agent to synthesize nanoalloys. As a further approach, stronger reducing agent sodium borohydride ($NaBH_4$) was used for the reduction of metal ions. Although $NaBH_4$ is successful in silver ions' reduction process, its strength is not enough for synthesis of stable AgCu NAs in long term. Carefully controlled synthesis of AgCu NAs under specific conditions such as purging of reaction medium, only very little amount of reduced copper was detected after allowing reaction for 1hour; information regarding chemical state and amount of copper was obtained from XPS spectrum of AgCu NAs (Figure 12). During the reduction process hydride ions enable the electron donation for silver and copper ions but this reduction process was not rapid as the oxidation of copper ions.

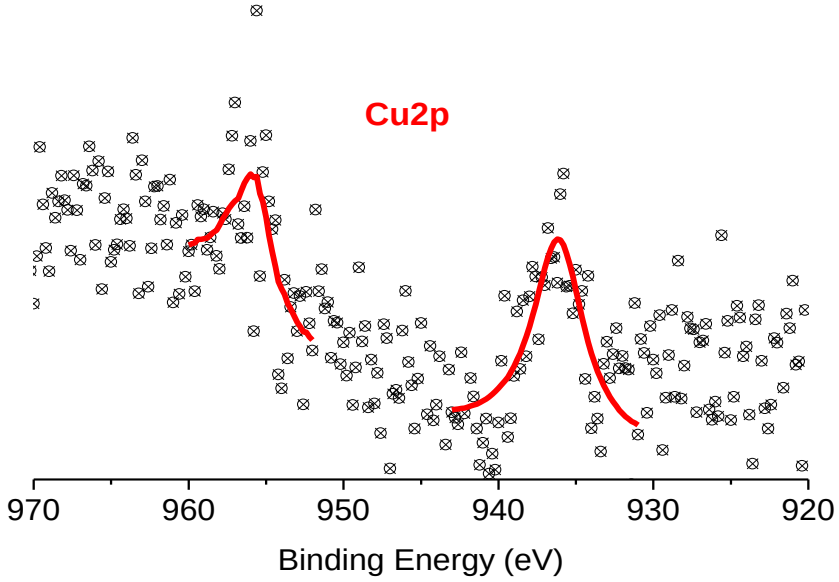

Figure 12. Cu 2p region of the XPS spectrum of AgCu nanoalloys which were synthesized in the presence of $NaBH_4$ as the reducing agent.

Sufficient amount of Cu without any oxide contamination existed in the AgCu NAs, exactly when it was prepared by very strong reducing agent hydrazine hydrate, corresponding to sharp Cu 2p spin orbit peaks in Cu2p region as shown in Figure 13, protecting it against oxidation under ambient conditions. Attributable to higher hydrogen content and very high affinity toward oxidation reaction of hydrazine hydrate ($NH_2NH_2.H_2O$), this reducing agent used effectively to prevent oxidative contamination of AgCu nanoalloys as a result of immediate reduction of copper ions to zero-valent copper in nanoalloy. Furthermore, oxidation product of hydrazine hydrate after the reduction of both metal ions of silver and copper is non-toxic nitrogen gas which creates automatically inert gas atmosphere. This decomposition product was preferred over the formation of boric oxides resulting from the $NaBH_4$ reduction and averted the immediate oxidation of copper ions to its copper oxide counterparts.[101]

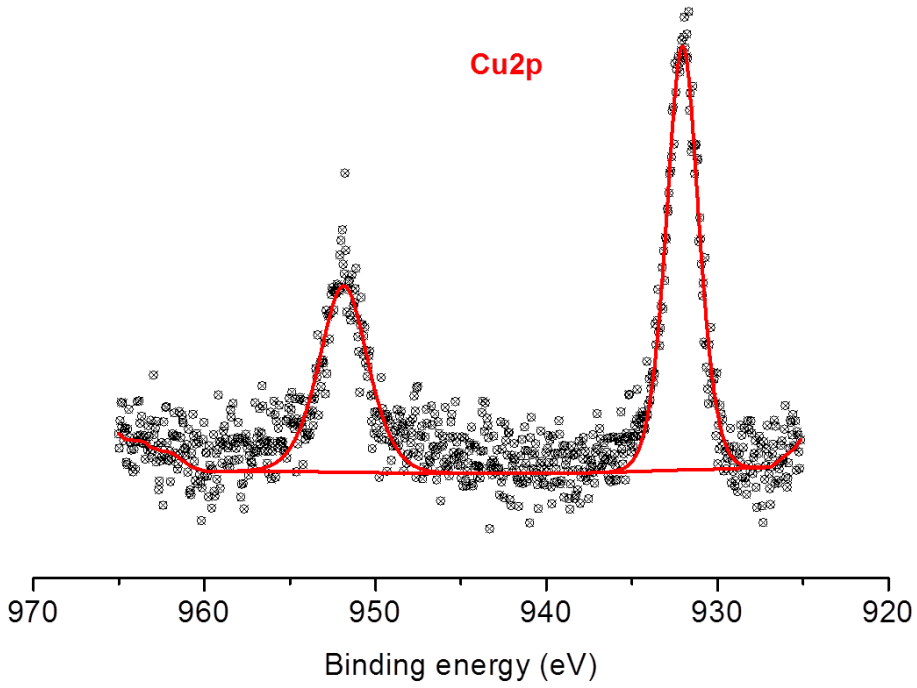

Figure 13. Cu 2p region of the XPS spectrum of AgCu nanoalloys which were synthesized in the presence of $NH_2NH_2.H_2O$ as reducing agent.

Hence, hydrazine hydrate leading immediate reduction of copper ions before being oxidized was used for both the synthesis, against the difficulties in handling, and against high air sensitivity problems during AgCu nanoalloy formation.

3.2.3. Reaction Media Purging Effect on Ag-Cu Nanoalloy Synthesis

In order to protect Cu nanoparticles against oxidation and to minimize the copper oxide formation deionized water, which was used for the preparation of all solutions, was purged by nitrogen gas and synthesis were done by bubbling nitrogen gas into the reaction media to purge it because of the reason that highly reactive nature of the copper requires atmosphere of inert gases for the formation of copper oxide free nanoalloys in the presence of

relatively weaker reducing agents (formaldehyde or sodium borohydride). Because under ambient conditions and without strong protection of synthesized nano sized particles aqueous media contain enough reactive oxygen species which readily form a complex with copper ions resulting copper oxide at the end product. Nevertheless, after purging period of reaction medium, AgCu nanoalloys' copper oxide contamination could not be avoided because copper requires high purity of nitrogen atmosphere.[99, 100] Thus, the color of the solutions that contains AgCu NAs turning into light-bright yellow was unstable without inert gas indication oxide contamination once more.

The duration of nitrogen purge was lengthened up to one-hour for solutions and nitrogen purge was continued after the expected wine-brown color of solution was observed to see whether the longer purging time was effective in the stability of copper. With increasing time interval for nitrogen purging process, oxide contamination of copper was observed in longer waiting periods like 2 or 3 days. As a result of investigation on purging reaction media with inert nitrogen gas, it was seen that anhydrous media or inert atmosphere of nitrogen gas was required for continuous stability of copper in AgCu alloys when relatively weaker reducing agents, stabilizer or complexing agent were used.

3.2.4. Stabilizer Effect on AgCu Nanoalloy Synthesis

In an attempt to ensure the stability of the nano-sized copper during synthesis and storage period protecting agents - stabilizers were also introduced because the limited shell life of nanoalloys leads limitations for various applications of these particles.

Initially, polyvinylpyrrolidone (PVP) was used in preparation of colloidal metal particles as a protecting polymer to control the formation of zero-valent copper in nanoalloys and to stabilize them. The experiments showed that; after reduction of silver and copper salts in the presence of PVP and strong reducing agent hydrazine hydrate the nanoalloys in

solutions were oxidized in longer time interval than the stabilizer-free experiments. Nonetheless, this stabilizer was not strong enough to stop conversion of nano-copper at zero oxidation state into copper oxide species. During storage period under ambient conditions the color of the nanoalloy solution turned into light yellow within few days owing to the formation of copper oxide species. Therefore, higher stabilizing polymer concentrations were required to impart stability to copper particles in water but as a result of strong interaction between water molecules and protective polymer, the interaction between side-chain of the polymer and metal nanoparticles weakens.[22, 98, 99] However, unstable behavior against oxidation in the case of polymer-protected synthesis was attributed to the poor protective property of polymers in water where PVP was not successful to obtain air-stabilized AgCu nanoalloys.

Surface modifications to impart further stability should be performed, in order that compensation of the high surface energy of nano-sized particles with suitable reagents. Rather than the other weaker complexing agents or stabilizers, such as polymers or electrostatically protecting agents or ligands containing deprotonated negatively charged carboxylic acid groups, thiol group (-SH) containing stabilizers provide enhanced stability. Because carbon bonded sulfhydryl groups have high tendency toward metal nanoparticles.[18-20] In this respect, cysteine which has carbon bonded –SH group at its terminal position is an anchor group to impart enriched stability to AgCu nanoalloys preventing particle oxidation.

Hence, as an alternative to the polymer protection for the synthesis of stable AgCu nanoalloys, although cysteine was not very successful for stabilizing the copper nanoparticles against oxidation when relatively weaker reducing agents were used, where the time interval for the oxidation of the copper nanoparticles were lengthened compared to the polymer stabilized experiments; in the presence of both strong reducing agent hydrazine hydrate and stabilizer cysteine oxidation of copper in the alloy was successfully prevented. Instead of

electrostatic interactions for attachment of stabilizing agents to nanoparticles, –SH group has capping ability via chemisorption through sulfhydryl bond that is very effective for preparing stable nanoparticles against particle agglomeration and oxidation. In terms of air-stability of copper, cysteine protected AgCu NAs retained feasibility of air-stabilization up to 50 days as a result of strong chemical interaction between functional group of cysteine and metal nanoalloys. Also being an amino acid, cysteine as protecting agent for effective capping is much more suitable for our aim of using synthesized nanoalloys for antibacterial applications, instead of other kind of stabilizers, since itself is antibacterial in nature.

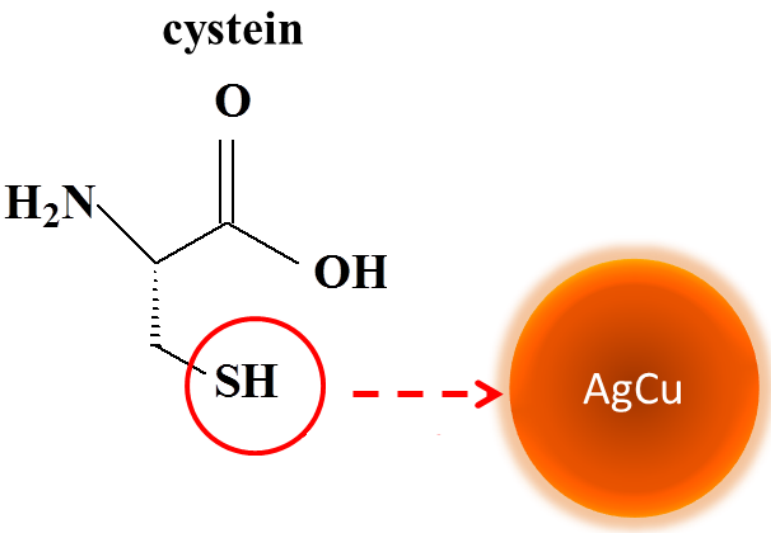

Figure 14. Schematic representation of affinity of thiol group at terminal position of cysteine toward AgCu nanoalloys.

3.2.5. Effect of Zn-salt addition on AgCu Nanoalloy Synthesis

Co-reduction of Ag and Cu metal ions in association with protective agent, surfactant and very strong reducing agent in solution as wet-chemical synthesis yields nanoalloys containing Ag and Cu metals in zero oxidation states but as it described previously in details in consequence of high reactivity, relatively low reduction potential and low stability of copper under ambient conditions, AgCu NAs are contaminated by copper oxide species during storage period.

Sacrificial anodes are often used to suppress the oxidation problem of metals involving metal-medium electrochemical potential bringing the reactive metal to the immunity zone for oxide contamination.[12, 102] Intended for metallic nanoparticles, rather than the oxidation by air or aqueous solutions, re-reduction of oxidized metal ions into zero-valent metal in nanostructure takes place straightforwardly, in the presence of sacrificial anodes. [12, 102, 103]

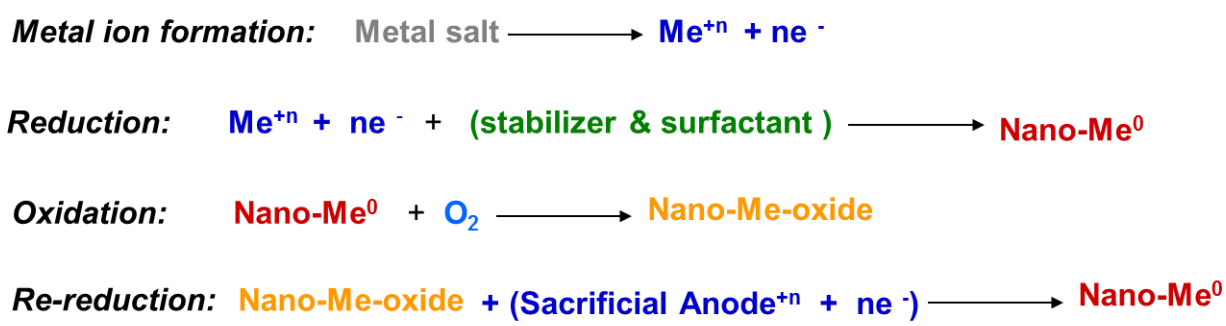

Figure 15. Representation of sacrificial anode effect on metal nanoparticle formation by re-reduction of metal ions after oxide contamination.

Inspiration with the idea of “sacrificial anode”, third metal “zinc” was added to the reduction medium of silver and copper metal salts with the ratio of Ag : Cu : Zn = 25 : 25 : 1

to prolong the stability of copper within AgCu nanoalloys. Zinc was chosen as the sacrificial anode during the synthesis due to its very low reduction potential where this very low reduction potential of zinc at -0.76V compared to the reduction potential of copper at +0.34V renders the inhibition of copper oxidation via preferential and much more rapid oxidation of zinc over copper.

AgCu-Zn ternary nanoalloys synthesis was confirmed by the wine-red color of the solution indicating successful nanoalloy synthesis without any copper oxide contamination. The oxide contamination was monitored by the color change of synthesized binary (AgCu) and ternary (AgCu-Zn) nanoalloys' solutions in the first place. Both AgCu and AgCu-Zn NAs solutions' color was dark wine-brown when they are freshly prepared, however the color of the solutions turned very light yellow as they are contaminated by copper oxide formation.

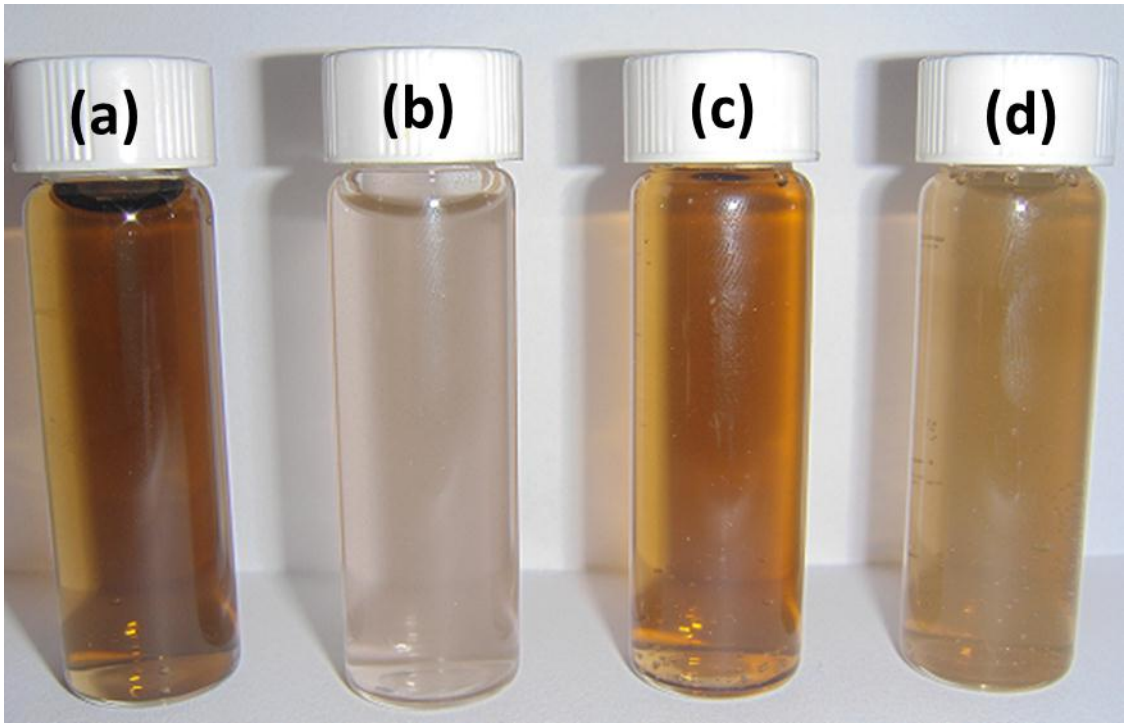

Figure 16. Images of **(a)** fresh AgCu **(b)** 14weeks-old AgCu **(c)** fresh AgCu-Zn **(d)** 14weeks-old AgCu-Zn nanoalloys' solutions.

Firstly, oxide contamination was followed by comparing the fresh and 14 weeks-old nanoalloy solution as depicted in Figure 16 and the basic sign for prolonged stability in presence of Zn was monitored by the darker color of 14 weeks-old AgCu-Zn NAs' solution while the color of AgCu NAs' solution turned very light yellow because of the higher degree of oxide contamination as compared to AgCu-Zn NAs.

Cu2p region of XPS spectrum indicates whether the chemical state of copper is zero or in its oxidized state (Cu^{+} or Cu^{2+}) with characteristic shake-up satellite structure. In order to elucidate the effect of Zn addition on stability of copper, further analyses on copper oxide contamination of AgCu and AgCu-Zn NAs were performed by XPS to precisely monitor the chemical state of copper. Hence XPS spectra of Cu2p region corresponding to AgCu and AgCu-Zn NAs were recorded after different storage intervals as shown in Figure 17. Accordingly fresh nanoalloys' Cu2p regions contain only copper in zero oxidation state for both AgCu and AgCu-Zn NAs without either oxide satellite or broadening of the peaks, After storage period of 7 weeks, copper oxide formation in AgCu NAs was distinguished easily by small oxide satellite formation and broadening of Cu2p peaks, though AgCu-Zn NAs did not contain oxide satellite or broadened peaks for the same storage period. Nonetheless, after 14 weeks of storage period Cu2p regions of both AgCu and AgCu-Zn NAs contain shake up satellites on account of copper oxide formation but it is obvious that AgCu-Zn NAs to a much lesser extent. The lower copper oxide contamination as a result of zinc addition is consistent with the "sacrificial anode" idea and the strong evidence for prolonged stability of copper against oxidation when Zn is added to the nanostructure.

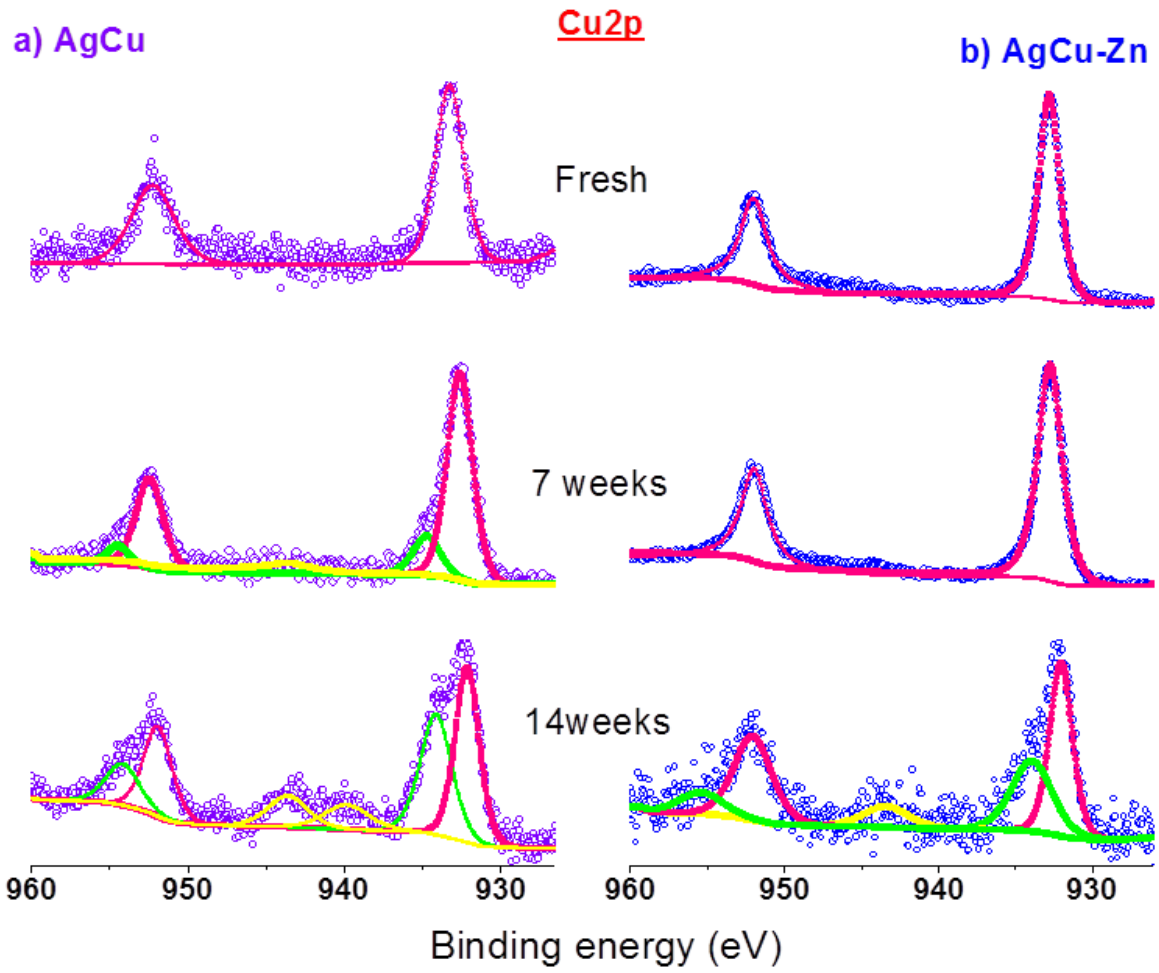

Figure 17. Cu2p region of the XPS spectra of **(a)** AgCu binary and **(b)** AgCuZn ternary nanoalloys recorded in fresh, after 7 and 14 weeks.

3.3. CHARACTERIZATION OF NANOPARTICLE AND NANOALLOY SOLUTIONS

For the characterization of synthesized Ag NPs with the characteristic yellow color of the silver nanoparticles, UV-vis spectrum of the solution was taken. Figure 18 shows the UV-vis spectrum recorded from synthesized Ag NPs and the existence for the silver-only nanoparticles in the solution was verified by the UV-vis optical absorbance spectrum with the absorbance at 390 nm corresponding to the silver surface plasmon frequency. The absorption spectrum of the AgCu nanoalloy solution is also shown in the same figure with, absorbance at 420nm that is different for the absorption of Ag-only nanoparticles dispersed in water, indicating the presence of silver – copper nanoparticles in the nanostructure.

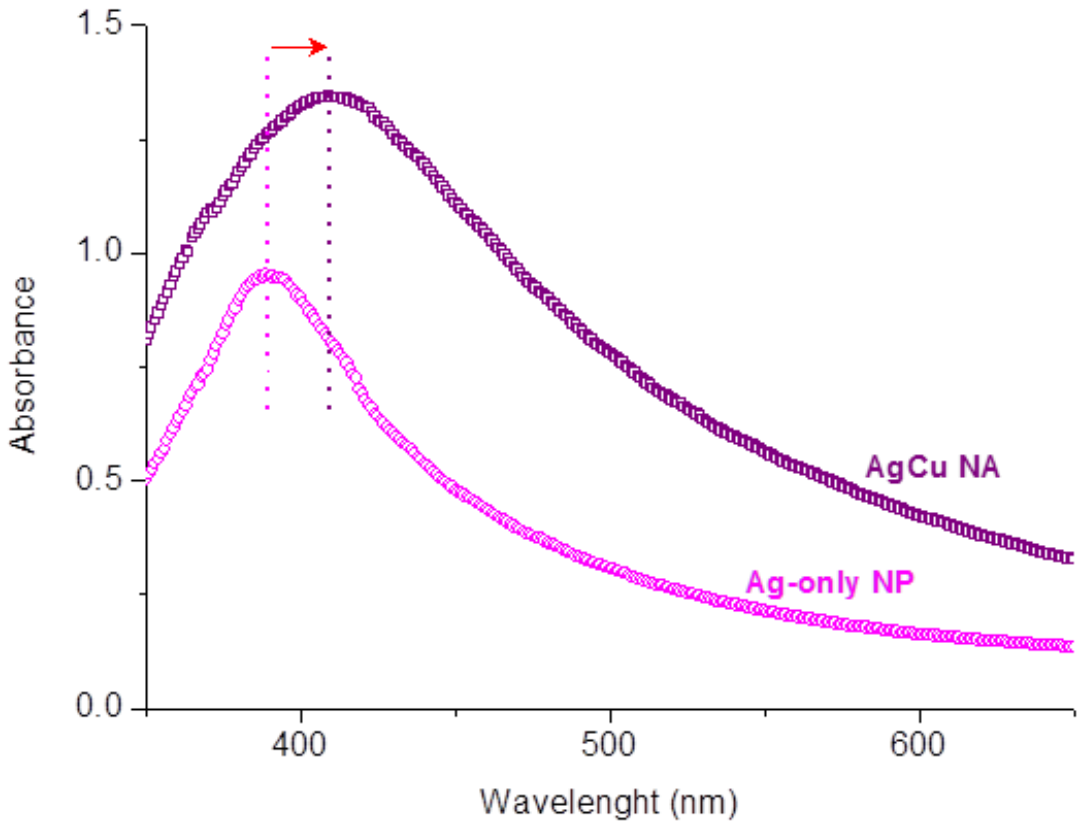

Figure 18. UV-visible absorption spectrum of aqueous solutions of Ag-only and AgCu alloy nanoparticles.

The figure shows that the silver absorbance at 390 nm corresponding to Ag-only nanoparticles was broadened and red-shifted toward 420 nm absorbance because of the presence of copper in the nanoalloy together with silver attributable to the interaction between copper and silver nanoparticles due to the fact that surface plasmon wavelength depends on the particle-particle interaction between silver and copper. UV-visible spectra of AgCu binary and AgCu-Zn ternary nanoalloys are represented in Figure 19. In the broadened peak of the AgCu NA no change was observed in the peak position after insertion of Zn into the binary nanoalloy. The peak at 420 nm in the absorption spectra indicates the presence of AgCu-Zn ternary nanoalloys in the solution.

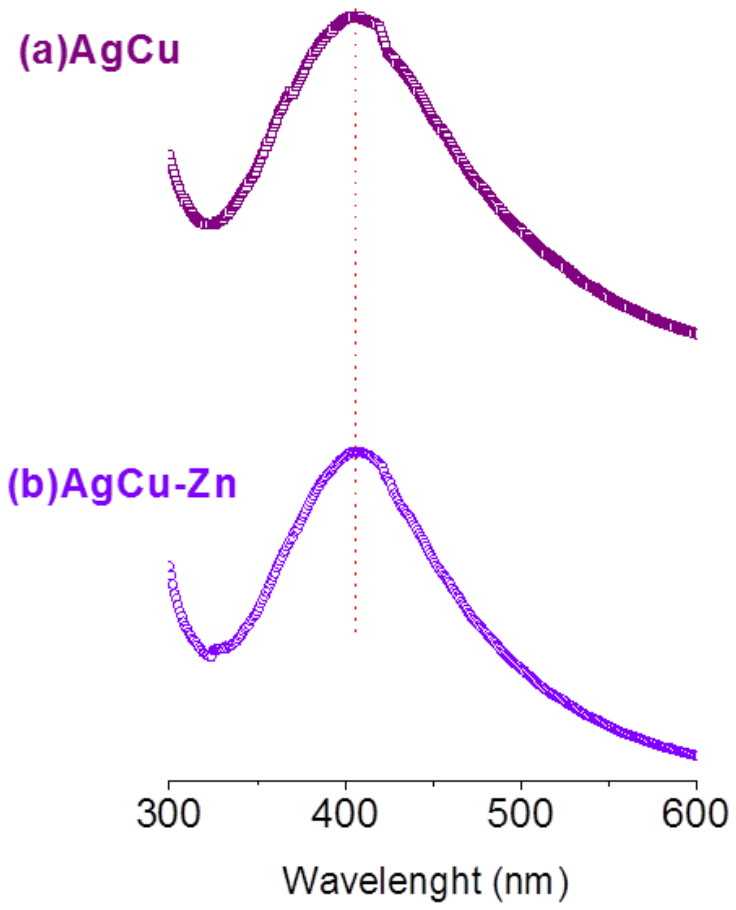

Figure 19. UV-visible absorption spectrum of aqueous solutions of AgCu binary and AgCu-Zn ternary alloy nanoparticles.

3.4. CHARACTERIZATION OF LAYER –BY-LAYER DEPOSITED ULTRA THIN POLYELECTROLYTE-METAL NANOPARTICLE FILMS

Layer-by-layer assembly was used both to construct ultra thin films consisting of polyelectrolyte multilayers and to deposit the pre-prepared nanoparticles/alloys on these thin films for the modification of the surfaces designed for anti-bacterial applications. Polyelectrolyte multilayers were coated on the glass and silicon surface where these surfaces were negatively charged and the construction of ultra thin films started with adsorption of PEI on substrates as first polyelectrolyte layer and continued with the sequential adsorption of PSS and PAH until desired multilayer configuration is reached.

Because of the fact that primary, secondary or tertiary amine and ammonia functional groups have the ability to form strong and irreversible interactions with transition metal particles,[33, 88] both use of positively charged polyelectrolytes PEI and PAH is convenient for LbL assembly. Hence, the use of PEI and PAH, containing amine and ammonia as functional group in their structure respectively, for the attachment of metal particles imparts additional stability against precipitation of particles on thin films over storage periods.

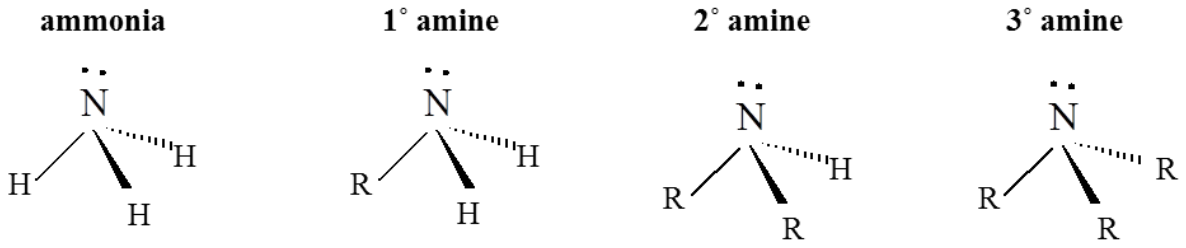

Figure 20. Structures of ammonia, primary amine, secondary amine and tertiary amine groups.

As a common thin film construction feature, properly charged pre-prepared Ag NPs or AgCu NAs were attached on thin films via alternating adsorption of oppositely charged nanoparticles/alloys and polyelectrolytes. Because, when Ag-only and AgCu nanoclusters are synthesized separately in the presence of sodium citrate as capping agent, in addition to the stabilization effect of citrate ions against particle agglomeration via repulsive forces between negatively charges, nanoclusters are capped with negative citrate ions what makes these particles applicable in Layer-by-Layer assembly to attach positively charged polyelectrolytes. As a result of electrostatic attachment of citrate capped Ag NPs or AgCu NAs on polyelectrolyte layers, desired multilayer configuration can be obtained for investigation of the films for antibacterial applications.

PEI which is branched and high molecular weight polyelectrolyte was used in our experiments as a base layer because PEI forms irreversibly bounded thin film on glass and silicon substrates through its amine group forming stable single-thin layer for further constructions. But in order to take full advantage of electrostatic interaction between glass or silicon surfaces and thin layer of PEI, metal nanoparticles can be released or not transferred directly on PEI layer to minimize their interaction. Therefore effective attachment of Ag NPS or AgCu NAs cannot be performed directly on PEI layer, so at least single PSS-PAH bilayer is constructed on top of the first layer for successful attachment of metal particles on polyelectrolyte multilayers.

3.4.1. Water-Contact-Angle Measurements of Ultra Thin Films

Water Contact Angle (WCA) measurements are used to determine wetting properties of different surfaces. For LbL deposited polyelectrolyte layers WCA is determined at where water droplet meets the negatively or positively charged polyelectrolyte layer thin surface and these oppositely charged thin surfaces display different wetting characteristics. Adsorption of positively charged PAH layer on the supporting surface results WCA at 70˚ and further adsorption of negatively charged polyelectrolyte layer on PAH layer reduce contact angle value to around 40˚. These characteristic contact angle values do not change with the number of adsorbed layers, so deposition of second layer on previous bilayer can be followed via conserved contact angle values. Hence, the successful adsorption of PAH and PSS polyelectrolyte layers was confirmed after each adsorption cycle by following the sharp change in surface wetting properties using WCA measurements as an practical and simple method before further spectroscopic analysis.

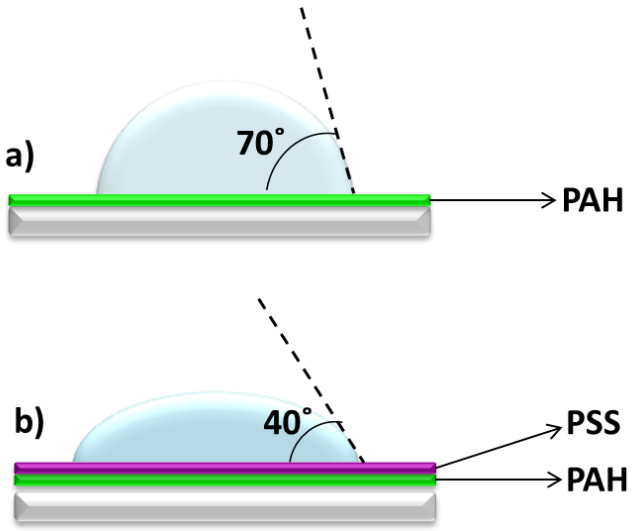

Figure 21. Schematic representation of Water Contact Angle measurements for **(a)** single PAH layer and **(b)** PSS/PAH bilayers on glass substrate.

Likewise for the preparation of ultra thin multilayers at optimum dipping time using optimum concentration for polyelectrolyte solutions, WCA measurements were used as the testing method. After each dipping cycle at constant polyelectrolyte solution concentration but changing the dipping time, successful adsorption was confirmed if the contact angle values reach 70˚ for PAH and 40˚ for PSS, such that optimum dipping time at a given concentration was determined. Also for constant dipping time in polyelectrolyte solutions, optimum concentration to form LbL layer was determined while changing the concentration of the dipping solutions under control of WCA values.

Table 1 represents the results for WCA measurements for different polyelectrolyte concentrations and dipping periods. Minus sign (-) indicates the unsuccessful deposition of PAH or PSS layers and plus sign (+) indicates the successful deposition of these polyelectrolytes at given concentration and time if WCA value reaches 70˚ for PAH and 40˚ for PSS. The optimum dipping time and concentration were chosen as 40 min at 1 g/l because shorter dipping periods were not successful for complete adsorption of polyelectrolytes and even at higher concentrations solubility problems were met for PSS other than non-uniform deposition of both polyelectrolytes.

Table 1. Water Contact Angle Measurements for given concentrations and time

	0.5 g/l		**1 g/l**		**1.5 g/l**		**2.0 g/l**	
Time	PAH	PSS	PAH	PSS	PAH	PSS	PAH	PSS
10min	-	-	-	-	-	-	-	-
15min	-	-	-	-	-	-	-	-
20min	-	-	-	-	-	-	-	+
25min	-	-	-	-	-	+	+	+
30min	-	-	-	-	-	+	+	+
35min	-	-	-	+	+	+	+	+
40min	-	-	+	+	+	+	+	+
50min	+	+	+	+	+	+	+	+

3.4.2. Characterization of Ag Nanoparticle Incorporated Ultra Thin Films

3.4.2.1. Optical Response of Ag Nanoparticle Ultra Thin Films

LbL assembled Ag-only nanoparticles can easily be recognized by their bright yellow color on colorless glass / polyelectrolyte layers. For optical characterization, UV-visible absorbance spectrum of ultra thin LbL multilayers containing Ag-only NPs can be used. Optical spectrum that revealed after the deposition of Ag-only NPs on top of the PEI-PSS-PAH thin layers has characteristics absorbance at 390 nm corresponding to the existence of NPs (Figure 22). When silver nanoparticles were deposited on multilayers of polyelectrolytes, optical properties were sustained as in the solution phase without any shift in the SPR band of Ag-only NPs, but with slight broadening.

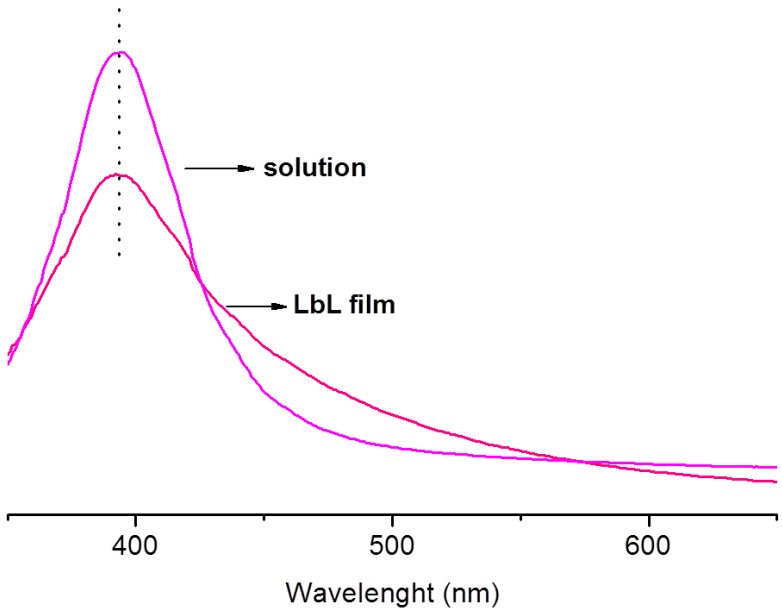

Figure 22. UV-visible absorption spectrum of silver-only nanoparticle solution and layer-by-layer assembled PEI-PSS-PAH / Ag-only NPs ultra thin film.

3.4.2.2. XPS Characterization of Ag Nanoparticle Ultra Thin Films

Since XPS is one of the most powerful techniques for sensitive surface analysis, characterization of LbL assembled ultra thin layers containing metal nanoparticles was performed as extracting information on elemental identification, chemical state or composition.

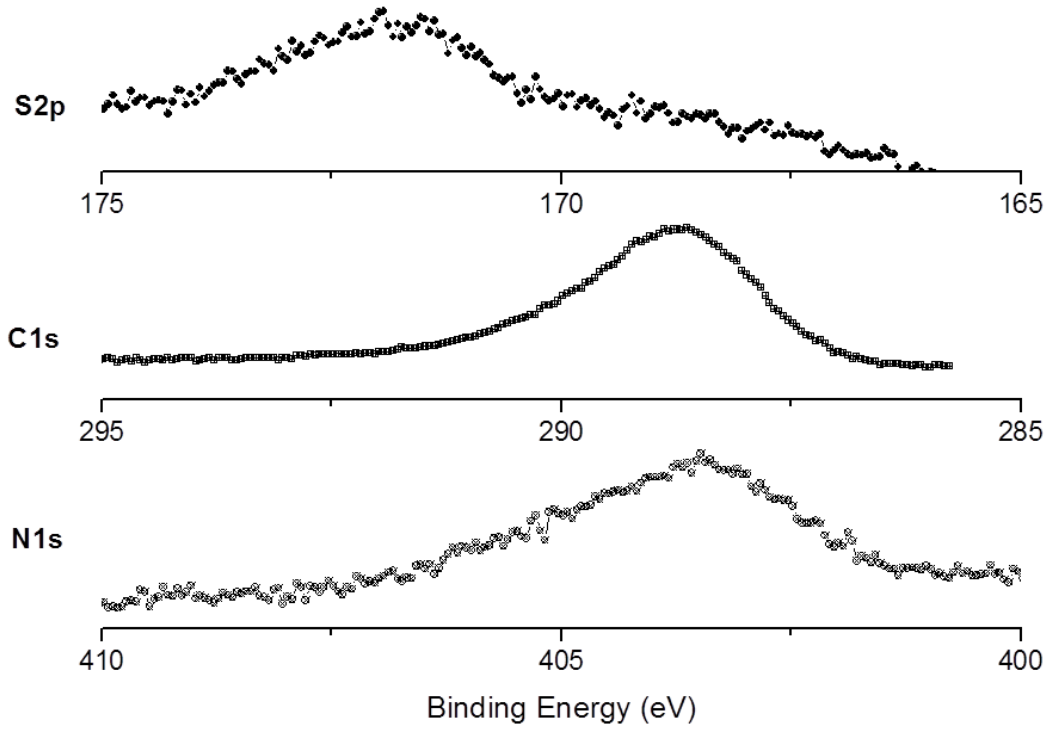

Figure 23. XPS spectrum of PEI-PSS-PAH / Ag-only NPs ultra thin layers showing S2p, C1s and N1s regions.

The ultra thin layers for XPS analysis were prepared as described in experimental part, starting with adsorption of PEI base layer on substrate and constructed further sequential adsorption of PSS and PAH layers. Incorporation of citrate capped Ag-only NPs was succeed by the adsorption of negatively charged silver nanoparticles on positively charged PAH and these Ag NPs inserted ultra thin layers were investigated by XPS. In the XPS spectra of PEI-

PSS-PAH/Ag-only NPs, corresponding to N1s, S2p and C1s peaks successful deposition of polyelectrolyte layers was confirmed (Figure 23).

C1s peak belongs distinctly to the carbon atoms of the polymer chains of each negatively and positively charged polyelectrolytes. N1s peak originates from the positively charged $–NH_3^+$ and $–NH^+$ groups corresponding to the polyelectrolyte layers of PAH and PEI respectively and the S2p peak originates from negatively charged $–SO_3^-$ group of PSS indicating the presence of these layers on the substrate. Existence of citrate capped Ag-only NPs on PEI-PSS-PAH layers was attested by the characteristic binding energy (368 eV) of silver at zero-oxidation state and 3d spin orbit splitting , as depicted in Figure 24, of silver nanoparticles. Therefore, LbL assembled multilayers consisting of polyelectrolytes and Ag-only metal nanoparticles was an evident in terms of explicit elemental and chemical state identification, while proving the successful creation of both nanoparticles and ultra thin layers.

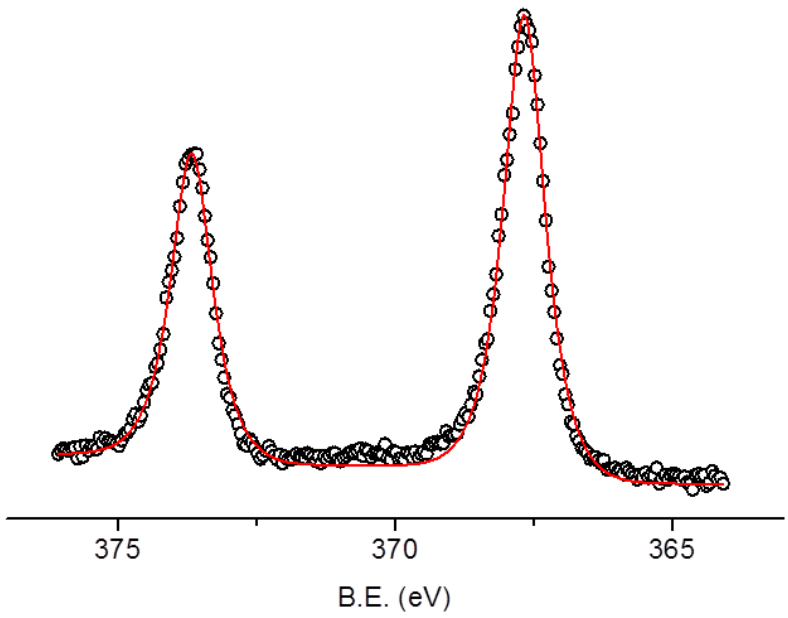

Figure 24. Ag 3d region of the XPS spectrum of LbL assembled PEI-PSS-PAH / Ag-only NPs ultra thin film.

3.4.3. Characterization of AgCu Nanoalloy Incorporated Ultra Thin Films

3.4.3.1. Optical Response of AgCu Nanoalloy Ultra Thin Films

LbL assembled AgCu nanoalloys were easily recognized by the wine-brown color of the deposited nanoalloys on colorless glass / polyelectrolyte layers. UV-vis absorption spectrum of AgCu NAs inserted ultra thin multilayers (Figure 25) over again indicates the presence of citrate capped AgCu NAs on PEI-PSS-PAH polyelectrolyte layers directly belonging to the characteristic absorbance of nanoalloys around 420 nm.

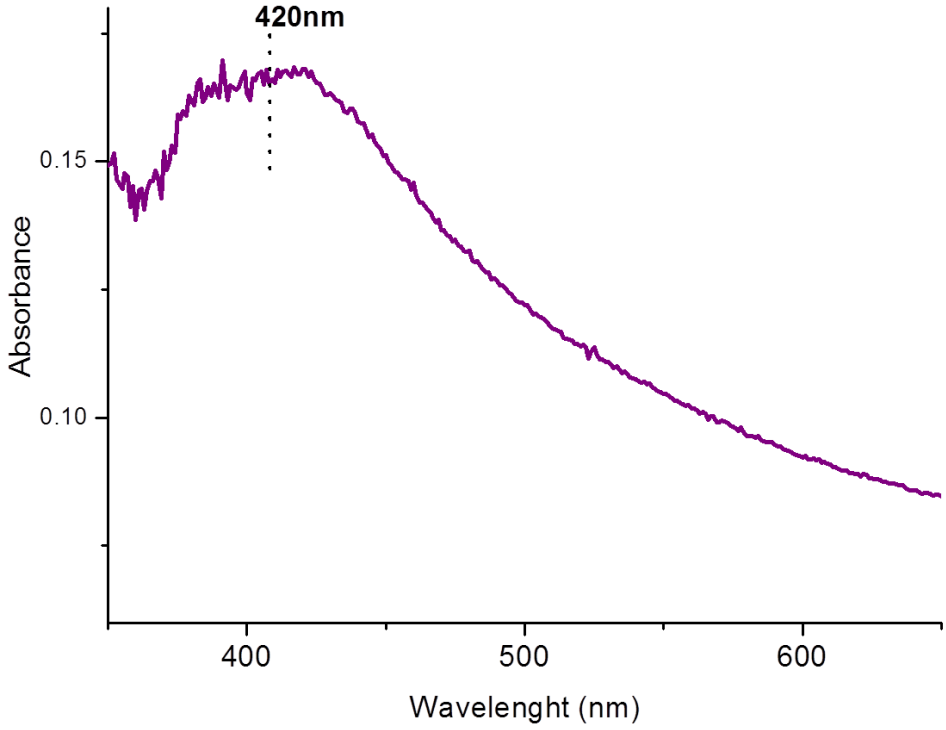

Figure 25. UV-visible absorption spectrum of layer-by-layer assembled PEI-PSS-PAH / AgCu NAs ultra thin film.

3.4.3.2. XPS Characterization of AgCu Nanoalloys Ultra Thin Films via "Static XPS"

The AgCu NAs ultra thin layers for XPS analysis was prepared in the same way with Ag-only NPs ultra thin layers preparation as described in experimental part, starting with adsorption of PEI base layer on substrate and constructed further sequential adsorption of PSS and PAH layers then the incorporation of citrate capped AgCu NAs on top of these polyelectrolyte layers as outermost layer.

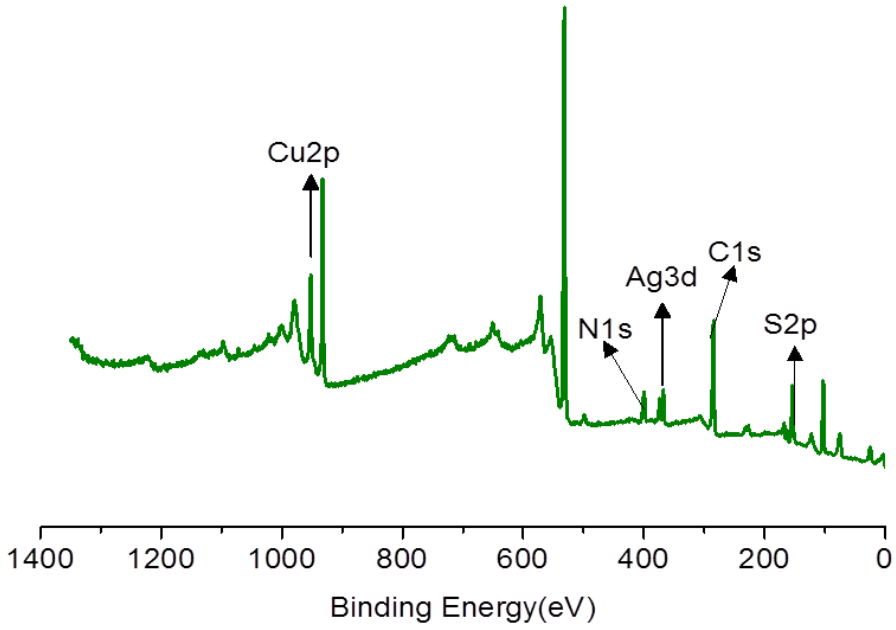

Figure 26. XPS survey of layer-by-layer assembled PEI-PSS-PAH / AgCu NAs ultra thin film.

The successful synthesis of citrate capped AgCu NAs and incorporation of pre-synthesized NAs into ultra thin LbL films was decisively monitored by the characteristic binding energies and atomic spin orbit splittings of Ag3d (6 eV) and Cu2p (19.6 eV) in XPS spectrum that was recorded for grounded sample via Static XPS method. XPS survey of PEI-

PSS-PAH/AgCu NAs thin film (Figure 26) also contains N1s, S2p and C1s peaks that resemble the successful deposition of PEI, PSS and PAH polyelectrolytes layers by virtue of nitrogen, sulphur and carbon atoms in the structure of positively and negatively charged polyelectrolytes.

Additionally, Static XPS method confirmed the synthesis of ternary AgCu-Zn nanoalloys corresponding to the Ag3d, Cu2p and Zn2p peaks in XPS survey of AgCu-Zn NAs which was recorded for grounded sample as depicted in Figure 27.

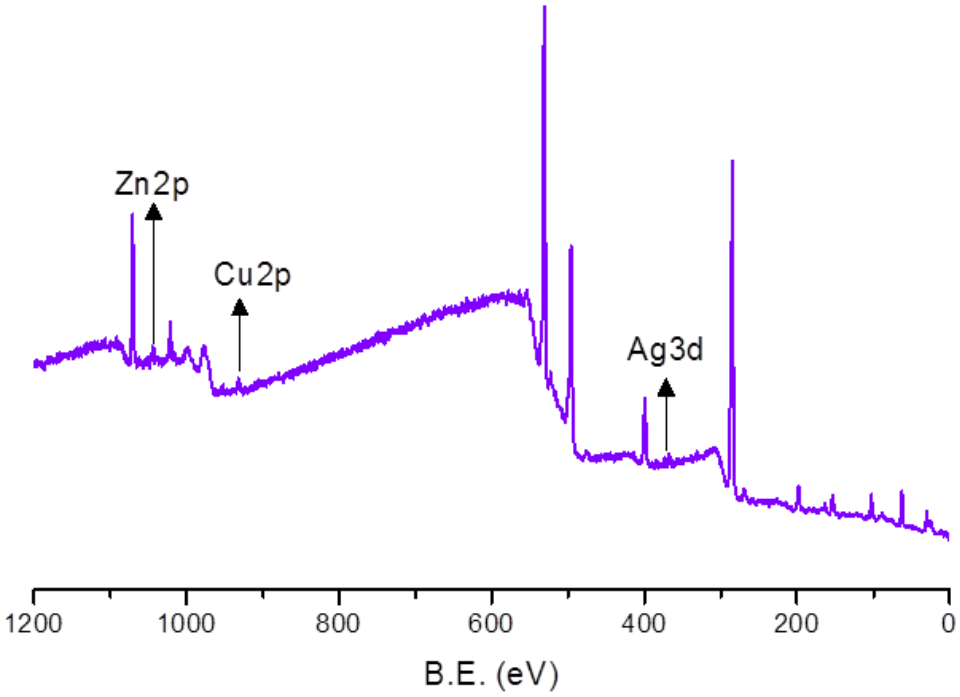

Figure 27. XPS survey of AgCu-Zn ternary nanoalloys thin film.

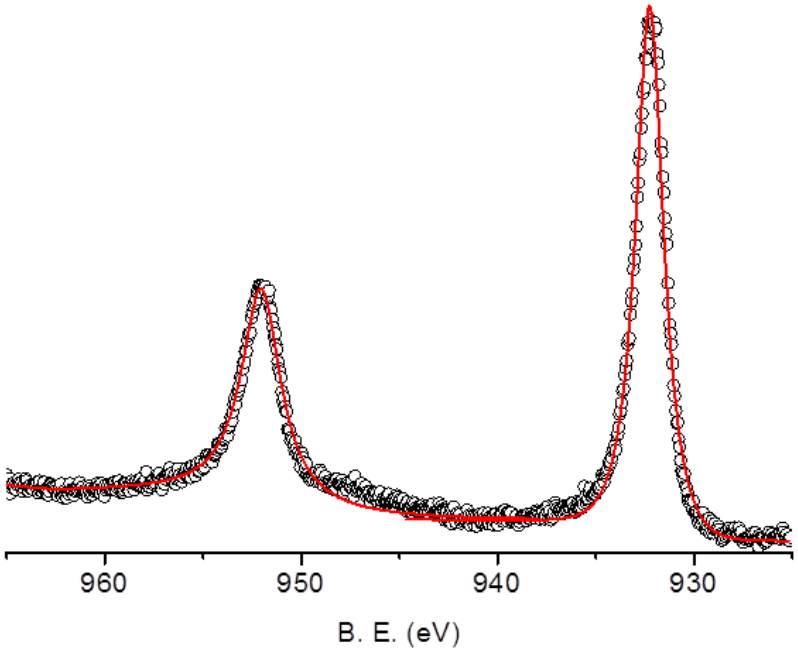

Figure 28. Cu 2p region of the XPS spectrum of LbL assembled PEI-PSS-PAH / AgCu NAs ultra thin film.

Besides the elemental identification, Cu2p region of the XPS spectrum includes chemical state information to distinguish the copper oxide species from zero-valent copper. Figure 28 depicts the Cu2p region of PEI-PSS-PAH / AgCu NAs ultra thin film's XPS spectrum where neither oxide satellites, which has different shape than the Cu2p peaks, nor peak broadening was detected. Binding energy of copper at zero-oxidation state (932.7 eV) verified the successful synthesis of nanoalloys without any copper oxide contamination under ambient conditions in the presence of strong reducing agent hydrazine hydrate, stabilizer and complexing agent . Unlike the distinction between CuO signal and zero valent copper signal, there was almost no difference between Cu_2O and zero valent copper in XPS spectra and XPS spectrum provided sufficient information about $Cu(OH)_2$. No signal was observed for hydroxide formation of copper as a result of complexing agent sodium citrate usage during

experiments, indicating that complexing agent addition prevent the hydroxide formation by providing better stability for citrate capped AgCu NAs.

Inspecting the S2p region of XPS spectrum of AgCu NAs (Figure 29) thin film in details, two different spin orbit doublets were detected corresponding to two different sulphur species: one of the S2p peaks at higher binding energy originates from negatively charged $-SO_3^-$ group corresponding to the LbL assembled negatively charged PSS layer and the other originates from the sulphur in the structure of cysteine that stabilize the AgCu NAs via surrounding nanostructures through sulfhydryl bond corresponding to the existence of silver-copper nanoalloys on ultra thin layers. Because of the fact that cysteine stabilized AgCu NAs were incorporated in ultra thin films as outermost layer on the top of PEI-PSS-PAH layers, the intensity of S2p peak that belongs to the sulfhydryl bond of cysteine is relatively higher than the intensity of S2p peak of underneath PSS layer which is another proof of successful thin film preparation with the desired nanoparticles within.

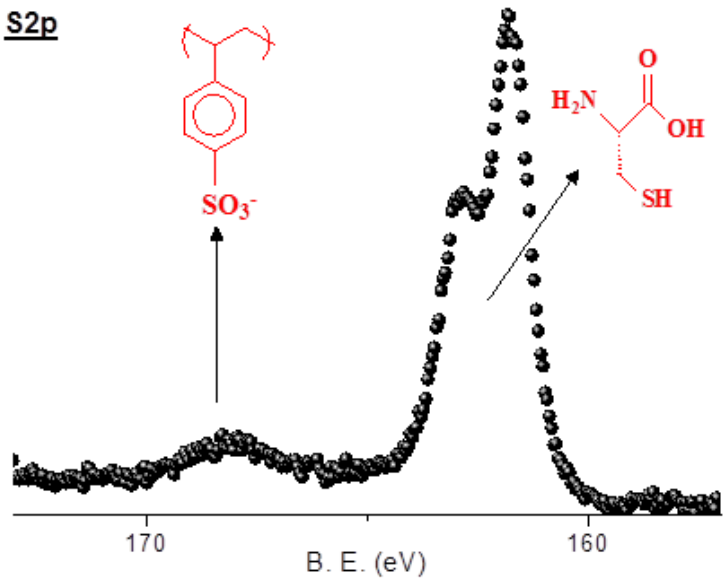

Figure 29. S2p region of the XPS spectrum of LbL assembled PEI-PSS-PAH / AgCuNAs ultra thin film showing chemical structures of PSS and cysteine.

3.4.3.3. XPS Characterization of AgCu Nanoalloys Ultra Thin Films via "Dynamic XPS"

It is known from the literature that Ag and Cu undergo phase separation under certain circumstances.[104] In order to verify that the AgCu nanoparticles form alloy structure Dynamic XPS is used. Hence with the intention of extracting detailed information from XPS analysis, LbL assembled PEI-PSS-PAH/AgCu NAs films on silicon substrates were analyzed under external stimuli. Films were prepared by alternative adsorption of positively charged and negatively charged polyelectrolytes on negatively charged silicon wafers containing silicon thermally grown silicon oxide layer as described in experimental part in details. As outermost layer, citrate capped AgCu NAs' thin layer was constructed on the top of polyelectrolyte layers.

XPS spectra of Ag3d, Cu2p, N1s, C1s and S2p regions (Figure 30 and Figure 31) were recorded while applying square wave pulses with frequency of 10 kHz and 0.001 Hz and +7 and -7 V amplitude so as to confirm the existence of the nano-sized copper together with nano-sized silver in the same nanostructure forming nanoalloys. The position of photoelectron peaks were shifted to higher and lower binding energy positions compared to the grounded binding energy position during the positive and negative DC voltage application because the sample attracts or repels electrons and negative or positive charges on the surface have been developed; so shifts in peak positions toward higher or lower binding energies had been followed as well as the charging phenomena depends on not only the application of external voltage stress but also the charging capacity of the domains, for both high and low frequencies. During square wave pulse application half of the time had been spent under -7 V where the other half had been spent under +7 V; subsequently the recorded XPS spectra contain photoelectron peaks that are split into two.

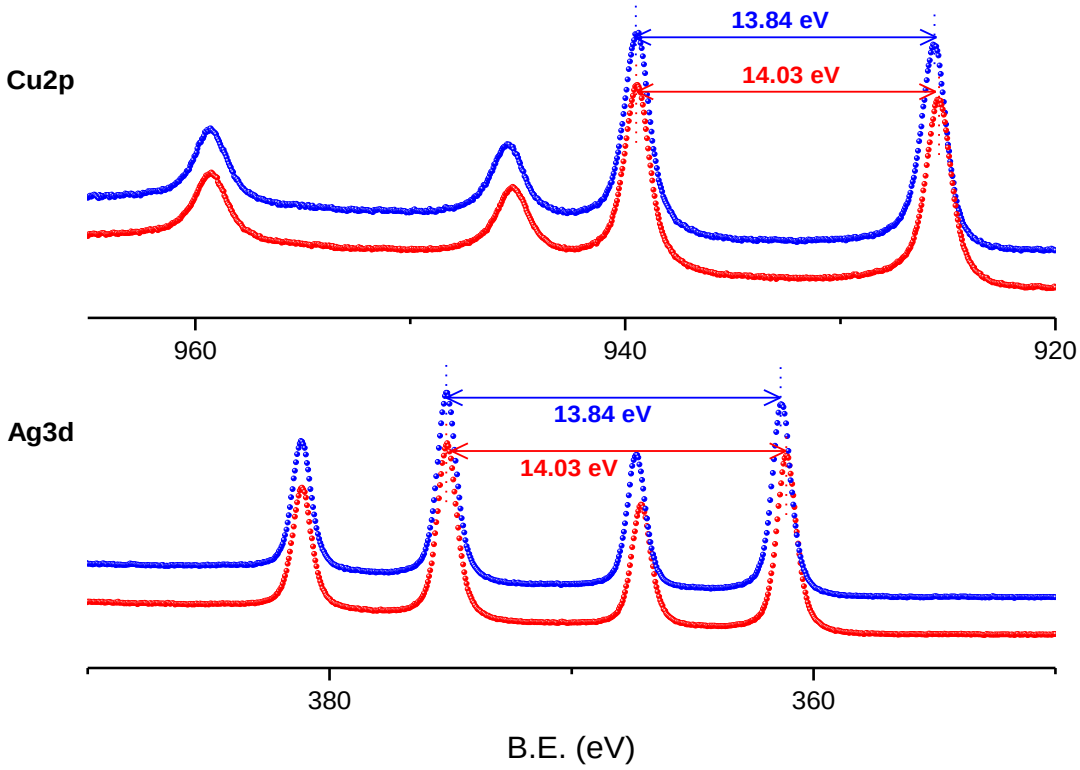

Figure 30. The XPS spectra of Cu2p and Ag3d regions of LbL assembled PEI-PSS-PAH / AgCu NAs ultra thin film subjected to +7 V(red) and –7 V (blue) external DC stress under square wave excitation at 10^{3} and 10^{-3}Hz.

When the binding energy differences between higher binding energy and lower binding energy were compared, binding energy difference of 14.03eV and 13.84eV under SQW pulses at 10^{3} Hz and at 10^{-3} Hz frequency respectively were detected for both Ag3d and Cu2p spin orbit splitting as depicted in Figure 30. Under high and the low frequencies (10^{3} Hz and 10^{-3} Hz) the shifts in peak positions of Ag3d spin orbit splitting were exactly as same as of Cu2p signifying that silver and copper are responding to external stimuli in same way revealing the fact that Ag and Cu atoms are in the same nanoalloy structure and their photoelectrons are similarly affected by the developed positive and negative potentials.

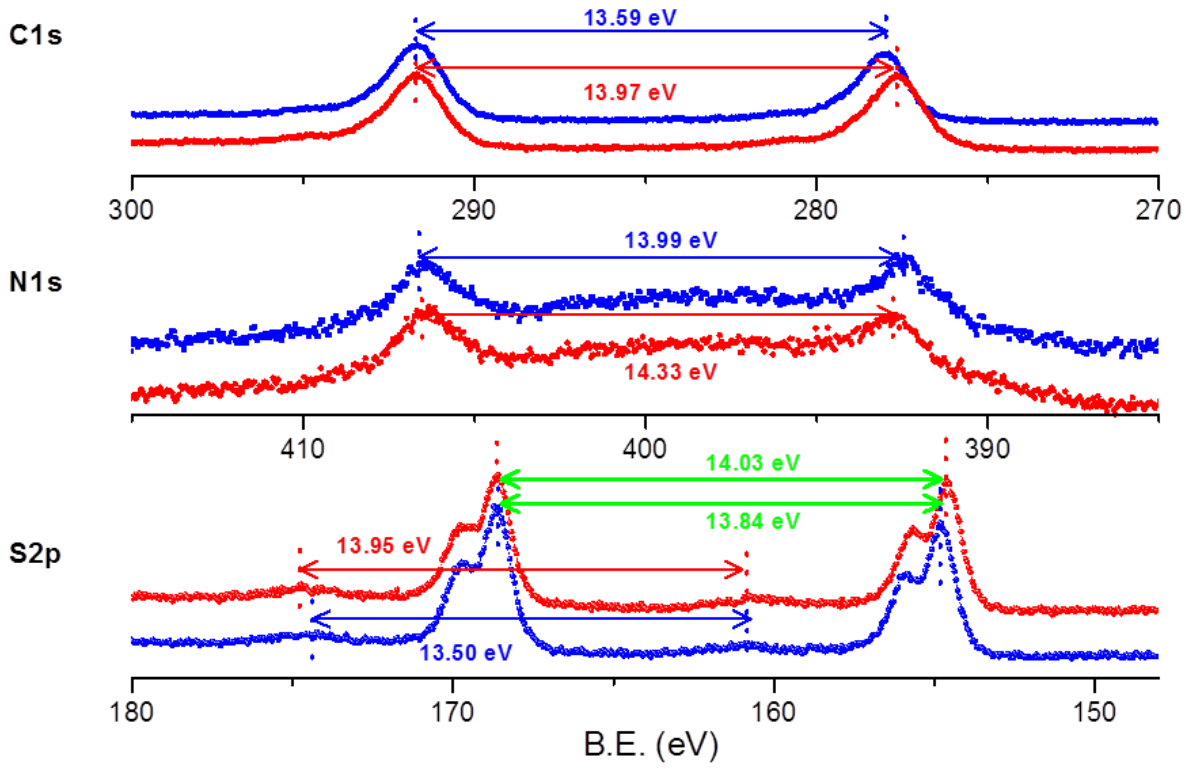

Figure 31. The XPS spectra of C1s, N1s and S2p regions of LbL assembled PEI-PSS-PAH / AgCu NAs ultra thin film subjected to +7 V(red) and –7V (blue) external DC stress under square wave excitation at 10^{3} and 10^{-3}Hz.

On the other hand binding energy difference under SQW pulses at 10^{3} Hz and at 10^{-3} Hz frequency for C1s (13.97eV and 13.59eV), N1s (14.33eV and 13.99eV) and S2p (13.95eV and 13.50eV) photoelectron peaks originating from the polyelectrolyte layers were different than Cu2p and Ag3d counterparts which is consistent with the fact that these peaks belongs to different layers not to nanostructure. As observed by Static XPS investigations previously, two different peaks were observed in the S2p region of XPS spectrum; one of them corresponding to the polyelectrolyte layers and the other one correspond to the stabilizer cysteine. Binding energy shifts of S2p belonging to sulphur of the cysteine, with binding

energy shifts of 14.03eV and 13.84eV, around AgCu NAs were also in agreement with the shifts in Ag3d and Cu2p binding energies for higher and lower frequencies where these shifts were obviously different for S2p belonging to the $-SO_3^-$ group of PSS layer.

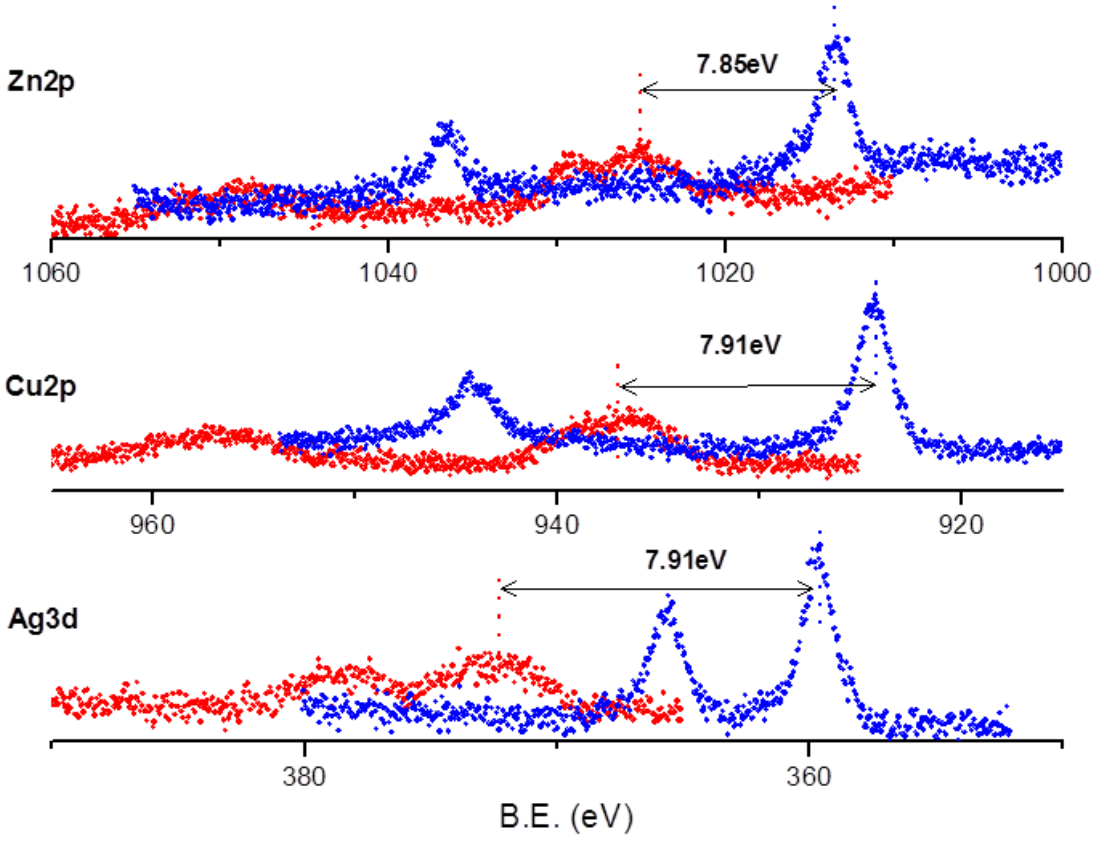

Figure 32. The XPS spectra of Zn2p, Cu2p and Ag3d regions of LbL assembled PEI-PSS-PAH / AgCu-Zn NAs ultra thin film subjected to +10 V (red) and –10V (blue) external DC stress.

Also the formation of ternary AgCu-Zn NAs was studied under +10 V and -10 V external DC stress to establish that silver, copper and zinc are responding to external stimuli in similar way with nearly same binding energy shifts 7.85 eV, 7.91 eV and 7.91 eV corresponding to Zn2p, Cu2p and Ag3d peaks as shown in Figure 32, due the fact that all of the Ag, Cu and Zn atoms are in the same nanoalloy structure and so their photoelectrons are similarly affected by the developed positive and negative potentials.

Therefore, both Static and Dynamic XPS attested the successful synthesis of AgCu NAs in the presence of very strong reducing agent hydrazine hydrate, stabilizing agent cysteine and complexing agent sodium citrate and construction of LbL assembled ultra thin polyelectrolyte layers of PEI, PSS, PAH and pre-synthesized citrate capped AgCu NAs.

3.5. ANTIBACTERIAL APPLICATIONS OF METAL NANOPARTICLES

3.5.1. Antibacterial Investigation of Ag Nanoparticles and AgCu Nanoalloys Dispersed in Solution

3.5.1.1. Antibacterial Test on Solid Agar Plates

Sterile LB agar plates were prepared from gelation of nutrient media containing all elements which are required for bacteria growth and these LB agar plates are appropriate for the visual observation of colony growth. Before spreading E.*coli* cells on agar plates, bacteria cells were grown to optical densities of 0.2 OD, 0.1OD and 0.05 OD, and then inoculated with same concentration (0.01M) of Ag-only nanoparticle or AgCu nanoalloy solutions under same conditions. All agar plates were left upside down in incubator to prevent any possible weeping. After overnight incubation of the LB agar plates inoculated with known concentration of bacteria and Ag NPS or AgCu NAs, antibacterial effectiveness of nanoparticles and nanoalloys were compared by the visual colony growth on plates. Figure 33, shows the representative images of LB agar plates after 18 hours incubation time including both Ag-only NPs and AgCu NAs containing plates at different *E. coli* DH5α concentrations. These bacteria concentrations were chosen as much higher than the realistic bacteria concentrations of real-life systems in order to highlight the superior antibacterial effectiveness of AgCu NAs over Ag-only NPs even at lower concentrations.

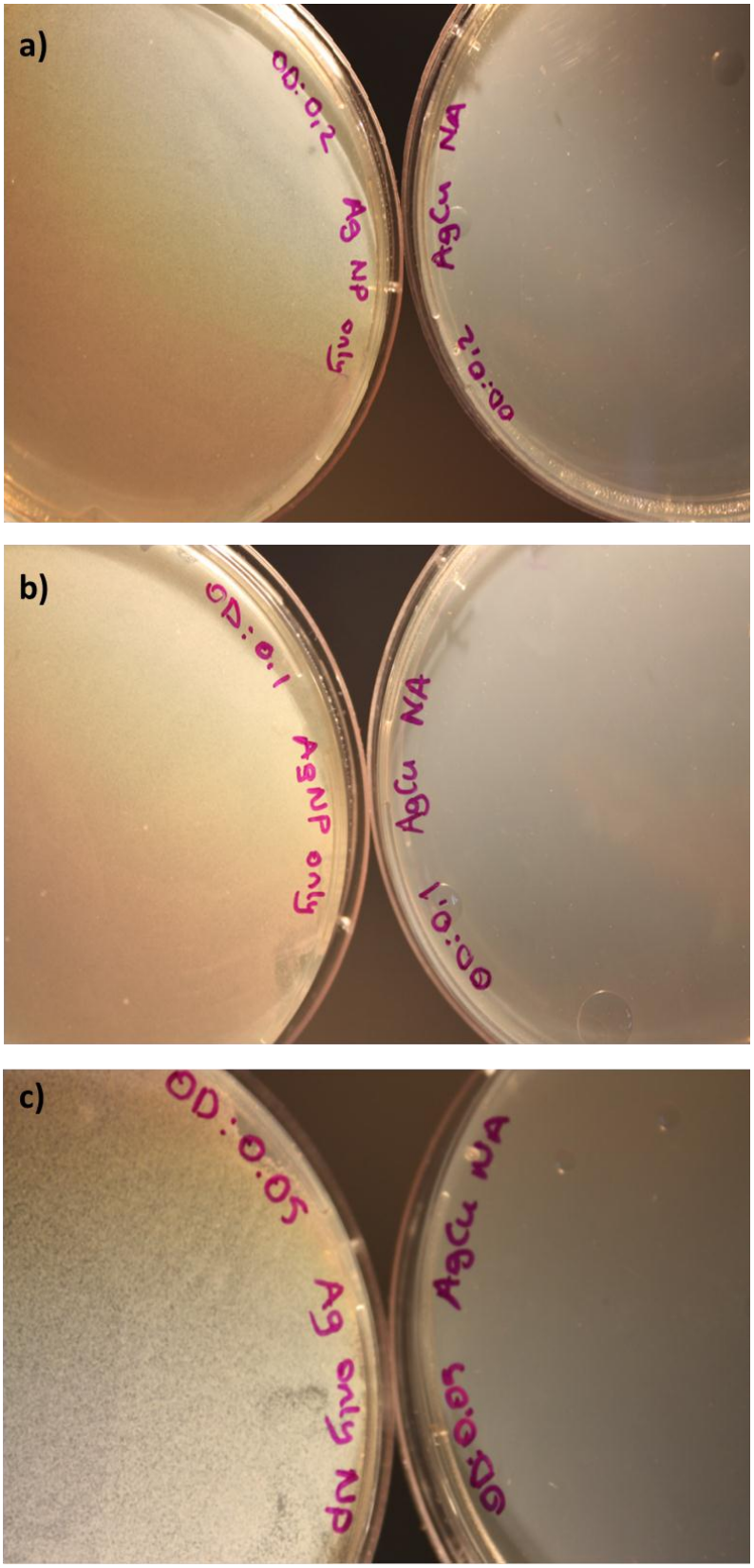

Figure 33. Representative images of agar plates containing an equal amount of Ag-only nanoparticles bacteria colony formation and AgCu nanoalloys without colonies with initial *E. coli* DH5α concentration at **(a)** 0.2 OD_{600} **(b)** 0.1 OD_{600} and **(c)** 0.05 OD_{600}.

In Figure 33 (A) and (B), corresponding to the 0.2 OD_{600} and 0.1 OD_{600} initial bacteria concentration respectively, *E. coli* DH5α colonies spread over whole agar plates containing Ag-only NPs and these colonies could not be distinguished from each other because of their high number. For lower *E. coli* DH5α concentration at 0.05 OD_{600} in Figure 33 (C) colonies on Ag-only NPs inserted plates can be observable as cloudy dots with uncountable number. On the other hand, for all AgCu NAs containing plates no bacterial colony growth was observable indicating total bacteria-killing effect of AgCu NAs superior to Ag-only NPs.

3.5.1.2. Batch Growth Profiles of Ag Nanoparticles and AgCu Nanoalloys

Bacterial population growth in the presence of synthesized Ag-only NPs and/or AgCu NAs was analyzed by the growth curve, which is obtained by the determination of cell number in the culture at the beginning and then after certain time intervals, of *E. coli* DH5α inoculated in liquid LB medium. Because of the fact that all bacteria cells in a liquid culture volume cannot be counted, cell density that is determined optically in spectrophotometer is related with the number of bacteria at a specified sample volume. In the spectrophotometer, the light beam passing through analysis cuvette containing sample culture is scattered by bacteria cells, so this scattering light intensity which is optical density, is directly proportional with the bacterial cell number. Optical density measurements were performed at a constant wavelength of 600 nm to compare the intensity of light scattering.

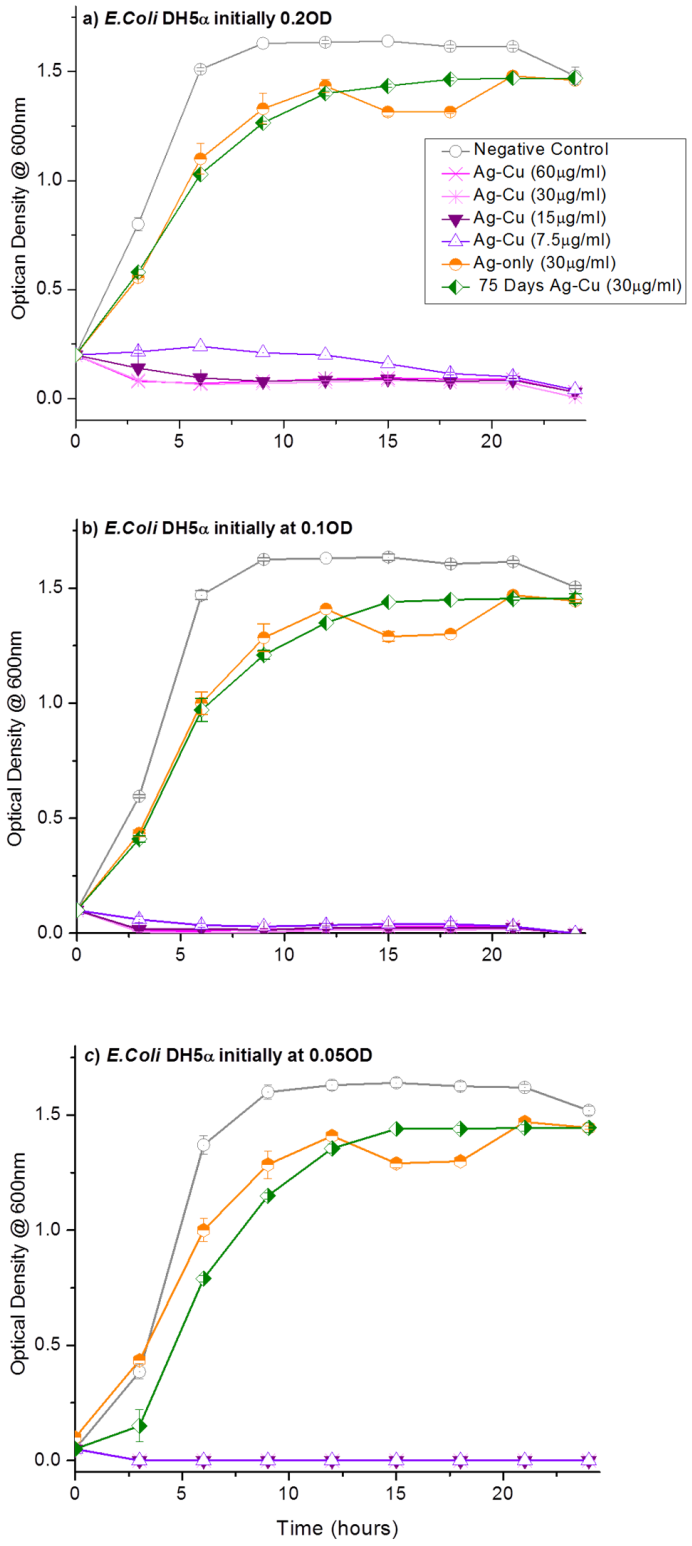

Figure 34. Representative batch growth profiles in the presence of Ag-only nanoparticles and AgCu nanoalloys for initial concentrations of *E.Coli* DH5α: **(a)** 0.2 OD_{600} and **(b)** 0.1 OD_{600} and **(c)** 0.05 OD_{600}.

For our antibacterial analysis, *E. coli* DH5α bacterial density at 0.2 OD_{600}, 0.1 OD_{600} and 0.05 OD_{600} were used as initial concentration of bacteria cell and inoculated under constant agitation in the presence of Ag-only NPs and AgCu NAs at different concentrations under same controllable parameters such as incubation time, concentration, incubation and application conditions. Optical density of suspensions containing *E. coli* cells, liquid LB broth and Ag-only or AgCu nanoclusters was monitored by the change in the optical density at a constant wavelength of 600 nm after each 3 hours during 24 hours incubation period. Dynamics of the bacterial growth was depicted in Figure 34 for different concentrations of bacteria and metal solutions. As it is clear in the figure, Ag-only nanoparticles show a decrease in the growth of *E. coli* DH5α for all the three optical densities when compared to the negative control. In the case of AgCu nanoalloys, optical density not only decreased for all 0.2 OD, 0.1 OD and 0.05 OD initial bacterial concentrations and but also did not increase within the total incubation period as a result of irreversible inhibition of bacterial growth due to bacteria killing activity of nanoalloys. This decisive dual antibacterial action of AgCu NAs was sustainable even after 24 hours, whereas Ag-only nanoparticle supplemented culture cells reached to the degree of the stationary phase. AgCu NAs have definitely better antibacterial property than Ag-only NPs even at lower concentrations. Additionally, for the analysis of antibacterial investigations it is remarkable to state that AgCu NAs, hydrazine hydrate was not carried to the final nanoalloy product due its total decomposition during reduction process so did not have additional bacteria-killing effect on synthesized nanoalloys

When growth curves in Figure 34 (a), (b) and (c) for 75 days old AgCu NAs were analyzed. A sharp decrease existed in the antibacterial effectiveness of old NAs solution and their growth curves resemble to growth curves of Ag-only NPs for different bacteria concentrations. It is obvious that, AgCu NAs lost their novel dual antibacterial activity. Accordingly irreversible inhibition of bacterial growth could not be proceed and they can only

cause a decrease in the growth profile of bacteria cells as Ag-only NPs. The decline in antibacterial effectiveness after 75 days was attributed to the copper oxide contamination of AgCu NAs during storage period under ambient conditions as the formation of oxide species was monitored from the Cu 2p region of AgCu NAs' XPS spectrum after storage period.

For further investigation on antibacterial characteristics of AgCu NAs after formation of ternary AgCu-Zn alloys the zinc salt was added to suppress the copper oxide contamination problem and bacterial growth profiles of AgCu-Zn ternary alloys were also monitored to control whether the antibacterial efficiency of nanoalloys prolonged or not in the presence of zinc. Figure 35 (a) and (b) depict the dynamics of bacterial growth of AgCu and AgCu-Zn NAs for fresh and 14 weeks old solutions.

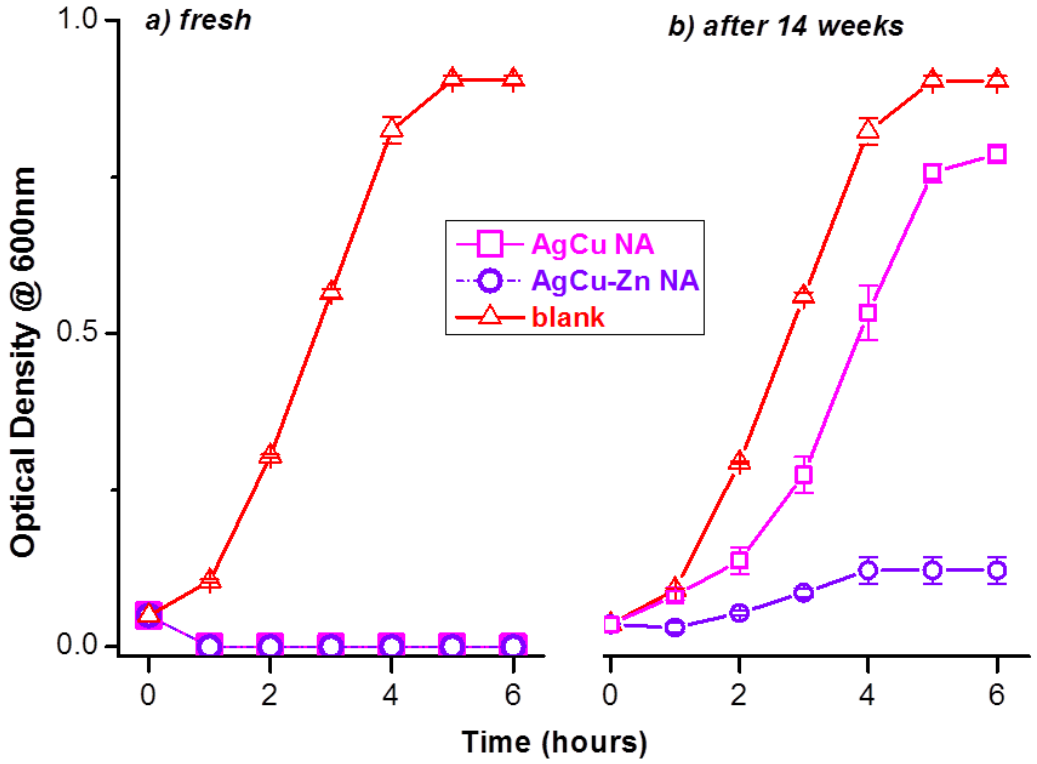

Figure 35. Representative batch grow profiles in the presence of AgCu and AgCuZn nanoalloys **(a)** fresh and **(b)** after 14 weeks

Inhibition of bacterial growth was similar for both of the freshly prepared AgCu and AgCu-Zn ternary nanoalloy solutions. But then again the antibacterial effectiveness of AgCu NAs sharply decreased after 14 weeks storage period due to copper oxide formation. Although there was decline in the effectiveness of AgCu-Zn ternary NAs after 14 weeks, they were far more effective than their AgCu counterparts as consistent with the prolonged stability of AgCu-Zn NAs against copper oxide contamination as a result of sacrificial anode (zinc) addition.

3.5.1.3. Quantification of Antibacterial Efficiency

Colony forming ability of bacteria cells is used to describe the antibacterial property of the nanoclusters in quantitative way. Biochemically induced irreversible inhibition of bacterial growth as a result of death of bacteria and inhibition of bacterial growth are determined quantitatively by determination of Minimum Bactericidal Concentration (MBC) and Minimum Inhibitory Concentration (MIC) for synthesized nanoclusters. MIC values express the inhibition ability against growth of bacterial cells as lowest concentration of nano-particles/alloys and MBC values express the lowest concentration nano-particles/alloys inhibiting the bacteria colony growth in terms of killing 99.9% of bacteria.

MIC values, in the case of 2-512 times dilution of NAs or NAs solutions after 24 hours incubation at 37°C under constant shaking at 225 rpm, was determined via following visual turbidity of the tubes both before and after the incubation period for Ag NPs and AgCu NAs to reveal the antibacterial effectiveness of particles. MBC was also determined after 18 hour incubation at 37°C by plating 100µl LB broth and bacteria having no bacterial cell growth that was chosen from MIC analysis with no visual colony growth as observable turbidity, on agar plates as described in details in experimental part.

Table 2. MIC (μg ml^{-1}) and MBC (μg ml^{-1}) of silver nanoparticles and silver – copper nanoalloys for *E. coli* DH5α

MIC/μg ml^{-1}		**MBC/μg ml^{-1}**	
Ag NP	**AgCu NA**	**Ag NP**	**AgCu NA**
>150 μg ml^{-1}	0.5 μg ml^{-1}	N/A	0.5 μg ml^{-1}

Table 2 shows the MIC and MBC values for both nanoparticles and nanoalloys for better clarification of superior antibacterial activity of AgCu NAs over Ag-only NPs. Ag Cu NAs are much more effective and have lower MIC value of 0.5μg/ml than their Ag- only counterparts in terms of antibacterial activity. Moreover dual antibacterial action of AgCu NAs was exposed with MBC at 0.5μg/ml as same as its MIC, where the bactericidal effectiveness of the Ag-only NPS cannot be defined in terms of MBC. This revealed that the concentrations at which the bacteria growth is irreversibly inhibited were also adequate to kill the bacteria in the growth medium totally.

AgCu nanoalloys lost their antibacterial efficiency because of the oxide contamination of the copper particles in the alloy and this was discussed previously with batch growth profiles of fresh and old nanoalloys. Additionally, it was shown that zinc addition forming AgCu-Zn ternary nanoalloys prolongs the antibacterial activity excessively as represented in their batch growth profiles. Henceforward, MIC and MBC values of AgCu NAs and AgCu-Zn ternary NAs were used to quantify the bacterio-static and bactericidal properties. Corresponding MIC and MBC values for fresh, 7weeks and 14weeks old nanoalloys are given in Table 3.

Table 3. Comparison of the Antibacterial Activity (MIC and MBC values) of fresh, 7 weeks-old and 14 weeks-old AgCu NAs and AgCu-Zn ternary NAs on *E. coli* DH5α

Samples	MIC/μg ml^{-1}	MBC/μg ml^{-1}
Fresh AgCu	0.5	0.5
7 weeks-old AgCu	1.0	1.0
14 weeks-old AgCu	2.0	2.0
Fresh AgCu-Zn	1.0	1.0
7 weeks-old AgCu-Zn	0.5	0.5
14 weeks-old AgCu-Zn	1.0	4.0

AgCu-Zn NAs show less antibacterial activity at the beginning of storage period with MIC value of 1.0 μg/ml as compared to their AgCu counterparts with MIC value of 0.5 μg/ml. But at the end of 7 weeks, they are more active and have lower MIC value of 0.5 μg/ml than AgCu NAs in terms of bacterio-static activity and though AgCu-Zn ternary NAs had a decline in their antibacterial effectiveness at the end of 14 weeks, these particles were still more effective than AgCu NAs as well. This retained antibacterial property is attributed to the prolonged stability of ternary nanoalloys with the addition of Zn and the formation of strong and tough antibacterial zinc-oxide species.[25, 105]

Assessment of irreversible inhibition of bacterial growth was performed by comparing of the bactericidal effectiveness so as the MBC values of AgCu and AgCu-Zn ternary NAs. Except for 14 weeks old AgCu-Zn NAs, MBC values revealed that the concentrations at which the bacteria growth is inhibited, were also adequate to kill the bacteria in the growth medium totally for all samples. 14 weeks old AgCu-Zn ternary nanoalloys inhibited observable bacterial growth effectively at lower concentrations compared to AgCu showing a decline in bactericidal effectiveness.

The bacterial assays should be performed with a known number of cells for accuracy, stated as CFU/ml although this colony forming units can be derived from the optical density readings roughly where optical density readings are directly related to the bacterial cell number. Also the inhibition can only be quantified by known concentration of bacteria as wells as by colony forming units of bacteria used in the experiments. Colony forming abilities of nanoparticles and nanoalloys were deduced by plating dilution series of bacteria with different dilutions in the range of 10^0 - 10^7 from initial culture at 0.2OD on agar plates containing dilutions of Ag NPs and AgCu NAs with 10^1-10^5 dilutions through sterile diluent LB broth and water. Then agar plates were incubated for 18 h at 37 °C before counting observable colonies. Initial bacterial concentrations of optical densities at 0.05, 0.1 and 0.2 were determined as $1.7x10^8$ CFU/ml, $3.5x10^8$ CFU/ml, and $7.0x10^8$ CFU/ml respectively by calculating the ratio between number of colonies on the plate for given dilution factor and volume of inoculated culture on the agar plate.

Table 4: Effect of different concentrations of NP and NAs on dilution series of *E. coli* DH5α

	Number of colonies for given dilution factors (DF)							
NPs/NAs	**DF**	**1**	**10^1**	**10^2**	**10^3**	**10^4**	**10^5**	**10^6**	**10^7**
AgCu(30 μg/ml)		0	0	0	0	0	0	0	0
AgCu(3 μg/ml)		0	0	0	0	0	0	0	0
AgCu(0.3 μg/ml)		UNC	UNC	UNC	316	542	42	42	0
AgCu (30 ng/ml)		UNC	UNC	UNC	3040	388	372	192	14
Ag (150 μg/ml)		UNC	UNC	UNC	3376	960	482	304	32
Ag (15 μg/ml)		UNC	UNC	UNC	3208	1496	860	236	32
No NP/NA		UNC	UNC	UNC	UNC	1313	703	445	18

Table 4 represents the effect of different concentrations of Ag-only NPs and AgCu NAs on dilution series and the abbreviation UNC represents the uncountable number of observable bacterial colonies on agar plates. Number of colonies quantifies the antibacterial efficiency and states expressly the superior antibacterial activity of AgCu NAs over Ag-only NPs. But also, due to colony forming abilities of nano-sized metals it is remarkable that as concentration of NPs or NAs decreases their antibacterial efficiency decreases.

With the intention of quantification of difference between the antibacterial effectiveness of fresh and old AgCu NAs to analyze the oxide contamination consequences, and also to effect of Zn addition colony forming abilities were studied for fresh and 14 weeks of AgCu binary and AgCu-Zn ternary NAs in the presence of different concentrations of NP and NAs on dilution series of *E. coli* DH5α. The results, which were obtained by before counting observable colonies after incubation of agar plates containing dilutions of Ag NPs and AgCu NAs for 18 h at 37 °C with different dilutions in the range of $10^0 – 10^3$ from initial *E. coli* DH5α culture at 0.2OD, were represented in Table 5. Due to colony forming abilities so as the number of growth bacteria, both fresh samples of AgCu binary and AgCu-Zn ternary NAs are highly efficient in terms of antibacterial activity, whereas antibacterial efficiency has decreased as a result of copper-oxide contamination after 14 weeks storage period under ambient conditions. Nonetheless there exists a sharp decline in the antibacterial effectiveness of AgCu NAs therewith Zn addition prolongs the stability of AgCu NAs so as the antibacterial activity as represented with colony forming abilities of samples.

Table 5: Effect of different concentrations of NAs on dilution series of *E. coli* DH5α for fresh and 14 weeks old samples

	Number of colonies for given dilution factors (DF)			
NAs	**DF 1**	**10^1**	**10^2**	**10^3**
Fresh				
AgCu (30 µg/ml)	0	0	0	0
AgCu(3 µg/ml)	0	0	1	0
AgCu (0.3µg/ml)	972	201	32	10
AgCu-Zn (30 µg/ml)	0	0	0	0
AgCu-Zn (3 µg/ml)	147	24	0	4
AgCu-Zn (0.3 µg/ml)	1332	84	38	4
14 Weeks Old				
AgCu (30 µg/ml)	0	1	0	0
AgCu(3 µg/ml)	417	17	3	2
AgCu (0.3 µg/ml)	1984	194	64	23
AgCu-Zn(30 µg/ml)	1	0	0	0
AgCu-Zn(3 µg/ml)	347	5	3	2
AgCu-Zn (0.3 µg/ml)	1224	225	36	15

3.5.2. Antibacterial Investigation of Ag Nanoparticles and AgCu Nanoalloys Incorporated Ultra Thin Films

Before exploration of antibacterial characteristics of ultra thin films, they were prepared by LbL assembly as described in experimental part in details with the integration of excellent antibacterial reagent AgCu NAs on the top of PEI-PSS-PAH multilayers which were prepared by immersion into 1g/l polyelectrolyte solutions for 40 min and overnight immersion into nanoalloy solution. As the next step LbL samples were placed into solid agar plates and 100µl of E.*coli* strain at OD_{600} = 0.6 ($2.1x10^7$ CFU/ml) was inoculated directly on the ultra thin film samples. Also 100µl of liquid LB medium was injected on the samples to elicit nutrients for bacterial growth and to prevent desiccation of bacterial cells.

AgCu NAs containing LbL films were investigated to verify the innovative approach of surface functionalization for antibacterial purposes after inoculation E.*coli* strain on the ultra thin films and overnight incubation at 37^{o}C. Antibacterial property of AgCu NAs LbL films were assessed by focusing on visual bacteria colonization on ultra thin films using 100x optical microscope and E.*coli* colonies are recognized as white smudge on the films. Images of two different sides (right and left) of the sample films have been taken by this optical microscope to monitor the difference between the regions where bacteria colonies developed on the ultra thin layers containing AgCu NAs and PEI-PSS-PAH layers (Figure 36). Because very high bacterial concentration of $2.1x10^7$ CFU/ml was used for inoculation of E.*coli* cells and very low amount of AgCu NAs can be inserted by LbL deposition technique on the PEI-PSS-PAH ultrathin layers growth of E.*coli* colonies can be observed slightly on the films as depicted in Figure 36 (a) and (c). On the other hand when reference sample consisting of only polyelectrolyte multilayers without AgCu NAs and the AgCu NAs containing polyelectrolyte layers on glass substrate have been compared, growth of bacterial colonies on PEI-PSS-PAH film, as represented for different regions of the film in Figure (b) and (d), is strikingly high

and these results unroll the antibacterial property of AgCu NAs even at very small amounts and against very high bacterial concentration. In retrospect, our innovative approach of combining two antibacterial metal particles enters upon a new phase for antibacterial reagent and using layer-by-layer deposition technique construction of antibacterial thin layers is established.

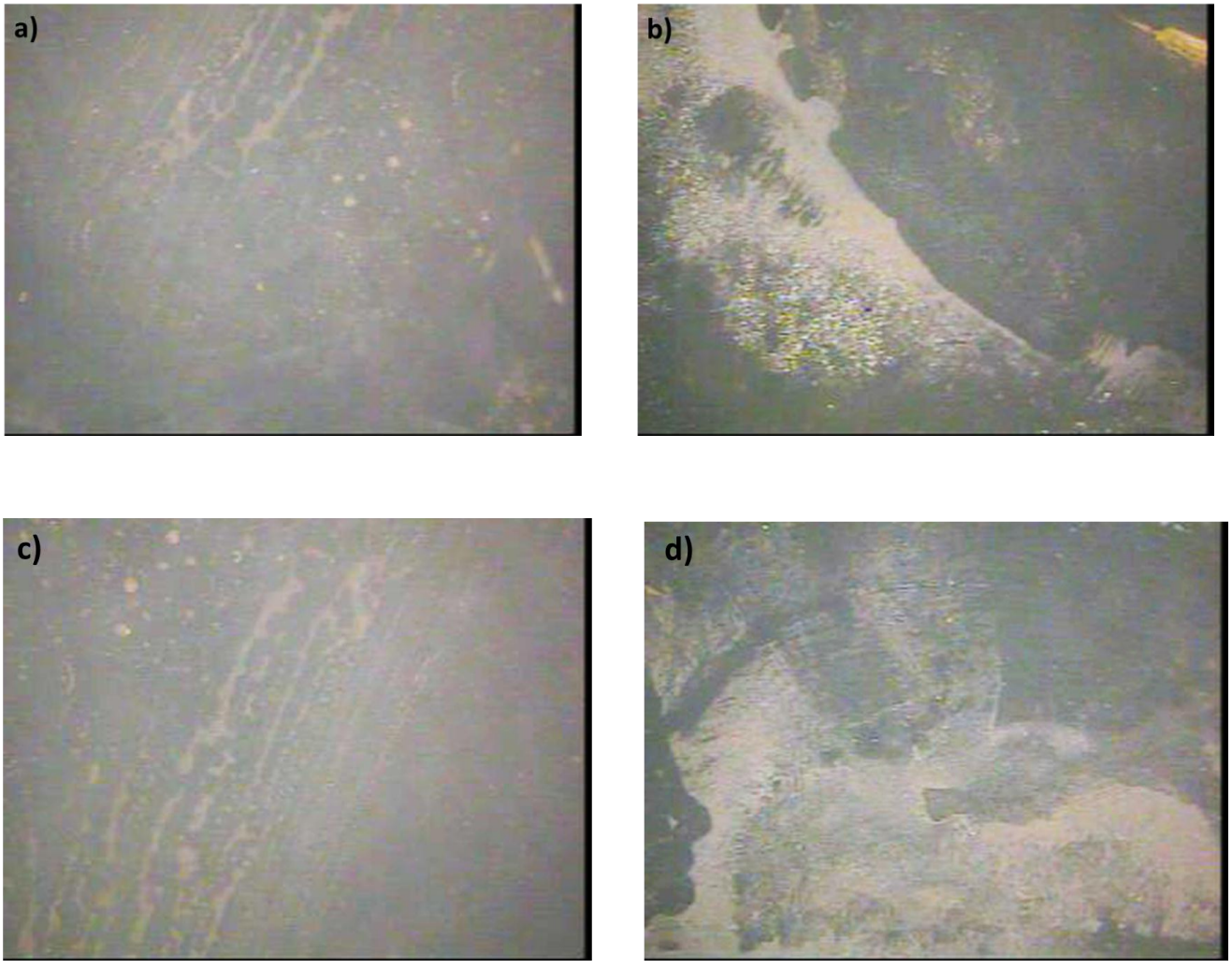

Figure 36. Microscope images of **(a)** AgCu/PEI-PSS-PAH film right side **(b)** PEI-PSS-PAH film right side **(c)** AgCu/PEI-PSS-PAH film left side and **(d)** PEI-PSS-PAH film left side.

4. CONCLUSIONS

In this thesis, preparation, characterization and antibacterial investigation of ultra thin films containing silver-copper nanoalloys using layer-by-layer assembly were presented. Combination of two antibacterial nano sized metal particles increased the antibacterial efficiency and layer-by-layer assembly provided an opportunity to construct ultra thin films containing these antibacterial nanoparticles. These thin films were also characterized by spectroscopic techniques.

As first contribution to this thesis work, preparation of Ag-only nanoparticles and AgCu nanoalloys were comprehensively investigated with the intention of preventing oxidation of highly reactive copper to copper oxide to synthesize stable nanoalloys. Stable AgCu NAs synthesis was managed in the presence of very strong reducing agent hydrazine hydrate, stabilizer cysteine and complexing agent sodium citrate. LbL films were constructed through the sequential adsorption of positively charged polyelectrolytes PEI and PAH, negatively charged PSS and citrate capped nanoparticles and nanoalloys.

In the second part of the thesis characterization of the ultra thin films was represented firstly via optical spectroscopy and then by Static and Dynamic XPS analysis. Chemical and elemental information were acquired via Static XPS method to confirm the successful preparation of Ag-only and AgCu nanoparticles containing thin films without any copper oxide contamination attributable to characteristic binding energies, spin orbit splittings, shape of the peaks and oxide satellites. For further analysis in the direction of extracting additional information from AgCu NAs-PEI-PSS-PAH ultra thin films, samples were analyzed under external DC voltage as well as square wave pulse stresses at 10^{-3} -10^{3} Hz frequency to follow the response of Ag, Cu and polyelectrolyte layer components against external electrical stimuli by comparing the measured binding energy differences between the split peaks arising from application of the square wave pulses. The results showed that Ag and Cu are

together in the alloy structure since they respond to external stimuli in the same way which is different that the response of C1s, N1s and S2p regions arising from polyelectrolyte layers.

Lastly, the antibacterial properties of Ag nanoparticles and AgCu nanoalloys were investigated to assess the bactericidal effectiveness of these particles against E. *coli* DH5α stain. Novel dual antibacterial action of AgCu NAs was confirmed by batch growth profiles, agar plate tests and determination of colony forming abilities of particles in addition to their much more lower MIC and MBC values than Ag-only nanoparticles. Also the durability of AgCu NAs to prolong both antibacterial activity and air-stability was investigated in the presence of sacrificial anode Zn and the results indicated that Zn preserve these properties of AgCu NAs. Finally the ultra thin films containing AgCu NAs showed antibacterial property against very high bacterial concentration as confirmed by the visual colony formation on LbL films.

5. REFERENCES

1. Shon, Y. S.; Dawson, G. B.; Porter, M.; Murray, R. W., Monolayer-protected bimetal cluster synthesis by core metal galvanic exchange reaction. *Langmuir* **2002,** *18* (10), 3880-3885.
2. Gerbec, J. A.; Magana, D.; Washington, A.; Strouse, G. F., Microwave-enhanced reaction rates for nanoparticle synthesis. *Journal of the American Chemical Society* **2005,** *127* (45), 15791-15800.
3. Schmid, G., *Clusters and colloids: from theory to applications*. Wiley-VCH: 2008.
4. Feldheim, D. L.; Foss, C. A., *Metal nanoparticles: synthesis, characterization, and applications*. CRC: 2002.
5. Khanna, P. K.; Singh, N.; Charan, S.; Viswanath, A. K., Synthesis of Ag/polyaniline nanocomposite via an in situ photo-redox mechanism. *Materials Chemistry and Physics* **2005,** *92* (1), 214-219.
6. Mukherjee, P.; Ahmad, A.; Mandal, D.; Senapati, S.; Sainkar, S. R.; Khan, M. I.; Parishcha, R.; Ajaykumar, P. V.; Alam, M.; Kumar, R., Fungus-mediated synthesis of silver nanoparticles and their immobilization in the mycelial matrix: a novel biological approach to nanoparticle synthesis. *Nano Letters* **2001,** *1* (10), 515-519.
7. Burda, C.; Chen, X.; Narayanan, R.; El-Sayed, M. A., Chemistry and properties of nanocrystals of different shapes. *Chemical Reviews-Columbus* **2005,** *105* (4), 1025-1102.
8. Karadas, F.; Ertas, G.; Ozkaraoglu, E.; Suzer, S., X-ray-induced production of gold nanoparticles on a SiO2/Si system and in a poly (methyl methacrylate) matrix. *Langmuir* **2005,** *21* (1), 437-442.
9. Ozkaraoglu, E.; Tunc, I.; Suzer, S., Preparation of Au and Au-Pt nanoparticles within PMMA matrix using UV and X-ray irradiation. *Polymer* **2009,** *50* (2), 462-466.
10. Henglein, A., Physicochemical properties of small metal particles in solution:" microelectrode" reactions, chemisorption, composite metal particles, and the atom-to-metal transition. *The Journal of Physical Chemistry* **1993,** *97* (21), 5457-5471.
11. Grouchko, M.; Kamyshny, A.; Ben-Ami, K.; Magdassi, S., Synthesis of copper nanoparticles catalyzed by pre-formed silver nanoparticles. *Journal of Nanoparticle Research* **2009,** *11* (3), 713-716.
12. Reetz, M. T.; Helbig, W., Size-selective synthesis of nanostructured transition metal clusters. *Journal of the American Chemical Society* **1994,** *116* (16), 7401-7402.
13. Henglein, A.; Giersig, M., Formation of colloidal silver nanoparticles: capping action of citrate. *The Journal of Physical Chemistry B* **1999,** *103* (44), 9533-9539.
14. Dubas, S. T.; Kumlangdudsana, P.; Potiyaraj, P., Layer-by-layer deposition of antimicrobial silver nanoparticles on textile fibers. *Colloids and Surfaces A: Physicochemical and Engineering Aspects* **2006,** *289* (1-3), 105-109.
15. Bootharaju, M. S.; Pradeep, T., Uptake of toxic metal ions from water by naked and monolayer protected silver nanoparticles: An X-ray photoelectron spectroscopic investigation. *The Journal of Physical Chemistry C* **2010,** *114* (18), 8328-8336.
16. Chen, S.; Sommers, J. M., Alkanethiolate-protected copper nanoparticles: spectroscopy, electrochemistry, and solid-state morphological evolution. *The Journal of Physical Chemistry B* **2001,** *105* (37), 8816-8820.
17. Cioffi, N.; Ditaranto, N.; Torsi, L.; Picca, R. A.; De Giglio, E.; Sabbatini, L.; Novello, L.; Tantillo, G.; Bleve-Zacheo, T.; Zambonin, P. G., Synthesis, analytical characterization and bioactivity of Ag and Cu nanoparticles embedded in poly-vinyl-methyl-ketone films. *Analytical and bioanalytical chemistry* **2005,** *382* (8), 1912-1918.

18. Aryal, S.; Bkc, R.; Dharmaraj, N.; Bhattarai, N.; Kim, C. H.; Kim, H. Y., Spectroscopic identification of SAu interaction in cysteine capped gold nanoparticles. *Spectrochimica Acta Part A: Molecular and Biomolecular Spectroscopy* **2006,** *63* (1), 160-163.
19. Varghese, M. V.; Dhumal, R. S.; Patil, S. S.; Paradkar, A. R.; Khanna, P. K., Synthesis and In-Vitro Antimycobacterial Studies of Cysteine Capped silver Nano-Particles. *Synthesis and Reactivity in Inorganic, Metal-Organic, and Nano-Metal Chemistry* **2009,** *39* (9), 554-558.
20. Wei, Y.; Chen, S.; Kowalczyk, B.; Huda, S.; Gray, T. P.; Grzybowski, B. A., Synthesis of Stable, Low-Dispersity Copper Nanoparticles and Nanorods and Their Antifungal and Catalytic Properties. *The Journal of Physical Chemistry C* **2010,** *114* (37), 15612–15616.
21. Elechiguerra, J. L.; Burt, J. L.; Morones, J. R.; Camacho-Bragado, A.; Gao, X.; Lara, H. H.; Yacaman, M. J., Interaction of silver nanoparticles with HIV-1. *Journal of Nanobiotechnology* **2005,** *3* (6), 1-10.
22. Cioffi, N.; Torsi, L.; Ditaranto, N.; Tantillo, G.; Ghibelli, L.; Sabbatini, L.; Bleve-Zacheo, T.; D'Alessio, M.; Zambonin, P. G.; Traversa, E., Copper nanoparticle/polymer composites with antifungal and bacteriostatic properties. *Chem. Mater* **2005,** *17* (21), 5255-5262.
23. Sambhy, V.; MacBride, M. M.; Peterson, B. R.; Sen, A., Silver bromide nanoparticle/polymer composites: dual action tunable antimicrobial materials. *Journal of the American Chemical Society* **2006,** *128* (30), 9798-9808.
24. Martinez-Castanon, G. A.; Nino-Martinez, N.; Martinez-Gutierrez, F.; Martinez-Mendoza, J. R.; Ruiz, F., Synthesis and antibacterial activity of silver nanoparticles with different sizes. *Journal of Nanoparticle Research* **2008,** *10* (8), 1343-1348.
25. Zhang, L.; Jiang, Y.; Ding, Y.; Povey, M.; York, D., Investigation into the antibacterial behaviour of suspensions of ZnO nanoparticles (ZnO nanofluids). *Journal of Nanoparticle Research* **2007,** *9* (3), 479-489.
26. Malcher, M.; Volodkin, D.; Heurtault, B.; Andre, P.; Schaaf, P.; Mo hwald, H.; Voegel, J. C.; Sokolowski, A.; Ball, V.; Boulmedais, F., Embedded silver ions-containing liposomes in polyelectrolyte multilayers: Cargos films for antibacterial agents. *Langmuir* **2008,** *24* (18), 10209-10215.
27. Falletta, E.; Bonini, M.; Fratini, E.; Lo Nostro, A.; Pesavento, G.; Becheri, A.; Lo Nostro, P.; Canton, P.; Baglioni, P., Clusters of poly (acrylates) and silver nanoparticles: structure and applications for antimicrobial fabrics. *The Journal of Physical Chemistry C* **2008,** *112* (31), 11758-11766.
28. Ruparelia, J. P.; Chatterjee, A. K.; Duttagupta, S. P.; Mukherji, S., Strain specificity in antimicrobial activity of silver and copper nanoparticles. *Acta biomaterialia* **2008,** *4* (3), 707-716.
29. Smoukov, S. K.; Bishop, K. J. M.; Kowalczyk, B.; Kalsin, A. M.; Grzybowski, B. A., Electrostatically "Patchy" Coatings via Cooperative Adsorption of Charged Nanoparticles. *Journal of the American Chemical Society* **2007,** *129* (50), 15623-15630.
30. Decher, G., Fuzzy nanoassemblies: toward layered polymeric multicomposites. *Science* **1997,** *277* (5330), 1232.
31. Decher, G.; Schlenoff, J. B., *Multilayer thin films*. Wiley Online Library: 2003.
32. Tang, Z.; Wang, Y.; Podsiadlo, P.; Kotov, N. A., Biomedical Applications of Layerâ€□byâ€□Layer Assembly: From Biomimetics to Tissue Engineering. *Advanced Materials* **2006,** *18* (24), 3203-3224.
33. Dai, J.; Bruening, M. L., Catalytic nanoparticles formed by reduction of metal ions in multilayered polyelectrolyte films. *Nano Letters* **2002,** *2* (5), 497-501.

34. Dubas, S. T.; Schlenoff, J. B., Factors controlling the growth of polyelectrolyte multilayers. *Macromolecules* **1999,** *32* (24), 8153-8160.
35. Decher, G.; Eckle, M.; Schmitt, J.; Struth, B., Layer-by-layer assembled multicomposite films. *Current opinion in colloid & interface science* **1998,** *3* (1), 32-39.
36. Srivastava, S.; Kotov, N. A., Composite layer-by-layer (LBL) assembly with inorganic nanoparticles and nanowires. *Accounts of chemical research* **2008,** *41* (12), 1831-1841.
37. Podsiadlo, P.; Choi, S. Y.; Shim, B.; Lee, J.; Cuddihy, M.; Kotov, N. A., Molecularly engineered nanocomposites: layer-by-layer assembly of cellulose nanocrystals. *Biomacromolecules* **2005,** *6* (6), 2914-2918.
38. Brender, C.; Danino, M., Screening in Short Polyelectrolyte Chains. A Monte Carlo Study. *The Journal of Physical Chemistry* **1996,** *100* (44), 17563-17567.
39. Lourenço, J. M. C.; Ribeiro, P. A.; do Rego, A. M. B.; Fernandes, F. M. B.; Moutinho, A. M. C.; Raposo, M., Counterions in Poly (allylamine hydrochloride) and Poly (styrene sulfonate) Layer-by-Layer Films. *Langmuir* **2004,** *20* (19), 8103-8109.
40. Hammond, P. T., Form and function in multilayer assembly: New applications at the nanoscale. *Advanced Materials* **2004,** *16* (15), 1271-1293.
41. Kharlampieva, E.; Sukhishvili, S. A., Release of a dye from hydrogen-bonded and electrostatically assembled polymer films triggered by adsorption of a polyelectrolyte. *Langmuir* **2004,** *20* (22), 9677-9685.
42. Radziuk, D.; Shchukin, D. G.; Skirtach, A.; Möhwald, H.; Sukhorukov, G., Synthesis of silver nanoparticles for remote opening of polyelectrolyte microcapsules. *Langmuir* **2007,** *23* (8), 4612-4617.
43. Sukhorukov, G. B.; Donath, E.; Lichtenfeld, H.; Knippel, E.; Knippel, M.; Budde, A.; Möhwald, H., Layer-by-layer self assembly of polyelectrolytes on colloidal particles. *Colloids and Surfaces A: Physicochemical and Engineering Aspects* **1998,** *137* (1-3), 253-266.
44. Donath, E.; Sukhorukov, G. B.; Caruso, F.; Davis, S. A.; MÃ¶hwald, H., Novel hollow polymer shells by colloidâ€templated assembly of polyelectrolytes. *Angewandte Chemie International Edition* **1998,** *37* (16), 2201-2205.
45. Cheung, J. H.; Stockton, W. B.; Rubner, M. F., Molecular-level processing of conjugated polymers. 3. Layer-by-layer manipulation of polyaniline via electrostatic interactions. *Macromolecules* **1997,** *30* (9), 2712-2716.
46. Kotov, N. A., Layer-by-layer self-assembly: The contribution of hydrophobic interactions. *Nanostructured Materials* **1999,** *12* (5-8), 789-796.
47. Shimazaki, Y.; Mitsuishi, M.; Ito, S.; Yamamoto, M., Preparation of the layer-by-layer deposited ultrathin film based on the charge-transfer interaction. *Langmuir* **1997,** *13* (6), 1385-1387.
48. Shiratori, S. S.; Rubner, M. F., pH-dependent thickness behavior of sequentially adsorbed layers of weak polyelectrolytes. *Macromolecules* **2000,** *33* (11), 4213-4219.
49. Ramsden, J. J.; Lvov, Y. M.; Decher, G., Determination of optical constants of molecular films assembled via alternate polyion adsorption. *Thin Solid Films* **1995,** *254* (1-2), 246-251.
50. Bromberg, L.; Hatton, T. A., Poly (N-vinylguanidine): Characterization, and catalytic and bactericidal properties. *Polymer* **2007,** *48* (26), 7490-7498.
51. Kenawy, E. R.; Worley, S. D.; Broughton, R., The chemistry and applications of antimicrobial polymers: a state-of-the-art review. *Biomacromolecules* **2007,** *8* (5), 1359-1384.
52. Lewis, K.; Klibanov, A. M., Surpassing nature: rational design of sterile-surface materials. *TRENDS in Biotechnology* **2005,** *23* (7), 343-348.
53. Wang, Y.; Kim, H. J.; Vunjak-Novakovic, G.; Kaplan, D. L., Stem cell-based tissue engineering with silk biomaterials. *Biomaterials* **2006,** *27* (36), 6064-6082.

54. Lichter, J. A.; Van Vliet, K. J.; Rubner, M. F., Design of antibacterial surfaces and interfaces: polyelectrolyte multilayers as a multifunctional platform. *Macromolecules* **2009,** *42* (22), 8573-8586.
55. Lee, D.; Cohen, R. E.; Rubner, M. F., Antibacterial properties of Ag nanoparticle loaded multilayers and formation of magnetically directed antibacterial microparticles. *Langmuir* **2005,** *21* (21), 9651-9659.
56. Kim, Y. H.; Lee, D. K.; Cha, H. G.; Kim, C. W.; Kang, Y. S., Synthesis and characterization of antibacterial Ag-SiO2 nanocomposite. *The Journal of Physical Chemistry C* **2007,** *111* (9), 3629-3635.
57. Zhang, B.; Lin, Y.; Tang, X.; He, S.; Xie, G., Synthesis, characterization, and antimicrobial properties of Cu-inorganic antibacterial material containing lanthanum. *Journal of Rare Earths* **2010,** *28* (1), 451-455.
58. Pang, M.; Hu, J.; Zeng, H. C., Synthesis, Morphological Control, and Antibacterial Properties of Hollow/Solid Ag2S/Ag Heterodimers. *Journal of the American Chemical Society* **2010,** *132* (31), 10771–10785.
59. Sondi, I.; Salopek-Sondi, B., Silver nanoparticles as antimicrobial agent: a case study on E. coli as a model for Gram-negative bacteria. *Journal of Colloid and Interface Science* **2004,** *275* (1), 177-182.
60. Podsiadlo, P.; Paternel, S.; Rouillard, J. M.; Zhang, Z.; Lee, J.; Lee, J. W.; Gulari, E.; Kotov, N. A., Layer-by-layer assembly of nacre-like nanostructured composites with antimicrobial properties. *Langmuir* **2005,** *21* (25), 11915-11921.
61. Lee, H.; Lee, Y.; Statz, A. R.; Rho, J.; Park, T. G.; Messersmith, P. B., Substrate□ independent layer □by □layer assembly by using mussel □adhesive □inspired polymers. *Advanced Materials* **2008,** *20* (9), 1619-1623.
62. Yliniemi, K.; VahvaselkÃ¤, M.; Van Ingelgem, Y.; Baert, K.; Wilson, B. P.; Terryn, H.; Kontturi, K., The formation and characterisation of ultra-thin films containing Ag nanoparticles. *J. Mater. Chem.* **2007,** *18* (2), 199-206.
63. Li, Z.; Lee, D.; Sheng, X.; Cohen, R. E.; Rubner, M. F., Two-level antibacterial coating with both release-killing and contact-killing capabilities. *Langmuir* **2006,** *22* (24), 9820-9823.
64. Link, S.; El-Sayed, M. A., Spectral properties and relaxation dynamics of surface plasmon electronic oscillations in gold and silver nanodots and nanorods. *The Journal of Physical Chemistry B* **1999,** *103* (40), 8410-8426.
65. Kamat, P. V., Photophysical, photochemical and photocatalytic aspects of metal nanoparticles. *J. Phys. Chem. B* **2002,** *106* (32), 7729-7744.
66. Liz-MarzÃ¡n, L. M., Tailoring surface plasmons through the morphology and assembly of metal nanoparticles. *Langmuir* **2006,** *22* (1), 32-41.
67. Mulvaney, P., Surface plasmon spectroscopy of nanosized metal particles. *Langmuir* **1996,** *12* (3), 788-800.
68. Khanna, P. K.; Singh, N.; Kulkarni, D.; Deshmukh, S.; Charan, S.; Adhyapak, P. V., Water based simple synthesis of re-dispersible silver nano-particles. *Materials Letters* **2007,** *61* (16), 3366-3370.
69. Ohde, H.; Hunt, F.; Wai, C. M., Synthesis of silver and copper nanoparticles in a water-in-supercritical-carbon dioxide microemulsion. *Chem. Mater* **2001,** *13* (11), 4130-4135.
70. Khanna, P. K.; Gaikwad, S.; Adhyapak, P. V.; Singh, N.; Marimuthu, R., Synthesis and characterization of copper nanoparticles. *Materials Letters* **2007,** *61* (25), 4711-4714.
71. Ang, T. P.; Wee, T. S. A.; Chin, W. S., Three-dimensional self-assembled monolayer (3D SAM) of n-alkanethiols on copper nanoclusters. *The Journal of Physical Chemistry B* **2004,** *108* (30), 11001-11010.

72. Ang, T. P.; Chin, W. S., Dodecanethiol-protected copper/silver bimetallic nanoclusters and their surface properties. *The Journal of Physical Chemistry B* **2005,** *109* (47), 22228-22236.
73. Siegbahn, K., Electron spectroscopy for atoms, molecules, and condensed matter. *Science (Washington, DC);(United States)* **1982,** *217* (4555).
74. Briggs, D.; Seah, M. P., Practical surface analysis by Auger and X-ray photoelectron spectroscopy. *D. Briggs, & M. P. Seah,(Editors), John Wiley & Sons, Chichester 1983, xiv+ 533* **1983**.
75. Hüfner, S., *Photoelectron spectroscopy: principles and applications*. Springer Verlag: 2003.
76. Watts, J. F.; Wolstenholme, J.; Wiley, J., *An introduction to surface analysis by XPS and AES*. Wiley Online Library: 2003.
77. Bonzel, H. P.; Kleint, C., On the history of photoemission. *Progress in surface science* **1995,** *49* (2), 107-153.
78. Seah, M. P., The quantitative analysis of surfaces by XPS: a review. *Surface and interface analysis* **1980,** *2* (6), 222-239.
79. Hsieh, M. C.; Farris, R. J.; McCarthy, T. J., Surface "priming" for layer-by-layer deposition: Polyelectrolyte multilayer formation on allylamine plasma-modified poly (tetrafluoroethylene). *Macromolecules* **1997,** *30* (26), 8453-8458.
80. Suzer, S., Differential charging in X-ray photoelectron spectroscopy: a nuisance or a useful tool? *Analytical chemistry* **2003,** *75* (24), 7026-7029.
81. Ertas, G.; Suzer, S., XPS analysis with external bias: a simple method for probing differential charging. *Surface and interface analysis* **2004,** *36* (7), 619-623.
82. Conger, C. P.; Suzer, S., Response of Polyelectrolyte Layers to the SiO2 Substrate Charging As Probed by XPS. *Langmuir* **2009,** *25* (3), 1757-1760.
83. Dubey, M.; Gouzman, I.; Bernasek, S. L.; Schwartz, J., Characterization of self-assembled organic films using differential charging in X-ray photoelectron spectroscopy. *Langmuir* **2006,** *22* (10), 4649-4653.
84. Sezen, H.; Suzer, S., Dynamical XPS measurements for probing photoinduced voltage changes. *Surface science* **2010,** *604* (21-22), L59-L62.
85. Suzer, S.; Sezen, H.; Ertas, G.; Dana, A., XPS measurements for probing dynamics of charging. *Journal of Electron Spectroscopy and Related Phenomena* **2010,** *176* (1-3), 52-57.
86. Yoon, B.; Wai, C. M., Microemulsion-templated synthesis of carbon nanotube-supported Pd and Rh nanoparticles for catalytic applications. *Journal of the American Chemical Society* **2005,** *127* (49), 17174-17175.
87. Xue, X.; Wang, F.; Liu, X., One-step, room temperature, colorimetric detection of mercury (Hg2+) using DNA/nanoparticle conjugates. *Journal of the American Chemical Society* **2008,** *130* (11), 3244-3245.
88. Kidambi, S.; Bruening, M. L., Multilayered polyelectrolyte films containing palladium nanoparticles: synthesis, characterization, and application in selective hydrogenation. *Chemistry of materials* **2005,** *17* (2), 301-307.
89. Taner, M.; Sayar, N.; Yulug, I. G.; Suzer, S., Synthesis, characterization and antibacterial investigation of silver-copper nanoalloys. *Journal of Materials Chemistry* **2011,** *21*, 13150.
90. Jernigan, G. G.; Somorjai, G. A., Carbon monoxide oxidation over three different oxidation states of copper: metallic copper, copper (I) oxide, and copper (II) oxide-A surface science and kinetic study. *Journal of Catalysis* **1994,** *147* (2), 567-577.
91. Caruso, F.; Niikura, K.; Furlong, D. N.; Okahata, Y., 1. Ultrathin multilayer polyelectrolyte films on gold: construction and thickness determination. *Langmuir* **1997,** *13* (13), 3422-3426.

92. Laurent, D.; Schlenoff, J. B., Multilayer assemblies of redox polyelectrolytes. *Langmuir* **1997,** *13* (6), 1552-1557.
93. Chen, P.; Wu, X.; Lin, J.; Tan, K. L., Synthesis of Cu nanoparticles and microsized fibers by using carbon nanotubes as a template. *The Journal of Physical Chemistry B* **1999,** *103* (22), 4559-4561.
94. Park, B. K.; Jeong, S.; Kim, D.; Moon, J.; Lim, S.; Kim, J. S., Synthesis and size control of monodisperse copper nanoparticles by polyol method. *Journal of Colloid and Interface Science* **2007,** *311* (2), 417-424.
95. Joseph, Y.; Besnard, I.; Rosenberger, M.; Guse, B.; Nothofer, H. G.; Wessels, J. M.; Wild, U.; Knop-Gericke, A.; Su, D.; SchlÃ¶gl, R., Self-assembled gold nanoparticle/alkanedithiol films: preparation, electron microscopy, XPS-analysis, charge transport, and vapor-sensing properties. *The Journal of Physical Chemistry B* **2003,** *107* (30), 7406-7413.
96. Nakanishi, T.; Ohtani, B.; Shimazu, K.; Uosaki, K., Layer-by-layer self-assembly of composite films of CdS nanoparticle and alkanedithiol on gold: an X-ray photoelectron spectroscopic characterization. *Chemical physics letters* **1997,** *278* (4), 233-237.
97. Bell, W. C.; Myrick, M. L., Preparation and characterization of nanoscale silver colloids by two novel synthetic routes. *Journal of Colloid and Interface Science* **2001,** *242* (2), 300-305.
98. Vasan, H. N.; Rao, C. N. R., Nanoscale Ag-Pd and Cu-Pd alloys. *Journal of Materials Chemistry* **1995,** *5* (10), 1755-1757.
99. Huang, H. H.; Yan, F. Q.; Kek, Y. M.; Chew, C. H.; Xu, G. Q.; Ji, W.; Oh, P. S.; Tang, S. H., Synthesis, characterization, and nonlinear optical properties of copper nanoparticles. *Langmuir* **1997,** *13* (2), 172-175.
100. Ayyappan, S.; Gopalan, R. S.; Subbanna, G. N.; Rao, C. N. R., Nanoparticles of Ag, Au, Pd, and Cu produced by alcohol reduction of the salts. *Journal of Materials Research* **1997,** *12* (2), 398-401.
101. Lei, Y.; Jiang, C.; Liu, S.; Miao, Y.; Zou, B., A clean route for preparation of CdTe nanocrystals and their conjugation with bacterium. *Journal of Nanoscience and Nanotechnology* **2006,** *6* (12), 3784-3788.
102. Rabiot, D.; Dalard, F.; Rameau, J. J.; Caire, J. P.; Boyer, S., Study of sacrificial anode cathodic protection of buried tanks: Numerical modelling. *Journal of applied electrochemistry* **1999,** *29* (5), 541-550.
103. Dierstein, A.; Natter, H.; Meyer, F.; Stephan, H. O.; Kropf, C.; Hempelmann, R., Electrochemical deposition under oxidizing conditions (EDOC): a new synthesis for nanocrystalline metal oxides. *Scripta materialia* **2001,** *44* (8), 2209-2212.
104. Sanchez, J.; Stark, J.; Moruzzi, V., First-principles calculation of the Ag-Cu phase diagram. *Physical Review B* **1991,** *44* (11), 5411.
105. Raghupathi, K. R.; Koodali, R. T.; Manna, A. C., Size-dependent bacterial growth inhibition and mechanism of antibacterial activity of zinc oxide nanoparticles. *Langmuir* **2011,** *27* (7), 4020-4028.